Isomerization in Olefin Metathesis: Challenges and Opportunities

Carolyn Sarah Higman

Thesis submitted to the
Faculty of Graduate and Postdoctoral Studies
University of Ottawa
in partial fulfillment of the requirements for the degree of

Doctor of Philosophy

Ottawa-Carleton Chemistry Institute
Faculty of Science
University of Ottawa

Table of Contents

Abstract

The past two years have witnessed groundbreaking advances in the industrial deployment of olefin metathesis. While metathesis methodologies have been an integral part of the chemical manufacturing landscape for 60 years, implementation in pharmaceutical and specialty chemicals manufacturing represents a new frontier. The imperative to develop greener and more cost-effective manufacturing processes is anticipated to spur further improvements in sustainable synthesis. Advances in catalyst productivity, however, are critical to expansion of the uptake of metathesis methodologies in this and other manufacturing sectors.

Key to increased catalyst productivity is elimination of side reactions that lower yield and errode selectivity. Among such reactions, double-bond isomerization is by far most common. Accumulating evidence suggests that unwanted isomerization during olefin metathesis is due to ruthenium species generated via catalyst decomposition. The identification of these species and how they are formed is thus of great importance. Two hydride complexes, $RuHCl(CO)(H_2IMes)(PCy_3)$ and a dinuclear hydride, are known to form under some circumstances by decomposition of the second-generation Grubbs catalyst, $RuCl_2(H_2IMes)(PCy_3)(=CHPh)$, **GII**. These complexes have been widely viewed as responsible for unintended isomerization reactions. However, examination of their performance in olefin isomerization under conditions relevant to metathesis reveals that their activity is too feeble to account for the levels of isomerization observed during metathesis. Alternatively, kinetically competent culprits emerge from decomposition studies that reveal unexpected ruthenium products on decomposition of **GII** during metathesis; specifically, formation of ruthenium nanoparticles. The formation and catalytic non-innocence of RuNPs

constitutes a new paradigm in this field, which opens the door to new approaches to prevent or to harness olefin isomerization. Key to prevention, clearly, is circumventing the decomposition pathways that enable ligand stripping from the active catalyst. New approaches to catalyst design that involve use of truncated NHC ligands are also examined. Finally, the power and utility of isomerization when coupled with metathesis is explored. The opportunities and limitations of orthogonal isomerization–metathesis catalysis are examined in the context of the two-step synthesis of cinnamates from 1-allylbenzenes abundant in essential oils. An efficient one-pot, two-catalyst protocol is developed for conversion of these biorenewable feedstocks to high-value-added chemicals.

Acknowledgements

To my supervisor, Deryn Fogg, you have always encouraged me, and pushed me to become the person and scientist that you have seen in me since that day in transition metal lab many years ago. I have learned an incredible amount from you, both inside and outside the lab. To my first graduate student mentor (now Professor) Johanna Blacquiere, I feel extremely lucky to have had the chance to work with you. I hope that I am even a fraction as good as you are at teaching and mentoring. I have very much enjoyed watching you grow into an amazing supervisor and researcher.

To my many labmates over the years, I thank you for your teamwork, collaboration, and friendship. Gwen, you have taught me more than you know, and I have really enjoyed the time we've spent together teaching, travelling, and collaborating. Adrian and Justin, thank you for always being there to always bounce ideas off, and for all of the invaluable scientific discussions.

To all of my family and friends, you have supported me throughout what seems like a lifetime of schooling. Mom and Dad, you have always believed in me and encouraged me to be myself and do what makes me happy. To my friends Bianca, Liz, Rob, and Nick, I will always cherish our friendships and I love you all so much. I could not have made it through without you guys.

To my best friend, Ross, you keep me sane and grounded. You have been there for me through this journey with unwavering support and understanding. You are the kindest, most patient person I know, and I appreciate everything you've done for me.

Abbreviations

API	Active pharmaceutical ingredient
APTES	Aminopropyltriethoxysilane
BArF	Tetrakis[3,5-bis(trifluoromethyl)phenyl]borate
Boc	Di-tert-butyl dicarbonate
BSE	Back-scattered electrons
cGMP	Current good manufacturing practice
CM	Cross metathesis
CND	Crystal nanodiamond
COD	1,5-Cyclooctadiene
COMPO	Composition
COSY	Correlation spectroscopy
COT	1,3,5-Cyclooctatriene
DCE	1,2-dichloroethane
DCQ	2,6-dichloroquinone
DDM	Diethyldiallylmalonate
DLS	Dynamic light scattering
EDX	Energy-dispersive X-ray spectroscopy
ETG	Ethylene glycol
equiv	Equivalents
EM	Effective molarity
EXSY	Exchange spectroscopy
FESEM	Field-emission scanning electron microscopy
FETEM	Field-emission transmission electron microscopy
GC-FID	Gas chromatography-flame ionization detection
HCV	Hepatitis C virus
H_2IMes	1,3-bis-(2,4,6-trimethylphenyl)imidazolin-2-ylidene
HMBC	Heteronuclear multiple bond correlation experiment
HMQC	Heteronuclear multiple quantum coherence
HR-SEM	High-resolution scanning electron microscopy

HR-TEM	High-resolution transmission electron microscopy
Hz	Hertz
ICP-ES	Inductively coupled plasma emission spectrometry
IMes	1,3-bis-(2,4,6-trimethylphenyl)imidazol-2-ylidene
IMe_4	1,3,4,5-tetramethylimidazol-2-ylidene
IPr	1,3-bis(2,6-diisopropylphenyl)imidazol-2-ylidene
IR	Infrared
Isom	Isomerization
KTp	Potassium hydrotris(pyrazolyl)borate
MA	Methyl acrylate
MAP	Monoalkoxide pyrrolide
MCB	Metallacyclobutane
MCM	Mobil Composition of Matter
MDMA	3,4-methylenedioxy-methamphetamine
Mes	Mesityl
N.D.	Not determined
NHC	*N*-heterocyclic carbene
NMR	Nuclear magnetic resonance
NOESY	Nuclear Overhauser effect spectroscopy
NP	Nanoparticle
ORTEP	Oak Ridge thermal ellipsoid plot
ppm	Parts per million
py	Pyridine
RCM	Ring closing metathesis
RT	Room temperature
RuNPs	Ruthenium nanoparticles
SEM	Scanning electron microscopy
SM	Self-metathesis
TCE	Tetrachloroethane
TEM	Transmission electron microscopy
TEP	Tolman electronic parameter

THF	Tetrahydrofuran
TMB	1,3,5-trimethoxybenzene
TMS	Tetramethylsilane
TON	Turnover number
UHP	Ultra-high purity
UVA	Ultraviolet A
XPS	X-ray photoelectron spectroscopy
XRD	X-ray diffraction

List of Compounds

Metal complexes

#	Compound	#	Compound
GI	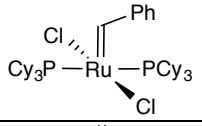	**GII**	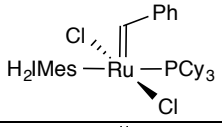
GIm	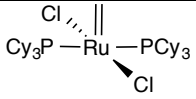	**GIIm**	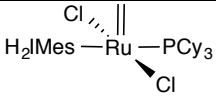
GI-py	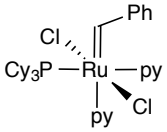	**GII-PPh$_3$**	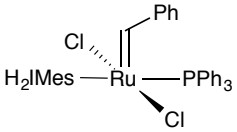
GIII	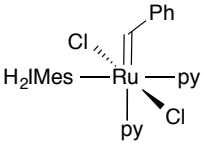	**GIII-Ind**	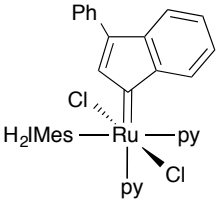
HI	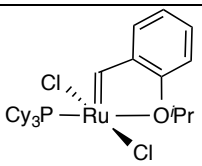	**HII**	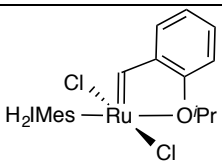
WH	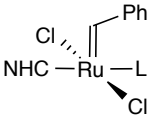	**PII**	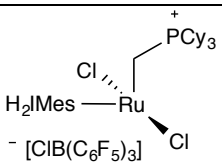
Z1b	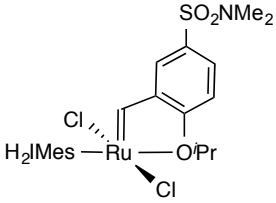	**nG**	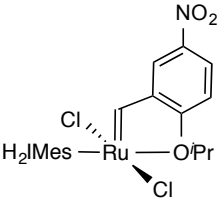
M2	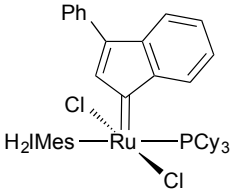	**Cat-RF1**	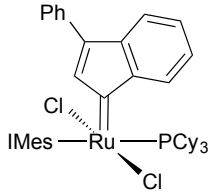
M51	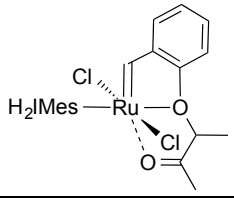	**Ru-1**	$RuCl_2(PPh_3)_3$

Ru-2	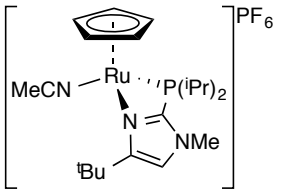	**Ru-2'**	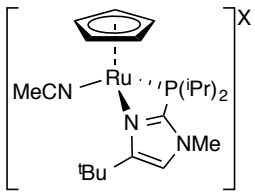
Ru-3	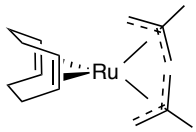	**Ru-4**	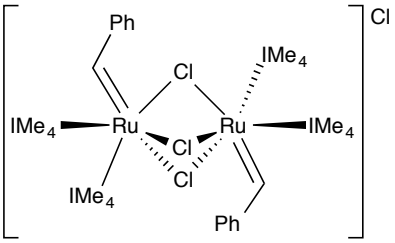
Ru-5	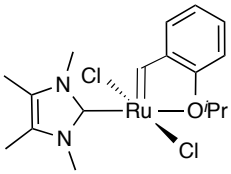	**Ru-6**	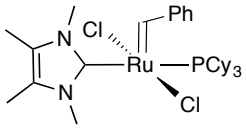
Ru-7	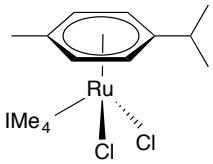	**Ru-8**	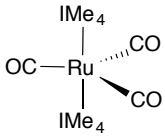
Ru-9	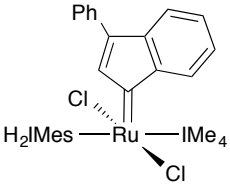	**Ru-10**	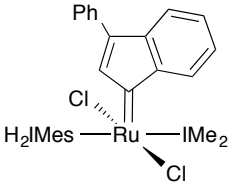
Ru-11	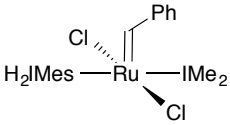	**MCB**	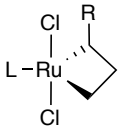
Ru-H1	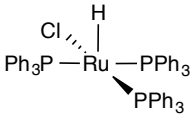	**Ru-H2**	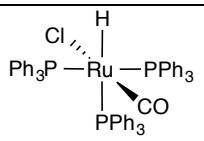
Ru-H3	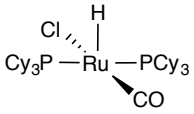	**Ru-H4**	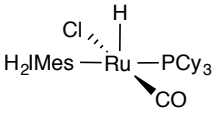
Ru-H5	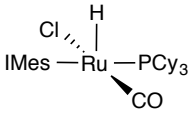	**Ru-H6**	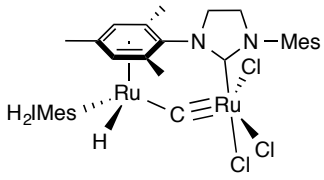

Ru-H7	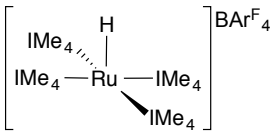	**Ru-H7'**	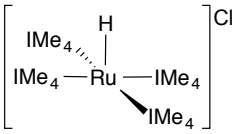
Ru-H8	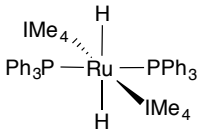	**Pd-1**	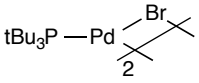
Mo-1	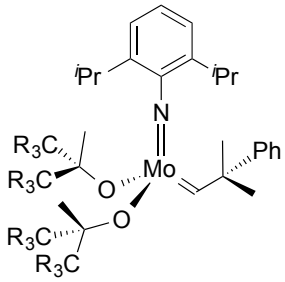	**Mo-2**	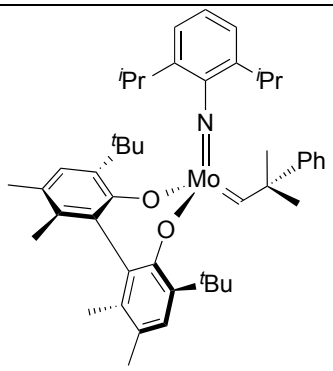
Mo-3	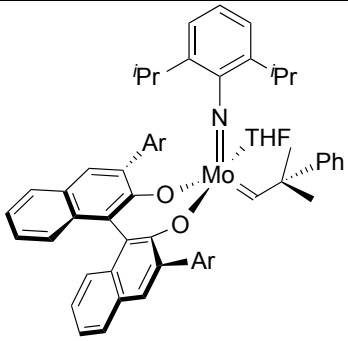	**Mo-P**	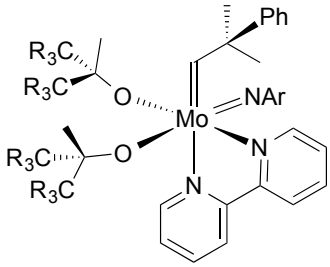
Mo-MAP	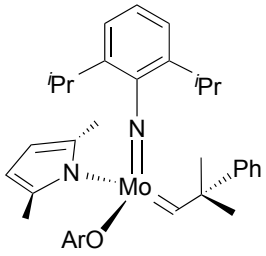	**W-MAP**	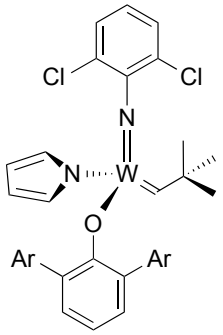

Organic Compounds

#	Compound	#	Compound	#	Compound
1a	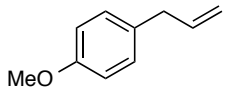	**1b**	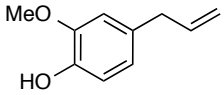	**1c**	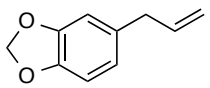
2a	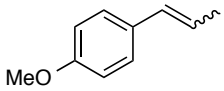	**2b**	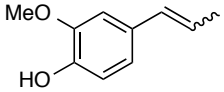	**2c**	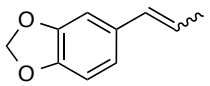
3a	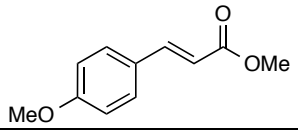	**3b**	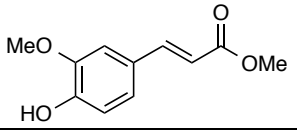	**3c**	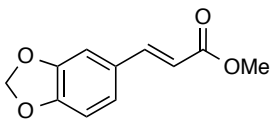
4a	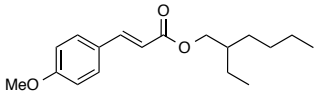	**4b**	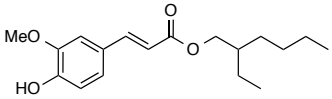	**4c**	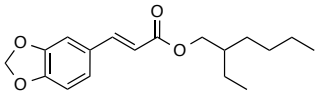
5a	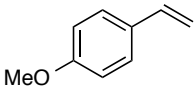	**5b**	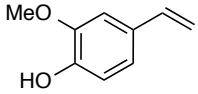	**5c**	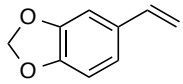
6a	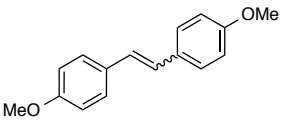	**6b**	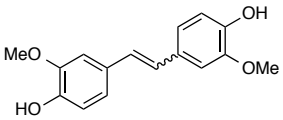	**6c**	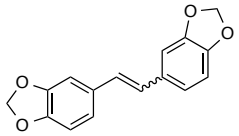

#	Compound	#	Compound
7a	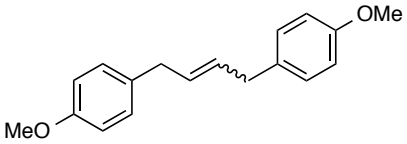	**8a**	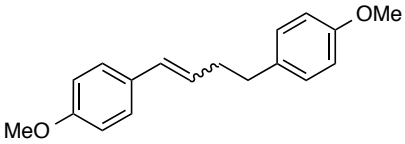
9a	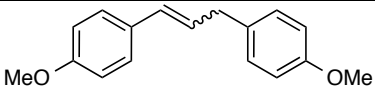	**10**	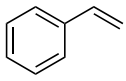
11	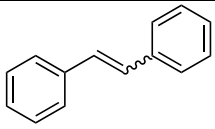	**12**	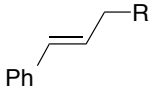
MA	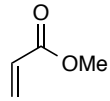	**EHA**	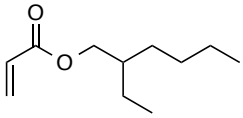
DDM	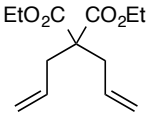	**TMB**	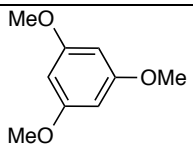
DMT	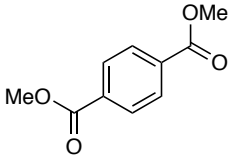	**IMe_4**	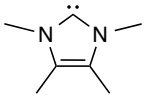
IMes	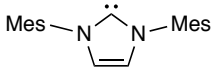	**H_2IMes**	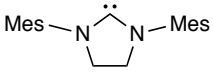

Chapter 1. Introduction

1.1. Published Contributions

Sections of this chapter have been published:

Olefin Metathesis at the Dawn of Implementation in Pharmaceutical and Specialty Chemicals Manufacturing.

Carolyn S. Higman,[†] Justin A. M. Lummiss,[†] and Deryn E. Fogg,* *Angew. Chem. Int. Ed.* **2016**, *55*, 3552–3565, invited review. [†]Equal contributions

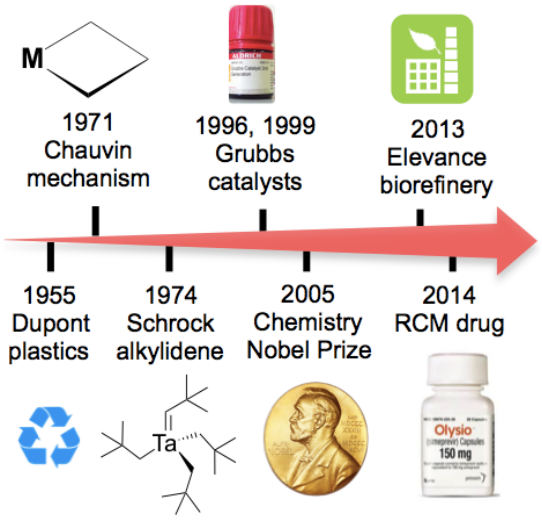

The uptake of olefin metathesis in pharmaceutical and specialty-chemicals manufacturing, anticipated for decades, is a recent reality. Metathesis has been a key industrial process since the 1950s, but applications to functional group-rich targets were long precluded by catalyst sensitivity. The advent of readily-handled, comparatively robust ruthenium catalysts, coupled with the discovery of the synthetic potential of ring-closing metathesis (RCM), brought metathesis methodologies to the attention of organic chemists. Applications to the synthesis of complex, biologically active organic molecules exploded.[1] Cross metathesis (CM)

benefited in parallel, particularly as the capacity to transform unsaturated seed oils into specialty chemicals gained impetus from new markets for sustainable products.[2,3] Given these advances, it is perhaps surprising the first industrial processes are only now emerging. Examined in this introductory chapter are recent advances and some of the challenges involved in implementation of the molecular metathesis catalysts in the industrial context. Ring-opening metathesis polymerization (ROMP) and acyclic diene metathesis (ADMET) of non-functionalized olefins have been utilized in industry for decades, following the original DuPont patent filing in 1955.[4] Fundamental to the new opportunities currently being developed in industry is the capacity to effect metathesis of functionalized substrates. These advances were made possible by the development of relatively robust molecular catalysts, born out of the pioneering advances of Schrock and Grubbs, and Chauvin's brilliant insight into the mechanism of the reaction.[5]

1.2. Molecular Metathesis Catalysts: The Research Context

Hundreds of metathesis catalysts have now been developed, of which more than 60 are now commercially available.[6] Particularly prominent are examples based on ruthenium and the group 6 metals molybdenum and tungsten. While the majority of these catalysts have been explored almost solely in the research context, Figure 1.1 highlights ruthenium catalysts known to have been adopted in industrial processes or in scaleup campaigns. Most of the catalysts in confirmed use are second-generation derivatives containing an *N*-heterocyclic carbene (NHC) ligand, which significantly expand catalyst scope and performance.

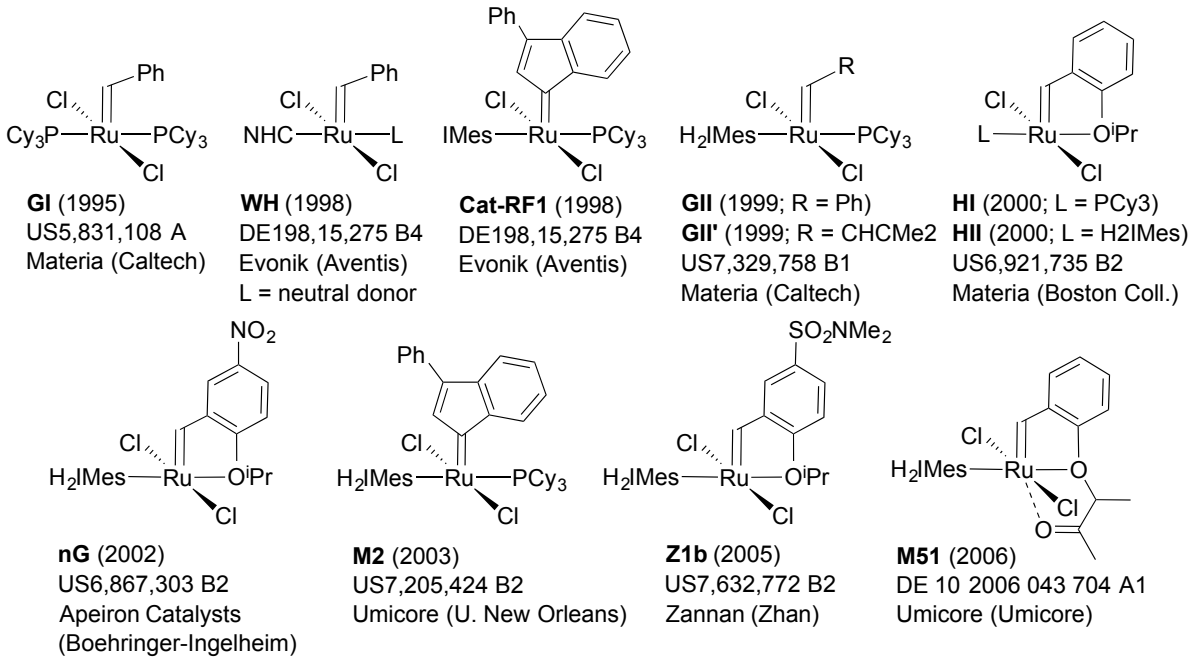

Figure 1.1. Commercially-available ruthenium metathesis catalysts, highlighting examples used in recently-disclosed industrial processes or scale-up, and the parent Grubbs catalyst **GI**. Shown are the priority year and the corresponding patent number, with the primary licensee and IP owner as of the time of writing. See: https://www.epo.org; www.uspto.gov.

As noted above, the greater ease of handling of the Ru systems led to their widespread adoption for target-directed synthesis. Nevertheless, the group 6 catalysts (Figure 1.2) stand out for their high, tunable reactivity and potential selectivity.[1] In particular, tempered-activity monoalkoxide-pyrrolide (MAP) catalysts have enabled spectacular advances in *Z*-selective metathesis.[7] Strategies developed to improve the ease of handling range from the use of masked, air-stable precursors such as **Mo-P**, to formulation of the active Mo catalysts into wax pills for convenient dosing of reactions.[8] No industrial processes utilizing these catalysts have yet been disclosed, however, although intriguing advances have been hinted by press release[9,10]

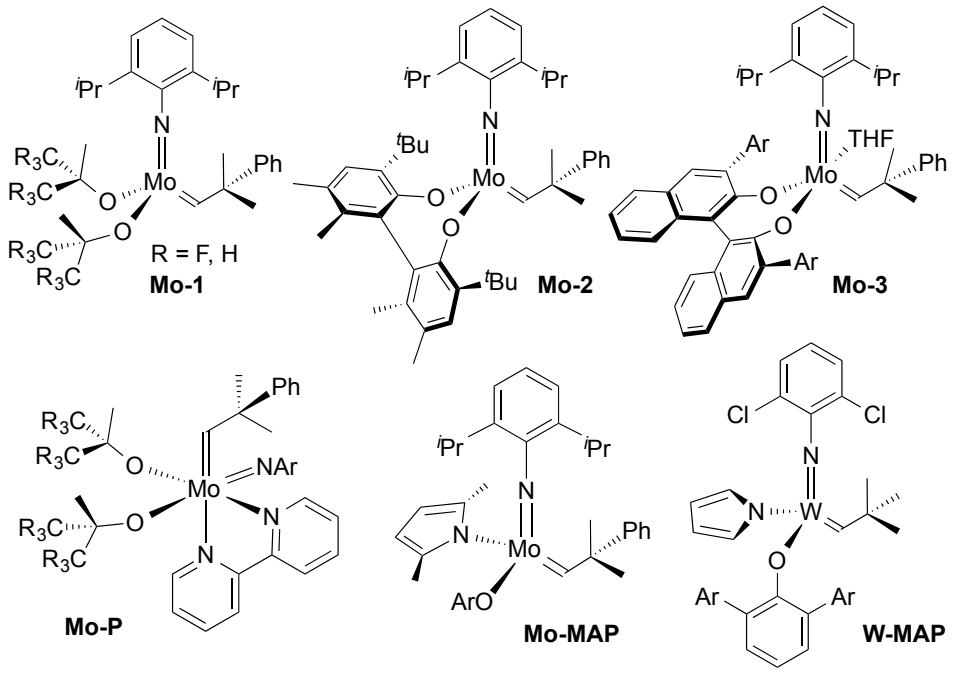

Figure 1.2. Leading, exemplary group 6 metathesis catalysts or (**Mo-P**) catalyst precursors.

1.3. The Chauvin Mechanism

Olefin metathesis operates via 2+2 cycloaddition (Figure 1.3), as first proposed by Chauvin in 1971.[11] The important Grubbs-class ruthenium catalysts enter the catalyst cycle via a dissociative mechanism involving rate-determining loss of PCy_3.[12] More rarely, as in the case of the Hoveyda catalyst **HII**, initiation can occur via an associative pathway in which substrate binds prior to loss of a neutral ancillary ligand.[13] Irrespective of the mechanism of initiation, substrate coordination is followed by metallacyclobutane (MCB) formation. Productive cycloreversion liberates the metathesis product, regenerating a four-coordinate active species. The active species can coordinate another olefin, or recapture the lost phosphine ligand to give an off-cycle, five-coordinate methylidene resting state, the concentration of which builds up during catalysis.

References page 24

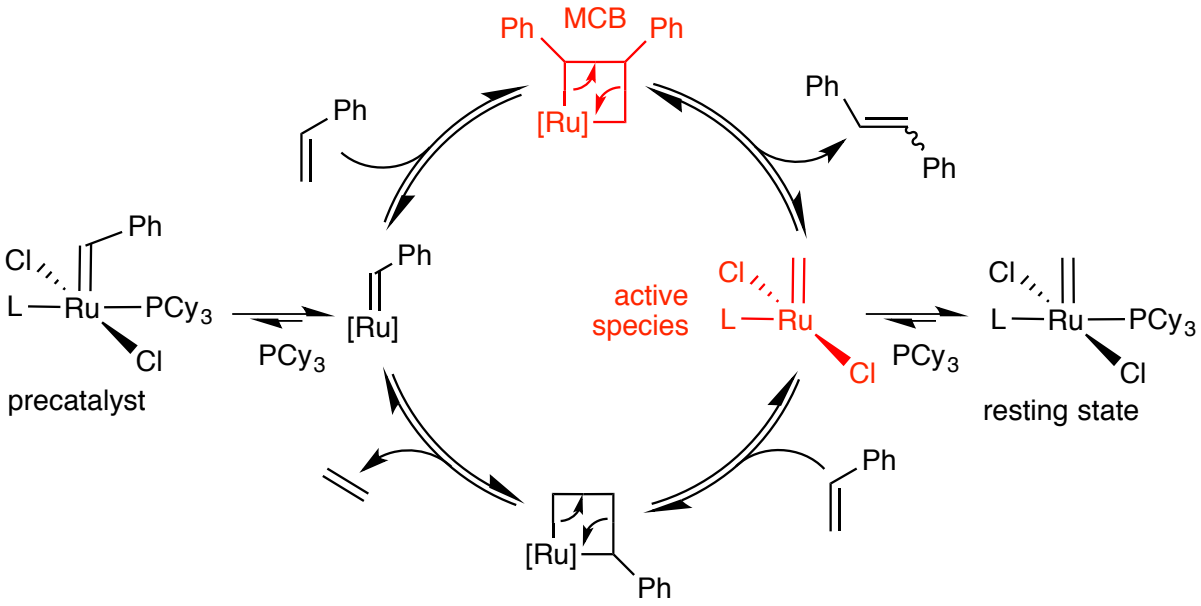

Figure 1.3. Chauvin mechanism for olefin metathesis, illustrated by cross-metathesis of a representative terminal alkene with a Grubbs-class catalyst.

1.4. Catalyst Choice in the Industrial Context

Catalyst choice in process development is governed by business considerations. Notwithstanding the importance of catalyst performance, primary issues are cost, freedom to operate, and security of supply on scale. Figure 1.1 shows the original patent number and priority year for the catalysts used in the processes discussed, the corporate entity that holds primary licensing rights, and the intellectual property (IP) owner.

Because the catalyst composition patents are still in force, the IP situation is complex, and concerns about freedom to operate have slowed commercial uptake of metathesis technologies. The concerns are illustrated by long-running litigation between Materia (exclusive licensee of the extensive Grubbs patent portfolio), and Evonik, which now holds the rights to Herrmann / Aventis patents claiming priority to Ru-NHC catalysts based on the

generic structure **WH**. Elevance Renewable Sciences, the dominant company involved in plant-oil metathesis, recently opted to license a subset of the Evonik patents as well as Materia's, to secure unambiguous rights to practice, and avert legal costs and implementation delays.[14,15] A limited number of companies supply metathesis catalysts, according to business models that have varied widely. Now increasingly common is bulk catalyst pricing that includes the associated IP, although uncertainties concerning freedom to operate remain incompletely resolved, as noted above. A further issue is security of supply on the ton scale required for large-scale industry.

1.5. Impact of Impurities

Robust, reliable catalyst performance is the cornerstone of plant-scale production. The issue is particularly acute in the manufacturing of active pharmaceutical ingredients (APIs), where a failed batch is not only very costly, but can potentially compromise both drug supply, and compliance with current Good Manufacturing Practice (cGMP) regulations. In general, metathesis catalysts are less stable than reports centered on target-directed synthesis tend to suggest. Oxidative degradation by air, reactions with solvent, and intrinsic C–H-activation pathways involving neutral ancillary ligands and the metallacyclobutane all limit productivity, as discussed in more detail in Section 1.7.

Further challenges become evident when very high turnover numbers (TONs) are required from technical-grade feedstocks. Certain impurities are severely detrimental to metathesis rates and yields, and ultimately to process reproducibility.[16-20] For Ru metathesis catalysts, both Brønsted and Lewis base functionalities are now known to be problematic (Figure 1.4).

This becomes critical at low catalyst loadings, where the concentration of adventitious contaminants may exceed that of the catalyst. Such destructive agents commonly derive from a prior reaction step. Minor impurities in industrial-grade solvents can likewise be important, particularly at the high dilutions frequently required for RCM. Undesired epimerization, a recurring problem in the RCM step for Ciluprevir and related APIs, was traced to ppm levels of morpholine in the toluene solvent.[18] Similar issues encountered during the synthesis of Simeprevir were eliminated by sequestering amine and phosphine residues.[20] A leading review from pharma suggested that a strategic purification stage – ideally, crystallization of the diene – be considered prior to any metathesis step, to safeguard process robustness.[20]

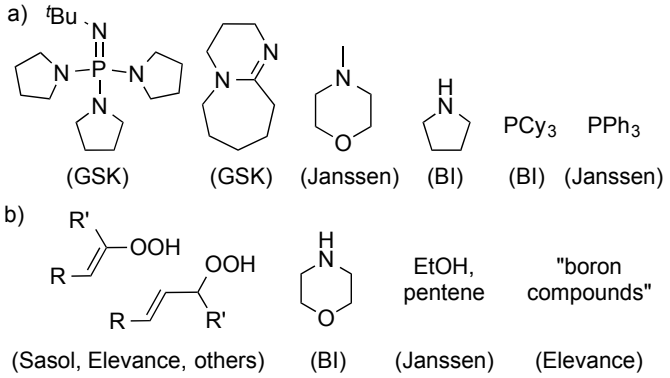

Figure 1.4. Exemplary contaminants identified as detrimental to metathesis in industrial applications. a) Residues from catalyst or prior step. b) Contaminants in solvent or feedstock.

Plant-oil feedstocks contain impurities that vary widely in distribution and proportion. Beyond the usual problems posed by Lewis bases, peroxides formed by autoxidation of unsaturated triglycerides are detrimental to catalyst productivity. Water and protic compounds also present difficulties, in part due to competing hydrolysis during the transesterification step used to liberate the desired unsaturated esters. The patent literature describes pre-treatment methods aimed at conserving catalyst productivity.[21,22] These range

from simply heating under N_2 to decompose peroxides, to treating with alumina, magnesol (magnesium silicates), silica gel, or other inorganic absorbents and desiccants, and with these or activated carbon to remove polar compounds. Acetic anhydride treatment is suggested as a potential means of removing alcohols and hydroperoxides.[21] While purification can protect the catalyst from poisons, and hence improve productivity, this adds to process and materials costs. Given the lower profit margins in the specialty chemicals sector, gains in catalyst productivity must be balanced against the cost of pre-treatment.

1.6. Pharmaceutical Applications

RCM is the most important application of metathesis in the production of APIs. To our knowledge, CM is not yet deployed in the pharmaceutical manufacturing sector on process scale. Summarized in Table 1.1 are recently disclosed examples for which RCM reactions have advanced into clinical trials and/or production. The majority of targets are macrocyclic peptidomimetics, which afford opportunities to address protein-protein interactions impervious to small molecules, while maintaining cell permeability and oral bioavailability.

Associated challenges are the cumulative impact of impurities in such large volumes of industrial-grade solvent, the bottleneck of solvent evaporation,[23] and poor mass transfer with respect to removal of ethylene from solution. In the original Ciluprevir campaign, ethylene removal proved inefficient even when sparging with N_2 at 1,000 L h^{-1} during RCM.[18] Retention of ethylene has multiple negative consequences, including regeneration of diene, unproductive cycling of the catalyst, and catalyst deactivation.

Table 1.1. RCM beyond the discovery stage, as used in synthesis of HCV protease inhibitors for production and/or clinical trials.

API name (company)	Catalyst (scale)	Ref.	Regulatory Status[a]
Ciluprevir (BI)	**nG** (400 kg)	18	halted in phase 2 (2002)
Simeprevir (Janssen)	**M2** (kg)	24	approved (2013-14)
Paritaprevir (AbbVie)	ND[b] (1.2 g)	25	approved (2014-15)
Vaniprevir (Merck)	**HII** (200 g)	26	approved (2014)
MK-6325 (Merck)	**Z1b** ("multi-kg")	27	completed phase 1 (2012)
IDX320 (Idenix)	**Z1b** (1 kg)	23	halted in phase 1 (2010)
Danoprevir (Roche)	Ru-NHC (13 g)	28,29	completed phase 2 (2015)

[a] See https://clinicaltrials.gov. [b]ND = not disclosed.

Abundant activity has centered on the RCM assembly of macrocycles that function as competitive inhibitors of proteases,[30] particularly the Hepatitis C virus protease (HCVP) NS3/4A. The first such drugs very recently reached the market. Simeprevir (Johnson & Johnson) was launched in December 2013, and rapidly achieved blockbuster status. Multiple therapeutic options are desirable to counter the emergence of drug-resistant strains arising from rapid virus mutation, and Simeprevir was followed in late 2014 by Vaniprevir (Merck) and Paritaprevir (AbbVie; Figure 1.5). Common features include a macrocyclic linker connecting peptide side-chains, and an endocyclic proline or proline mimic, elements also evident in Ciluprevir, the first such API to have been reported.[18,20,31] While Ciluprevir failed in clinical trials, it remains important for the insights its scaleup afforded into commercially

viable RCM macrocyclization, and the influence of these advances on subsequent synthetic campaigns.

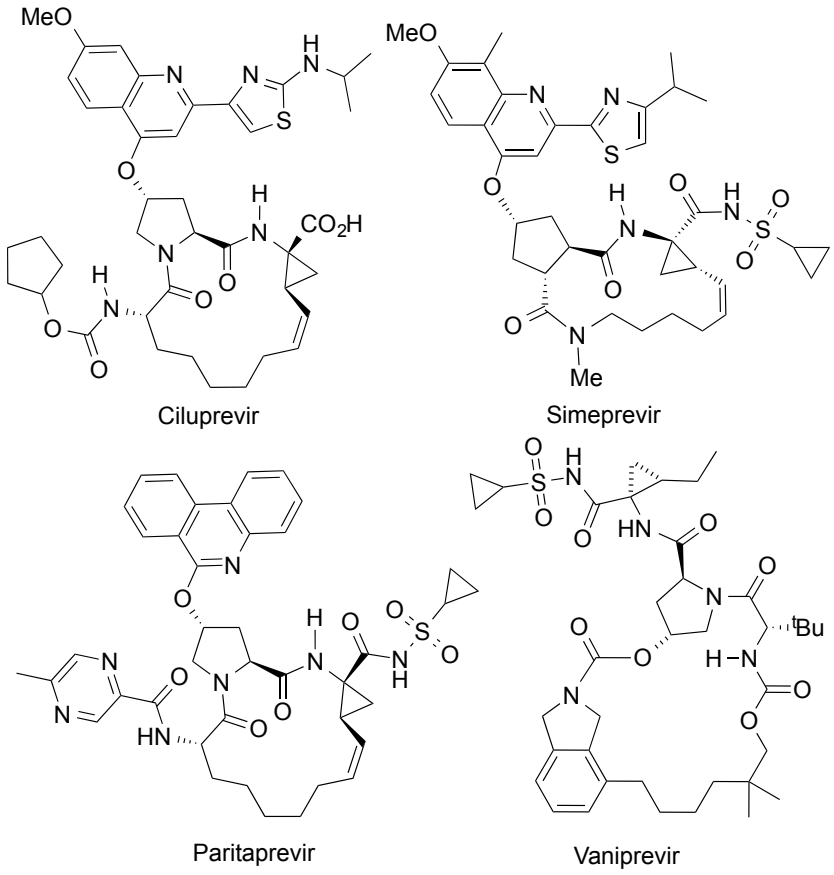

Figure 1.5. First-in class HCV drug candidate Ciluprevir, and currently approved HCV drugs prepared via RCM.

1.6.1. Ciluprevir

Boehringer-Ingelheim's 2005 report of the large-scale synthesis of Ciluprevir was a milestone: not only a first-in-class HCV protease inhibitor, but the first pilot-scale implementation of RCM.[18,32] The original scaleup was carried out at dilutions of 0.01 M (Figure 1.6a). Key to a more economical process was the discovery that acyl-protection of the endocyclic secondary amide significantly reduced ring strain, hence raising the effective molarity (EM) of the diene. Use of a Boc protecting group (Figure 1.6b) limited

oligomerization even at concentrations 10–20 times higher. Solvent requirements were thereby reduced from 150,000 L to 7,500 L per tonne of diene, enabling production in standard 2,000 or 4,000 L reactors, and eliminating the need for specialized rapid-evaporation equipment.[33] As an added, unanticipated advantage, *N*-protection favoured initiation at the sterically unencumbered olefin, rather than the vinylcyclopropane site. This adaptation suppressed epimerization, and prevented catalyst degradation by the unprotected amide. A switch to fast-initiating **nG** as catalyst, and to reaction in refluxing toluene, greatly improved space-time yields. The timescale for metathesis was compressed from days to minutes, such that the RCM step was no longer a bottleneck in operations. A 50-100 fold increase in catalyst productivity also facilitated catalyst quenching and removal. More recently, the synthetic strategies optimized for Ciluprevir were applied to the assembly of a closely related API still in pre-clinical study (BI201302).[34]

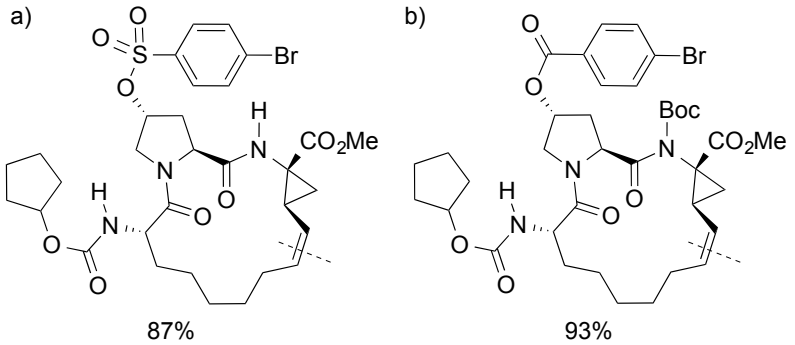

Figure 1.6. RCM scale-up conditions in production of Ciluprevir. a) Original conditions. b) Second-generation process. For API structure, see Figure 1.5.

References page 24

1.6.2. Simeprevir

The Medivir/Tibotec team recently reported process details for the synthesis of Simeprevir, the first RCM-enabled drug to come to market (Janssen Pharma).[24,35] Low diene EM was again a challenge. In the discovery route, partial oligomerization of the unprotected diene occurred even at dilutions of 0.01 M (Figure 1.7a). Epimerization was also an issue, but was circumvented by neutralizing residual bases present. Working concentrations were raised to 0.05 M by Boc-protection, as for Ciluprevir, and by adding diene slowly to limit intermolecular reaction (an approximation of the classic Ziegler "infinite-dilution" approach; Figure 1.7b).[24] To retard catalyst deactivation in refluxing toluene, **M2** was also added slowly. The catalyst loading was thereby reduced from 1.5 mol% to 0.3 mol%. No epimerization was observed for **M2** or other Ru-NHC catalysts, although such problems were encountered with **HI**. Despite the fact that Boc was originally chosen for its ease of installation and removal, recent Janssen patents note that deprotection required drastic conditions, which led to product decomposition.[36] Halogenated acyl groups proved more satisfactory, although dilutions of 0.02 M were required on the maximum scale reported (51 g).

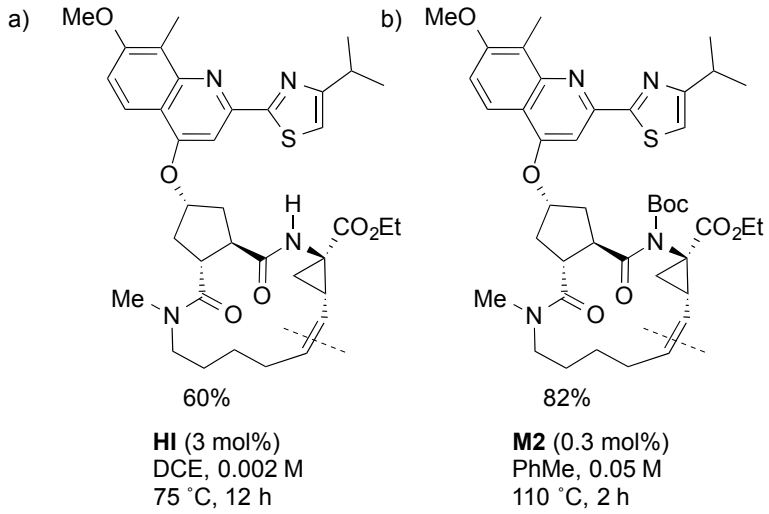

Figure 1.7. RCM step in the synthesis of Simeprevir. a) Discovery stage. b) reported process conditions, with slow addition of diene and catalyst.[24] For API structure, see Figure 1.5.

1.6.3. Paritaprevir

Paritaprevir (formerly ABT-450), developed by Enanta and marketed by AbbVie, is now approved for treatment of genotype 1 chronic HCV in the US and Canada, and for genotypes 1 and 4 in Europe.[35,37] Although neither process details nor the structure of the RCM precursor have been described, the macrocyclic core is identical to that in Ciluprevir (see Figure 1.5 above), and similar issues of dilution, epimerization, etc. are therefore probable. A 2009 patent describes use of a range of catalysts (**GI**, **GII**, **HII**, and variants), with up to 12 h reaction in refluxing CH_2Cl_2.[25] A subsequent update described RCM via **Z1b** in toluene, with post-metathesis quenching by imidazole.[38]

1.6.4. Vaniprevir

Approved in December 2014 in Japan, Vaniprevir contains the largest (20-membered) macrocyclic core of the HCV drug candidates openly pursued to date. A degree of

conformational constraint in the tripeptide–isoindoline diene **4a** is implied by the limited oligomerization (ca. 5%) observed even at 0.086 M diene, without Boc-protection. Slow diene addition enabled further reductions in the solvent volume, to 0.13 M (Scheme 1.1).[26] Initial challenges were posed by competing isomerization of the allylbenzene group, which resulted in contamination of the desired 20-membered ring with ca. 10% of the ring-contracted product. This side-reaction was limited to <2% by adding the catalyst slowly, sparging with N_2 to remove ethylene, and adding 2,6-dichloroquinone (DCQ). The importance of the first two factors tends to point toward catalyst decomposition as the cause of isomerization.

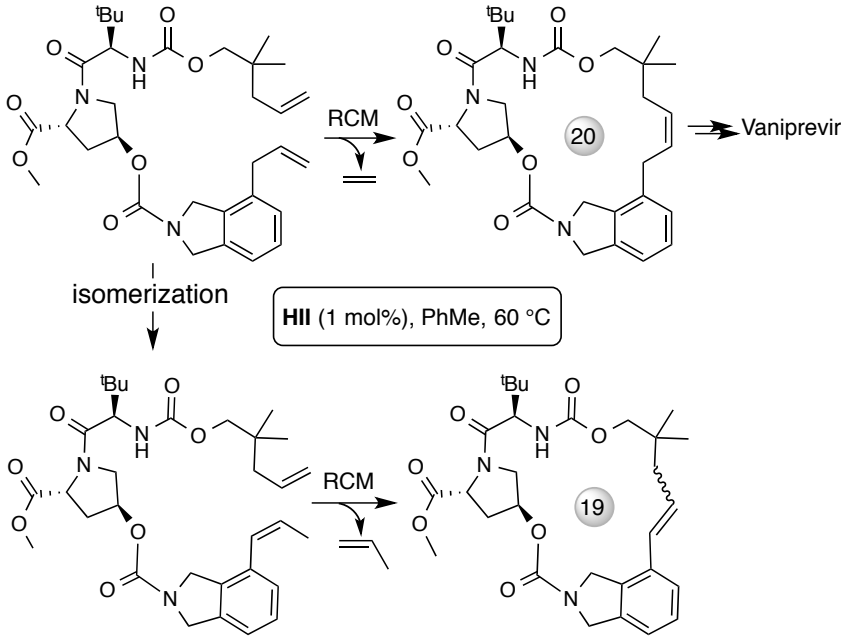

Scheme 1.1. Competing isomerization during the synthesis of Vaniprevir. For API structure, see Figure 1.5. Note: numbers in gray circles in the RCM products indicate the ring size.

1.7. Deactivation Mechanisms

Increased catalyst productivity has the potential to significantly expand uptake of the molecular metathesis catalysts in industrial processes. From the dual perspectives of process

chemistry and catalyst (re)design, an improved understanding of the fundamental pathways involved in catalyst deactivation is crucial. While several reports describe decomposition of key *precatalysts* by solvent,[18,39-41] adventitious oxygen,[42,43] or thermolysis,[44] this section focuses on decomposition of the metal species present during catalysis. A particular focus is **GII**, given its importance as the dominant catalyst currently used in metathesis.[45]

The mechanisms of decomposition are typically inferred from the organic byproducts observed. The fate of the ruthenium species has been identified under fewer, more specialized circumstances.[46] In one example, Hong and Grubbs identified the dinuclear ruthenium species **Ru-H6** as a major decomposition product on prolonged thermolysis of **GIIm** in the absence of substrate (Scheme 1.2).[47] This complex was isolated in 46% yield based on Ru. Also observed, but not quantified, was phosphonium salt $MePCy_3Cl$. Catalyst decomposition was proposed to proceed by loss of PCy_3 from **GIIm**, followed by attack of free phosphine on the methylidene carbon of four-coordinate **A** to generate intermediate **B**, and dimerization of **A**.[47] Elimination of the phosphine, a chloride, and methylidene ligands as $MePCy_3Cl$ then occurs, and **Ru-H6** is ultimately formed. Given the formation of hydride **Ru-H6** directly from the resting state species **GIIm**, and the observed isomerization activity of this complex, the authors suggested that **Ru-H6** could be responsible for the adventitious isomerization that is often observed during metathesis.

References page 24

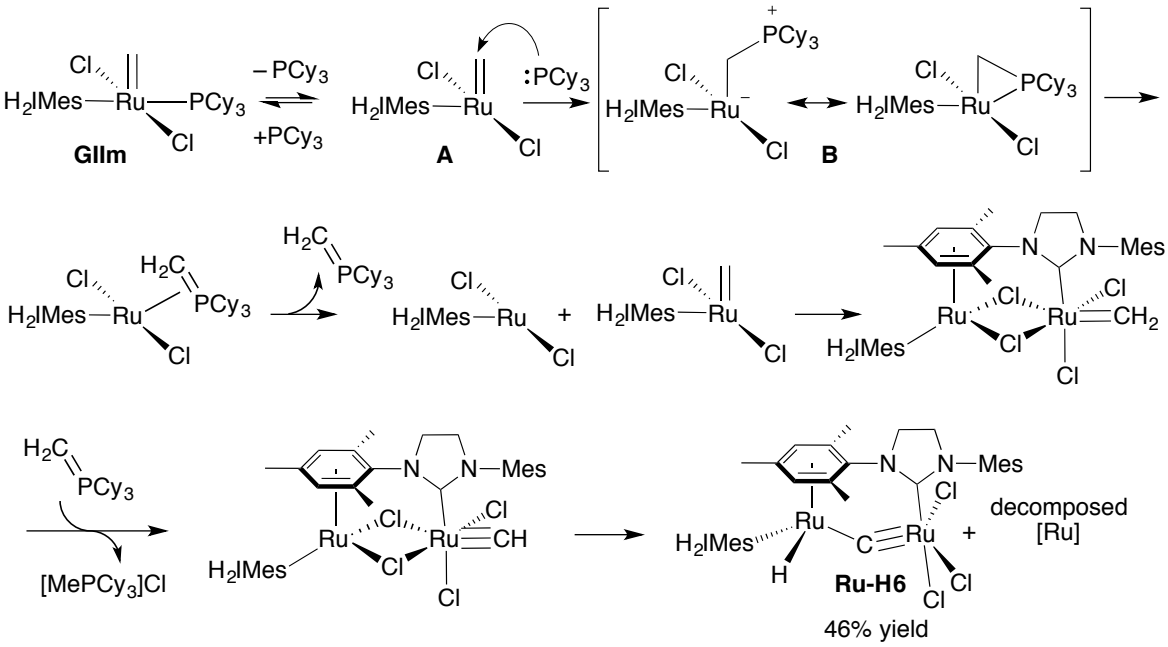

Scheme 1.2. Observation of **Ru-6** following thermolysis of **GIIm** (55 °C, benzene, 72 h), and proposed mechanism for its formation.

The relevance of **Ru-H6** to deactivation in the presence of substrate (i.e. during catalysis) is unclear, given the slow formation of this species, vs. the timescale of hours for decomposition of **GIIm** during metathesis. Likely much more relevant is liberation of the methylphosphonium salt. Nucleophilic attack of the PCy_3 ligand on the methylidene ligand is consistent with precedents for related complexes,[48-50] and the putative σ-alkyl intermediates appear to be highly reactive, readily participating in C-H activation processes.[50-52] Our group recently reported direct crystallographic evidence for the σ-alkyl moiety in the first-generation Grubbs system,[53] and quantified the "ligand-stripping" loss of $[MePCy_3]Cl$ following attack of PCy_3 on **GIIm**. Thus, formation of $[MePCy_3]Cl$ accounted for 85% of the total loss of **GIIm** at the first half-life (3 h) on thermolysis of **GIIm** at 60 °C in C_6D_6 (53% loss of methylidene; 45% conversion to $[MePCy_3]Cl$).[54] ^{13}C-Labelling studies with

$RuCl_2(H_2IMes)(PCy_3)(=^{13}CH_2)$ ***GIIm** confirmed that the methyl group of the phosphonium salt originates in the methylidene ligand.[55]

Dr. Justin Lummiss of this research group found that this process is greatly accelerated in the presence of donor ligands, a pathway we have termed "donor-induced deactivation" (Scheme 1.3).[54-56] Subsequent work by Mr. William McClennan demonstrated very rapid extrusion of the phosphonium salts (within minutes at RT) in the presence of a wide range of donors.

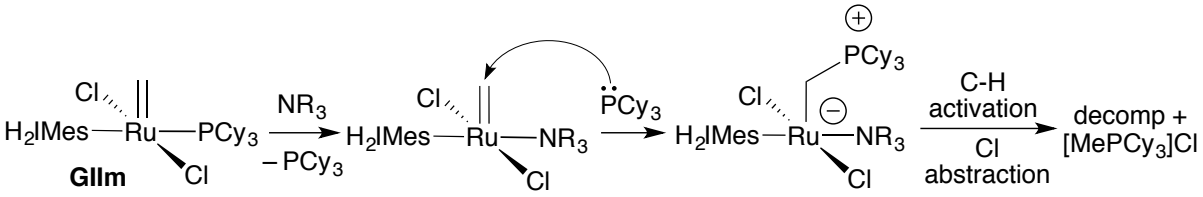

Scheme 1.3. Amine-induced deactivation of **GIIm**.

Forman and coworkers at Sasol reported that decomposition of **GIIm** under ethylene yields propylene and unidentified Ru products.[57] The mechanism was proposed to involve β-hydride elimination from the metallacyclobutane intermediate (**MCB**) to generate intermediate **C** (Scheme 1.4a). Ca. 40% decomposition of **GIIm** was observed after 16 h at 40 °C in C_6D_6. Notable is the greater rapidity of decomposition than evident from the half-lives subsequently reported in the absence of ethylene (Table 1.2).[58] Near-concurrent work from Dow described the negative impact of ethylene on the productivity (i.e. lifetime) of the Grubbs catalysts.[59]

Additional, four-carbon byproducts observed in minor amounts in the Sasol study were 2-butene, 1-butene, isobutene, and 1,3-butadiene. These species were proposed to arise by the participation of propene (the original β-hydride elimination product) in secondary metathesis reactions. Intriguingly, the imidazolium salt [H_2IMes]•HCl was not only observed, but was isolated in 13% yield. Formation of the phosphonium salt [$MePCy_3$]Cl was not reported.

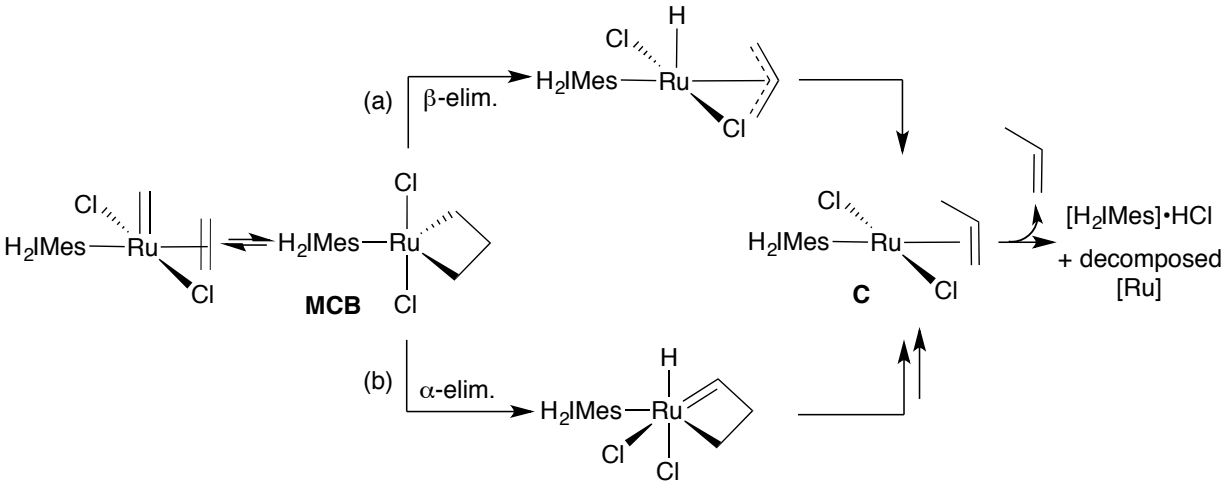

Scheme 1.4. Potential pathways for decomposition of **GIIm**. (a) β-hydride elimination, proposed by the Sasol group.[57] (b) Alternative mechanism for decomposition of **GIIm**, via α-elimination.

Table 1.2. Half-life data for decomposition of **GIIm** in the absence of substrate at various temperatures (assessed by ^{1}H NMR analysis in C_6D_6 vs. TMB used as internal standard).[58]

T (°C)	half-life (h)
40	63
60	4.1
80	0.4

The Forman mechanism of Scheme 1.4a was based on the observation of these organic byproducts. An accompanying DFT analysis supported the energetic feasibility of the β-elimination pathway, although this work preceded recognition of the fundamental importance of dispersion forces in quantitative evaluation of ligand binding energies.[60] Puddephatt's

studies of the decomposition of platinacyclobutanes point toward a potential alternative mechanism involving α-elimination (Scheme 1.4b).[61] While β-elimination pathways are normally presumed to be much lower in energy, labelling studies provided strong evidence for the α-elimination pathway in the platinacyclobutanes. The high energy of the classical β-elimination pathway may reflect the poor orbital overlap between the metal center and the β-C–H bond.

Hong and Grubbs subsequently reported formation of the C-H activated, edge-bridged dimer **D** from an analogue of **GII** in which PPh_3 replaces the PCy_3 ligand. Complex **D** was isolated in 70% yield on treating **GII-PPh$_3$** with ethylene (Scheme 1.5a).[62] Again, a methylphosphonium salt was observed: in this case, formation of $[MePPh_3]Cl$ was reportedly quantitative. A directly analogous species, uncovered in as-yet unpublished work by Dr. Justin Lummiss of this research group, crystallized during **GII**–promoted macrocyclization in the presence of added DBU (Scheme 1.5b). The bound styrene ligands originate in the benzylidene fragment of the **GII** precatalyst. This experiment formed part of a series of studies aimed at understanding the impact of base on decomposition pathways in metathesis,[54-56] a response to persistent reports[45] of amine-induced deactivation in metathesis. Of keen interest is the rapidity with which **D'** is formed in the presence of DBU, as well as the close correspondence to the structure of **D** itself. This tends to suggest that DBU is simply accelerating a decomposition pathway that is inherent to the active species formed during metathesis by **GIIm**.

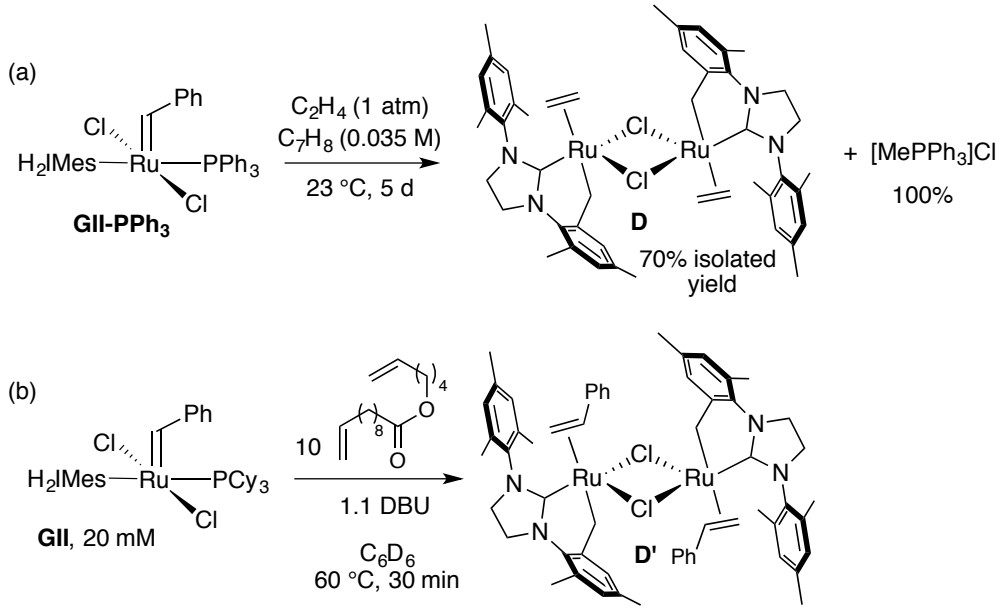

Scheme 1.5. (a) Decomposition of the methylidene species generated from **GII-PPh$_3$** by exposure to C_2H_4. (b) Decomposition of **GIIm** generated in situ during ring-closing macrocyclization (sealed-tube NMR experiment; trapped ethylene).

A related, face-bridged dimer (**E**, Scheme 1.6) was reported by Piers and coworkers following exposure of the second-generation Piers catalyst **PII** to 1,1-dichloroethylene. Complex **E** was formed in 40% yield in situ, although it was isolated in just 7% yield. The proposed pathway involves C-H activation of a mesityl *o*-methyl group, followed by dimerization.

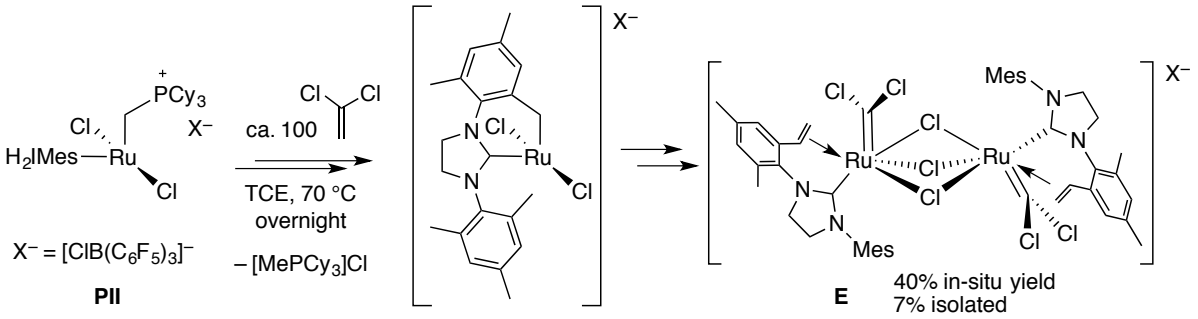

Scheme 1.6. Proposed decomposition pathway of **PII** to yield dimeric **E** by C-H activation and dimerization.[51] TCE = tetrachloroethane.

Additional decomposition pathways emerge from recent work by our research group. During the self-metathesis of styrene by **HII** in the presence of added amine, PhCH=CHCH$_2$R **F** was evolved (Scheme 1.7).[56] The presence of three added carbons in this byproduct pinpoints its origin in the metallacyclobutane ring. Deprotonation of the **MCB** ring by amine was postulated, affording an anionic Ru(σ-alkyl) complex related to those in the pathways outlined above. The strong basicity of this species is again proposed to trigger C-H activation to liberate **F**; the fate of the ruthenium fragment is unknown. While deprotonation of the metallacyclobutane ring could be favoured by the **MCB** C–C-agostic structure,[63] which should increase the acidity of these protons, initial deprotonation may alternatively occur at a mesityl methyl site, with subsequent attack on the **MCB** ring. The high pK_a characteristic of benzylic protons (ca. 41) may favour this pathway.

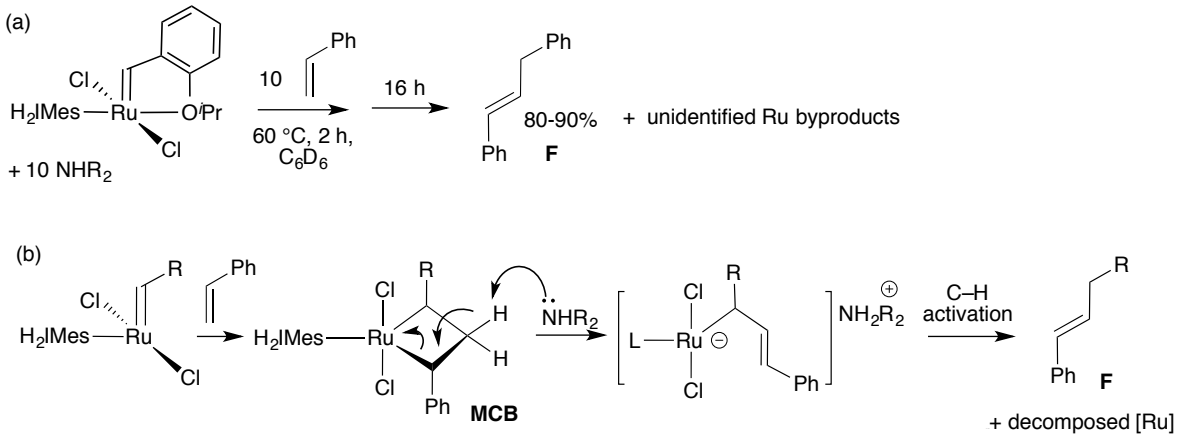

Scheme 1.7. (a) Decomposition of **HII** by added base during metathesis. (b) Proposed mechanism, involving deprotonation of the metallacyclobutane ring.

A related mechanism was proposed to account for the consistently feeble performance of **GII** (as compared to phosphine-free **HII**) in metathesis of electron-deficient olefins.[64] Thus, Michael addition of the dissociated PCy$_3$ ligand to methyl acrylate generates a highly

reactive carbanion (enolate), which deprotonates the MCB complex to liberate salt **G** (Scheme 1.8). Control reactions confirmed that **G** formed only when the metathesis catalyst or another proton source was present. Deprotonation of the **MCB** itself was postulated, but again, the relative pK_a values may favour attack on a benzylic C-H bond (i.e. a mesityl methyl group).

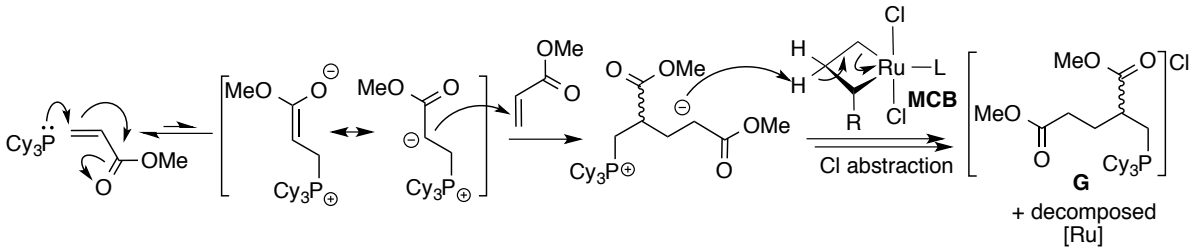

Scheme 1.8. Proposed pathway for decomposition of **GII** by deprotonation of **MCB** to give organic product **G**.

1.8. Scope of Thesis Work

It will be noted that the decomposition pathways summarized above fail to fully account for the mass balance in ruthenium. Minor ruthenium products have been noted to form under specific circumstances, but never do these account for all of the lost ruthenium. Ruthenium byproducts are widely presumed to be responsible for side reactions observed during olefin metathesis, of which double-bond isomerization is most common. This is the starting point for the work described in the following Chapters, which examine challenges and opportunities presented by isomerization in metathesis, and connects isomerization to previously overlooked catalyst decomposition pathways.

Chapter 2 considers the catalytic competence of the two complexes most commonly held to be responsible for competing isomerization during metathesis. Surprisingly, the actual isomerization activity of these species under conditions relevant to metathesis had not

previously been examined. Chapter 3 explores the potential formation of ruthenium nanoparticles by catalyst decomposition during metathesis, and involvement of these NPs in isomerization catalysis. Chapter 4 examines a potential means of circumventing "ligand-stripping" reactions that enable NP formation, by incorporation of a truncated NHC ligand into the Grubbs platform. Chapter 5 takes a different approach to isomerization, focusing on the opportunities rather than the problems associated with such pathways, when isomerization and metathesis are used in sequence for target-directed synthesis. Finally, Chapter 6 presents an overview of the major findings, and outlines opportunities emerging from this work.

References page 24

1.9. References

(1) Leading reviews of metathesis in natural products synthesis, including total synthesis: a) A. Fürstner, *Chem. Commun.* **2011**, *47*, 6505-6511; b) J. Cossy, S. Arseniyadis, C. Meyer, *Metathesis in Natural Product Synthesis: Strategies, Substrates and Catalysts* (Wiley-VCH, Weinheim, **2010**; c) W. H. C. Martin, S. Blechert, *Curr. Top. Med. Chem.* **2005**, *5*, 1521–1540; d) K. C. Nicolaou, P. G. Bulger, D. Sarlah, *Angew. Chem. Int. Ed.* **2005**, *44*, 4490–4527; *Angew. Chem.* **2005**, *117,* 4564–4601. For an overview of advances toward metathesis of directly-functionalized olefins, see: e) B. J. van Lierop, J. A. M. Lummiss, D. E. Fogg, in *Olefin Metathesis-Theory and Practice* (Ed.: K. Grela), Wiley, Hoboken, NJ, **2014**, pp. 85–152.

(2) Chikkali, S.; Mecking, S. *Angew. Chem., Int. Ed.* **2012**, *51*, 5802−5808.

(3) Biermann, U.; Bornscheuer, U.; Meier, M. A. R.; Metzger, J. O.; Schafer, H. J. *Angew. Chem. Int. Ed.* **2011**, *50*, 3854–3871.

(4) Anderson, A. W.; Merckling, N. G. Polymeric bicyclo[2.2.1]hept-2-ene. U.S. Patent No. 2721189, 1955.

(5) a) Schrock, R. R. *Angew. Chem.* **2006**, *118*, 3832–3844. b) Grubbs, R. H. *Angew. Chem., Int. Ed.* **2006**, *45*, 3760–3765. c) Chauvin, Y. *Angew. Chem., Int. Ed.* **2006**, *45*, 3741–3747.

(6) Grela, K., *Olefin Metathesis-Theory and Practice*. Wiley: Hoboken, NJ, 2014.

(7) Werrel, S. W.; L., J. C.; Donohoe, T. J. *Tet. Lett.* **2015**, *56*, 5261-5268.

(8) XiMo press release: "XiMo and Aspira Scientific Launch Air-Stable Metathesis Pills." October 13, 2015.

(9) Elevance press release: "Elevance Renewable Sciences, XiMo AG Announce Significant Advancements in Technology for Metathesizing Natural Oils". April 10, 2012.

(10) Versalis press release: "Versalis and Elevance Partner in Green Innovation for Premium Applications." February 6, 2014.

(11) Hérisson, J. L.; Chauvin, Y. *Makromol. Chem.* **1971**, *141*, 161–176.

(12) Sanford, M. S.; Love, J. A.; Grubbs, R. H. *J. Am. Chem. Soc.* **2001**, *123*, 6543–6554.

(13) Thiel, V.; Hendann, M.; Wannowius, K.-J.; Plenio, H. *J. Am. Chem. Soc.* **2012**, *134*, 1104–1114.

(14) Elevance Renewable Sciences, Inc., Form S-1 Registration Statement. Filed with the United States Securities and Exchange Commission, Sept. 20, 2011.

(15) Evonik Industries press release: "Elevance Renewable Sciences and Evonik Announce Metathesis Catalysts License Agreement." July 6, 2010.

(16) Cohen, S. A.; Anderson, D. R.; Wang, Z.; Champagne, T. M.; Ung, T. A. Methods for treating a metathesis feedstock with metal alkoxides / peroxide poisons. US20140275681A1, 2014.

(17) Lübbe, C.; Dumrath, A.; Neumann, H.; Schäffer, M.; Zimmermann, R.; Beller, M.; Kadyrov, R. *ChemCatChem* **2014**, *6*, 684–688.

(18) Nicola, T.; Brenner, M.; Donsbach, K.; Kreye, P. *Org. Process Res. Dev.* **2005**, *9*, 513–515.

(19) Wang, H.; Goodman, S. N.; Dai, Q.; Stockdale, G. W.; Clark, W. M. *Org. Process Res. Dev.* **2008**, *12*, 226–234.

(20) Farina, V.; Horváth, A., Ring-Closing Metathesis in the Large-Scale Synthesis of Pharmaceuticals. In *Handbook of Metathesis*, Grubbs, R. H.; Wenzel, A. G., Eds. Wiley-VCH: Weinheim, 2015; Vol. 2, pp 633–658.

(21) Kunz, L. A.; Pals, T. M.; Cohen, S. A.; Luetkens, M. L., Jr.; Balakrishnan, C.; Snyder, R. B. Diene-selective hydrogenation of metathesis derived olefins and unsaturated esters. U.S. Patent No. 20130217906A1, 2013.

(22) Cohen, S. A.; Luetkens, M. L.; Balakrishnan, C.; Snyder, R. Methods of refining and producing fuel from natural oil feedstocks. WO Patent No. 2011046872A2, 2011.

(23) Arumugasamy, J.; Arunachalam, K.; Bauer, D.; Becker, A.; Caillet, C. A.; Glynn, R.; Latham, G. M.; Lim, J.; Liu, J.; Mayes, B. A.; Moussa, A.; Rosinovsky, E.; Salanson, A. E.; Soret, A. F.; Stewart, A.; Wang, J.; Wu, X. *Org. Process Res. Dev.* **2013**, *17*, 811–828.

(24) Rosenquist, Å.; Samuelsson, B.; Johansson, P.-O.; Cummings, M. D.; Lenz, O.; Raboisson, P.; Simmen, K.; Vendeville, S.; de Kock, H.; Nilsson, M.; Horvath, A.; Kalmeijer, R.; de la Rosa, G.; Beumont-Mauviel, M. *J. Med. Chem.* **2014**, *57*, 1673−1693.

(25) Niu, D.; Liu, D.; Moore, J. D.; Xu, G.; Sun, Y.; Gai, Y.; Tang, D.; Or, Y. S.; Wang, Z. Preparation of quinoxalinyl macrocycles, especially quinoxalinyloxyproline-containing cyclic peptides, as hepatitis C virus (HCV) NS3-NS4A protease inhibitors for use in pharmaceutical compositions containing a cytochrome P450 monooxygenase inhibitor. U.S. Patent No. 20090005387A1, 2009.

(26) Kong, J.; Chen, C.-Y.; Balsells-Padros, J.; Cao, Y.; Dunn, R. F.; Dolman, S. J.; Janey, J.; Li, H.; Zacuto, M. J. *J. Org. Chem.* **2012**, *77*, 3820–3828.

(27) Li, H.; Scott, J. P.; Chen, C.-y.; Journet, M.; Belyk, K.; Balsells, J.; Kosjek, B.; Baxter, C. A.; Stewart, G. W.; Wise, C.; Alam, M.; Song, Z. J.; Tan, L. *Org. Lett.* **2015**, *17*, 1533–1536.

(28) Jiang, Y.; Andrews, S. W.; Condroski, K. R.; Buckman, B.; Serebryany, V.; Wenglowsky, S.; Kennedy, A. L.; Madduru, M. R.; Wang, B.; Lyon, M.; Doherty, G. A.;

Woodard, B. T.; Lemieux, C.; Geck Do, M.; Zhang, H.; Ballard, J.; Vigers, G.; Brandhuber, B. J.; Stengel, P.; Josey, J. A.; Beigelman, L.; Blatt, L.; Seiwert, S. D. *J. Med. Chem.* **2014**, *57*, 1753–1769.

(29) Puentener, K.; Scalone, M. New ruthenium complexes as catalysts for metathesis reactions. U.S. Patent No. 7939668B2, 2011.

(30) For an overview of these and other direct-acting antivirals and a prospective view of their ultimate clinical applications, see: E. De Clercq, *Biochem. Pharmacol.* **2014**, *89*, 441–452.

(31) Fandrick, K. R.; Savoie, J.; Jinhua, N. Y.; Song, J. J.; Senanayake, C. H., Challenges and Opportunities for Scaling The Ring-Closing Metathesis Reaction In The Pharmaceutical Industry. In *Olefin Metathesis – Theory and Practice*, Grela, K., Ed. Wiley: Hoboken, 2014; pp 349-366.

(32) Yee, N. K.; Farina, V.; Houpis, I. N.; Haddad, N.; Frutos, R. P.; Gallou, F.; Wang, X.-J.; Wei, X.; Simpson, R. D.; Feng, X.; Fuchs, V.; Xu, Y.; Tan, J.; Zhang, L.; Xu, J.; Smith-Keenan, L. L.; Vitous, J.; Ridges, M. D.; Spinelli, E. M.; Johnson, M.; Donsbach, K.; Nicola, T.; Brenner, M.; Winter, E.; Kreye, P.; Samstag, W. *J. Org. Chem.* **2006**, *71*, 7133–7145.

(33) Farina, V.; Shu, C.; Zeng, X.; Wei, X.; Han, Z.; Yee, N. K.; Senanayake, C. H. *Org. Process Res. Dev.* **2009**, *13*, 250–254.

(34) Wei, X.; Shu, C.; Haddad, N.; Zeng, X.; Patel, N. D.; Tan, Z.; Liu, J.; Lee, H.; Shen, S.; Campbell, S.; Varsolona, R. J.; Busacca, C. A.; Hossain, A.; Yee, N. K.; Senanayake, C. H. *Org. Lett.* **2013**, *15*, 1016–1019.

(35) For an overview of relevant patents, current through early 2014, see: World Health Organization working paper, "Patent Situation of Key Products for Treatment of Hepatitis

C." Prepared for the WHO by Thomson Reuters, Aug. 2014. (a) Simeprevir: http://www.who.int/phi/implementation/ip_trade/simeprevir_report_2014_09-02.pdf?ua=1. (b) ABT-450: http://www.who.int/phi/implementation/ip_trade/ABT-450_report_2014-09-02.pdf?ua=1.

(36) Horvath, A.; Wuyts, S.; Depré, D. P. M.; Couck, W. L. J.; Cuypers, J. L. J.; Harutyunyan, S.; Binot, G. F. S. Improved process for preparing an intermediate of the macrocyclic protease inhibitor TMC 435. U.S. Patent No. 2015/0152098 A1, 2015.

(37) Enanta Pharmaceutical. Annual Report. Filed with the United States Security and Exchange Commission, **2014**.

(38) Ku, Y.; McDaniel, K. F.; Chen, H.-J.; Shanley, J. P.; Kempf, D. J.; Grampovnik, D. J.; Sun, Y.; Liu, D.; Gai, Y.; Or, Y. S.; Wagaw, S. H.; Engstrom, K.; Grieme, T.; Sheikh, A.; Mei, J. Preparation of heterocyclic macrocyclic peptides as hepatitis C serine protease inhibitors. WO Patent No. 2010030359A2, 2010.

(39) Dinger, M. B.; Mol, J. C. *Eur. J. Inorg. Chem.* **2003**, 2827–2833.

(40) Kim, M.; Eum, M. S.; Jin, M. Y.; Jun, K. W.; Lee, C. W.; Kuen, K. A.; Kim, C. H.; Chin, C. S. *J. Organomet. Chem.* **2004**, *689*, 3535–3540.

(41) Beach, N. J.; Camm, K. D.; Fogg, D. E. *Organometallics* **2010**, *29*, 5450–5455.

(42) Dinger, M. B.; Mol, J. C. *Organometallics* **2003**, *22*, 1089–1095.

(43) Trnka, T. M.; Morgan, J. P.; Sanford, M. S.; Wilhelm, T. E.; Scholl, M.; Choi, T.-L.; Ding, S.; Day, M. W.; Grubbs, R. H. *J. Am. Chem. Soc.* **2003**, *125*, 2546–2558.

(44) Huang, J.; Stevens, E. D.; Nolan, S. P.; Petersen, J. L. *J. Am. Chem. Soc.* **1999**, *121*, 2674–2678.

(45) van Lierop, B. J.; Lummiss, J. A. M.; Fogg, D. E., Ring-Closing Metathesis. In *Olefin Metathesis-Theory and Practice*, Grela, K., Ed. Wiley: Hoboken, NJ, 2014; pp 85–152.

(46) Schrodi, Y., Mechanisms of Olefin Metathesis Catalyst Decomposition and Methods of Catalyst Reactivation. In *Handbook of Metathesis*, Grubbs, R. H.; Wenzel, A. G., Eds. Wiley-VCH: Weinheim, 2015; pp 323–342.

(47) Hong, S. H.; Day, M. W.; Grubbs, R. H. *J. Am. Chem. Soc.* **2004**, *126*, 7414–7415.

(48) Werner, H.; Stuer, W.; Weberndorfer, B.; Wolf, J. *Eur. J. Inorg. Chem.* **1999**, 1707–1713.

(49) Hansen, S. M.; Rominger, F.; Metz, M.; Hofmann, P. *Chem. Eur. J.* **1999**, *5*, 557–566.

(50) Galan, B. R.; Pitak, M.; Keister, J. B.; Diver, S. T. *Organometallics* **2008**, *27*, 3630–3632.

(51) Leitao, E. M.; Dubberley, S. R.; Piers, W. E.; Wu, Q.; McDonald, R. *Chem. Eur. J.* **2008**, *14*, 11565–11572.

(52) Leitao, E. M.; Piers, W. E.; Parvez, M. *Can. J. Chem.* **2013**, *91*, 935–942.

(53) Lummiss, J. A. M.; McClennan, W. L.; McDonald, R.; Fogg, D. E. *Organometallics* **2014**, *33*, 6738–6741.

(54) Lummiss, J. A. M.; Ireland, B. J.; Sommers, J. M.; Fogg, D. E. *ChemCatChem* **2014**, *6*, 459–463.

(55) Lummiss, J. A. M.; Botti, A. G. G.; Fogg, D. E. *Catal. Sci. Technol.* **2014**, *4*, 4210–4218.

(56) Ireland, B. J.; Dobigny, B. T.; Fogg, D. E. *ACS Catal.* **2015**, *5*, 4690−4698.

(57) van Rensburg, W. J.; Steynberg, P. J.; Meyer, W. H.; Kirk, M. M.; Forman, G. S. *J. Am. Chem. Soc.* **2004**, *126*, 14332–14333.

(58) Lummiss, J. A. M.; Higman, C. S.; Fyson, D. L.; McDonald, R.; Fogg, D. E. *Chem. Sci.* **2015**, *6*, 6739–6746.

(59) For studies demonstrating the detrimental effect of ethylene on the rates and yields of Ru-catalyzed cross-metathesis and ring-closing metathesis of olefins, see: (a) Burdett, K. A.; Harris, L. D.; Margl, P.; Maughon, B. R.; Mokhtar-Zadeh, T.; Saucier, P. C.; Wasserman, E. P. *Organometallics* **2004**, *23*, 2027–2047; (b) Lysenko, Z.; Maughon, B. R.; Mokhtar-Zadeh, T.; Tulchinsky, M. L. *J. Organomet. Chem.* **2006**, *691*, 5197–5203; (c) Lysenko, Z.; Maughon, B. R.; Mokhtar-Zadeh, T.; Tulchinsky, M. L. *J. Organomet. Chem.* **2006**, *691*, 5197–5203. In contrast, initiation rates for the Piers phosphonium alkylidene catalysts are dramatically increased by addition of a catalytic amount of ethylene. See: (d) Leitao, E. M.; van der Eide, E. F.; Romero, P. E.; Piers, W. E.; McDonald, R. *J. Am. Chem. Soc.* **2010**, *132*, 2784–2794.

(60) Nelson, D. J.; Percy, J. M. *Adv. Phys. Org. Chem.* **2014**, *48*, 81–188.

(61) Al-Essa, R. J.; Ling, S. S. M.; Puddephatt, R. J. *Organometallics* **1987**, *6*, 951–959.

(62) Hong, S. H.; Wenzel, A. G.; Salguero, T. T.; Day, M. W.; Grubbs, R. H. *J. Am. Chem. Soc.* **2007**, *129*, 7961–7968.

(63) Etienne, M.; Weller, A. S. *Chem. Soc. Rev.* **2014**, *43*, 242--259.

(64) Bailey, G. A.; Fogg, D. E. *J. Am. Chem. Soc.* **2015**, *137*, 7318–7321.

Chapter 2. Isomerization During Olefin Metathesis

2.1. Context and Objectives

Ruthenium metathesis catalysts promote a wide range of non-metathetical pathways.[1] Among these, olefin isomerization is particularly common.[2,3] Such reactions can be beneficial, where metathesis and isomerization manifolds are deliberately coupled via tandem catalysis.[4] More commonly, however, isomerization is an unintended side-reaction (widely believed, albeit with little direct evidence, to stem from catalyst decomposition), that represents a long-standing challenge in olefin metathesis.

Adventitious isomerization can precede or follow metathesis, and thus affects the integrity of both the reagents and the reaction products. While the problem of undesired isomerization is particularly acute for substrates bearing allylic substituents, as noted below, it is in fact much more general.[5-8] A useful discussion by Wagener and co-workers highlighted the possibility of ring expansion *or* contraction during RCM, arising from isomerization along the carbon backbone of metathesis oligomers.[5,9,10] A particularly high-profile instance of ring-contraction comes from the Merck synthesis of Vaniprevir (see Scheme 1.1).[11]

Instances of isomerization have been reported for the Schrock molybdenum catalysts[5,12-15] and for the first-generation Grubbs catalyst **GI**.[14,16-18] However, comparative studies indicate that isomerization becomes successively more problematic in the order **Mo-1** < **GI** < **GII**.[5,10,14,19] The challenge of competing isomerization associated with Ru-NHC catalysts[5,8,10,17,19,20] takes on heightened importance as such ruthenium metathesis catalysts enter industrial use. The species responsible have been the subject of much debate. At the

outset of this thesis work, molecular Ru hydrides were widely regarded as responsible for competing isomerization, but the assumption was untested. The work in this Chapter examines the validity of this proposition: specifically, whether the leading candidates are sufficiently active to account for the levels of isomerization observed during metathesis. Given the limited information in the literature about the relative isomerization activity of different catalysts, an important additional question lies in the relative activity of common ruthenium hydride complexes. A spectrum of isomerization activity was established, which is further developed in Chapter 5.

References page 44

2.1.1. Published Contributions

Isomerization During Olefin Metathesis: An Assessment of Potential Catalyst Culprits. Carolyn S. Higman, Lucie Plais, and Deryn E. Fogg *ChemCatChem* **2013**, 12, 3548–3551.

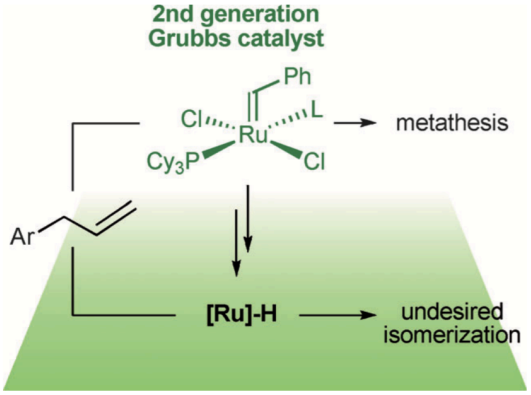

Two ruthenium hydride complexes commonly proposed as agents of unintended isomerization during olefin metathesis are examined for their activity in isomerization of estragole, a representative allylbenzene. Neither proves kinetically competent to account for the levels of isomerization observed during cross-metathesis of estragole by the second-generation Grubbs catalyst. A structure–activity analysis of selected ruthenium hydride complexes indicates that higher isomerization activity correlates with a more electrophilic metal center.

Author Contributions: The manuscript was written by CSH and DEF. CSH performed all experiments presented. LP performed initial experiments, under the supervision of CSH.

References page 44

2.2. Isomerization During Olefin Metathesis: An Assessment of Potential Catalyst Culprits.

2.2.1. Introduction

Double-bond isomerization is a common side-reaction in olefin metathesis, even for simple aliphatic olefins.[5,8,21,22] Isomerization is particularly problematic for substrates containing allylic amine, ether, or aromatic groups.[6,23-27] Comparative studies indicate that the problem is most acute for the second-generation Grubbs catalyst **GII**, as compared to the first-generation catalyst.[28] Isomerization-active species have been proposed to originate in contaminants introduced during catalyst synthesis[29,30] or use,[31] or in intrinsic catalyst deactivation pathways.[32,33] Most commonly cited in recent reports is the potential involvement of two hydride complexes (**Ru-H4** and **Ru-H6**), accessible by decomposition of **GII** (Chart 2.1).[34] Dinuclear **Ru-H6** was shown by Hong and Grubbs to form on thermolysis of the resting-state methylidene complex (albeit slowly),[33] while several reports describe routes to hydridocarbonyl complexes of type **Ru-H4** from **GII**.[3,35,36] Of particular interest, Percy and co-workers observed **Ru-H4** during RCM of 1,7-octadiene by **GII**,[37] and the Grubbs and Mol groups found that closely related carbonyl complexes form on exposure of the Grubbs catalysts to oxygen, albeit with low yields (ca. 10%)..[34] The latter findings raise the possibility that incomplete air-exclusion may contribute to isomerization.

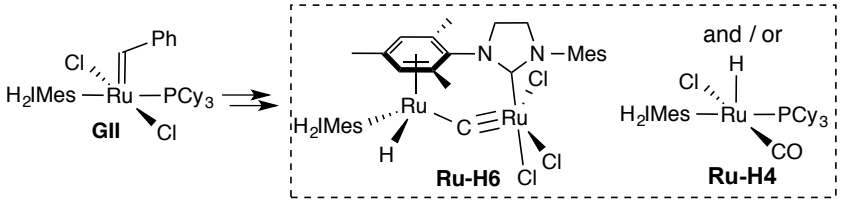

Chart 2.1. Complexes proposed to account for undesired isomerization during metathesis via **GII**.

Although both **Ru-H6**[33] and **Ru-H4**[38,39] have been shown to be isomerization-active, it is unclear whether they are kinetically competent to account for the levels of isomerization observed during metathesis reactions. Here we examine this point by explicitly comparing their isomerization activity with rates of isomerization seen during self-metathesis of the same substrate, under identical conditions. As a further goal, we sought to establish clear-cut structure-activity correlations for a series of selected Ru hydride complexes, which could ultimately aid in identification of plausible culprits.

For both purposes, we chose to study estragole **1a** as a representative, functionalized allylbenzene of keen interest as a renewable platform chemical.[40] Parallel recent work has pointed out the high value of products accessible from **1a** and isomeric phenylpropenoids via metathesis.[41-43] As noted above, allylbenzene substrates readily undergo isomerization to bring the double bond into conjugation with the phenyl ring, to the extent that they have been used as test substrates to assess potential isomerization inhibitors.[26] In a representative recent study, Bruneau and co-workers reported just 34% cross-metathesis (CM) on treating 2-methoxy-4-allyl-phenol (eugenol, **1b**) with methyl acrylate (**MA**) using **GII**.[24] Isomerized species, including secondary metathesis products, comprised the balance.

2.2.2. Results and Discussion

Consistent with the Bruneau report, we observed only minor amounts of self-metathesis (SM) on treating estragole **1a** with **GII** at 40 ˚C in toluene (1 mol% **GII**, 0.2 M **1a**; Figure 2.1). The yield of **7a** reached a maximum of 41%, then diminished, owing to competing isomerization and/or metathesis.[44] Additional products arise from isomerization of **1a** into

anethole **2a**, as well as isomerization-CM (see **9a**), SM-isomerization (see **8a**), and isomerization-SM (see **6a**), among other, less obvious pathways.[†]

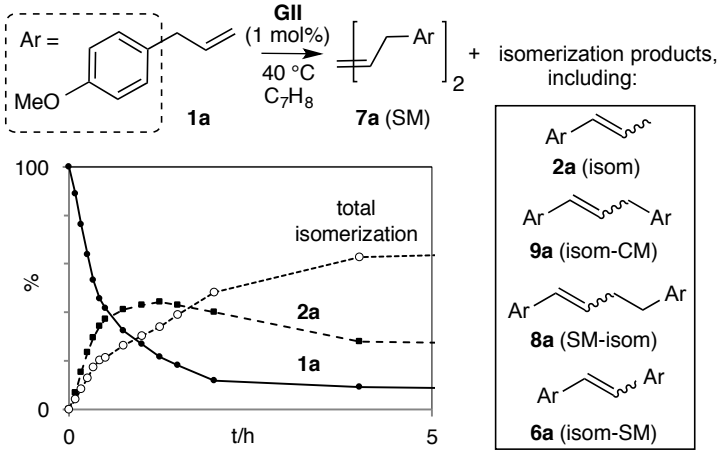

Figure 2.1. Rates of self-metathesis (SM), vs. isomerization, on treating **1a** with **GII** (0.2 M **1a**, 1 mol% **GII**); ±3% in replicate runs.

Having established a baseline for isomerization during metathesis, we turned to the question of whether **Ru-H6** and/or **Ru-H4** are sufficiently reactive to account for the levels of isomerization observed. These experiments were carried out under identical conditions of olefin concentration, temperature, and solvent, using the maximum proportion of hydride complex attainable assuming 100% transformation of the **GII** charge in Figure 2.1 (thus 0.5 mol% for the dimer **Ru-H6**, and 1 mol% for **Ru-H4**). Although clearly much higher than the proportion of any hydride species observed during metathesis, these loadings represented an inarguable upper limit. Nonetheless, both catalysts exhibited marginal isomerization activity (Figure 2.2). For **Ru-H6,** isomerization reached 6% by 5 h, and only 14% even after 24 h.[‡]

[†] For a useful representation of the isomerization products accessible, see Ref. 44a.

[‡] For the **Ru-H6** catalyzed reaction after 24 h, a 5% discrepancy emerged between conversions of **1a** (19%) and yield of **2a** (14%). Of the four additional products observed,

The low activity of **Ru-H6**, compounded by its slow formation (reported as ca. 50% after 3 d at 55 °C in the absence of substrate),[33] is strong evidence against its culpability in the levels of isomerization seen in Figure 2.1. Similarly feeble activity (maximum 8% isomerization) was seen for **Ru-H4**, despite the higher catalyst loading.

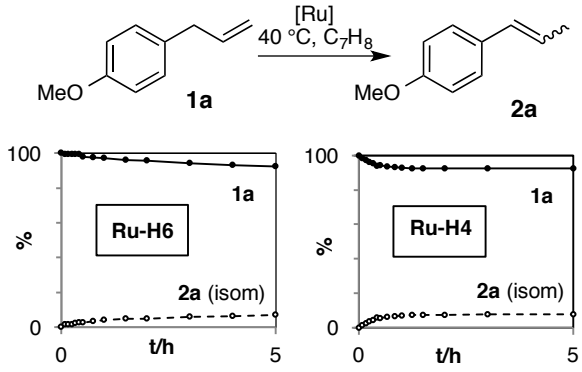

Figure 2.2. Isomerization of estragole **1a** to anethole **2a** by **Ru-H6** or **Ru-H4** (1 mol% Ru; 0.2 M **1a**); ±3% in replicate runs.

Having established the implausibility of these catalysts as candidates, we sought to clarify the nature of the ligands associated with higher isomerization activity. To this end, we screened a set of structurally related hydridochloro complexes in estragole isomerization. While reviews by the Schmidt and Krompiec groups examine the impact of substrate functional groups on isomerization activity,[3,45] systematic comparisons of ligand effects are more limited. As noted above, however, multiple studies suggest that second-generation (i.e. Ru-NHC) metathesis catalysts trigger more extensive isomerization side-reactions than their first-generation analogues.[28]

---

one minor constituent (2%) was identified as CM product **7a**, suggesting that **Ru-H6** is not completely metathesis-inactive, or that an alkylidene can be regenerated from the bridging carbido ligand.

To examine this point using well-defined catalysts, we compared the isomerization activity of PCy_3 complex **Ru-H3** with that of the NHC derivatives **Ru-H4** and **Ru-H5**. Also examined were two complexes of PPh_3 (**Ru-H2**, **Ru-H1**; Figure 2.3). We chose this labile ligand as a proxy for unknown weak donors potentially present during metathesis (for example, an unsaturated olefin or aryl site within the substrate itself). More fundamentally, it permits us to probe the correlation between isomerization activity and ligand donicity.

Given the low activity seen for **Ru-H4** at 40 °C (Figure 2.2), we evaluated the activity of these five complexes at 80 °C. Consistent with the prior reports,[28] levels of isomerization were considerably higher for H_2IMes complex **Ru-H4** than its PCy_3 analogue **Ru-H3** or, notably, IMes analogue **Ru-H5**. Dramatically higher activity, however, was seen for the PPh_3 derivatives **Ru-H2** and **Ru-H1**, suggesting that ligands of weaker donor ability favour isomerization. Decomposed ruthenium species from which the strong NHC and/or PCy_3 donors have been scavenged may thus be responsible for the high levels of isomerization activity seen in Figure 2.1 (see also Chapter 3).

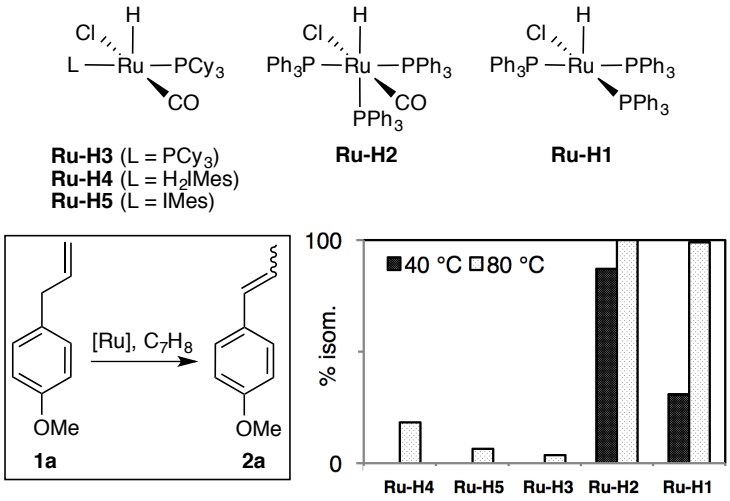

Figure 2.3. Isomerization of **1a** by various Ru hydrides (1 mol% Ru; 0.2 M **1a**, yield of anethole **2a** at 0.5 h; ±3% in replicate runs.

The correlations above have important mechanistic implications. While the higher activity of **Ru-H2**, vs. **Ru-H3**, could reflect the greater lability of PPh_3 than PCy_3, comparison of **Ru-H2** and **Ru-H1** tells a different story. In experiments carried out at 40 ˚C to maximize discrimination, the carbonyl complex **Ru-H2** is seen to be nearly three times more active, despite the fact that the π-acid ligand attenuates PPh_3 lability, vs. **Ru-H1**. Higher activity thus appears to be associated with a more electron-deficient Ru center (a factor that could contribute to the impressive activity of a cationic Ru complex reported by Grotjahn and co-workers).[43,46] This in turn suggests that olefin binding occurs in or before the rate-determining step. While early work on dihydride catalysts related to **Ru-H2** likewise suggested an associative pathway,[47] isomerization via catalysts of type **Ru-H4** has been presumed to proceed via a dissociative mechanism.[37]

To clarify this point, we evaluated rates of isomerization at a range of estragole concentrations (20 mM, 0.20 M, 1.0 M), using **Ru-H3** as catalyst. An approximately first-

order dependence on olefin concentration was observed, with the onset of saturation kinetics near 1 M. This indicates a mechanism that is associative in olefin, despite the bulk associated with the bulky PCy_3 and H_2IMes groups already present on the catalyst. Added PCy_3 inhibits reaction, however, consistent with a subsequent step involving rate-determining loss of PCy_3 (as also demonstrated in prior studies).[37,47]

2.2.3. Conclusions

Two lead candidates have been favoured in the recent literature as probable triggers for unintended double-bond isomerization during olefin metathesis. The foregoing provides strong evidence against their involvement. Indeed, the correlation between *weaker* donor ligands and higher isomerization activity tends to suggest that the isomerization-active species may arise from more extensive decomposition of the metathesis catalyst, in which the PCy_3 and/or NHC ligands have been scavenged. One intriguing possibility is that the observable hydride species are essentially bystanders, the true culprits instead being species that operate via a π-allyl mechanism. Finally, an associative pathway was uncovered in the mechanism for isomerization, even where rather bulky ligands are present on the metal. This corroborates earlier work showing similar behaviour for Ru-PPh_3 complexes. If this pathway is general, isomerization may be most problematic for metathesis reactions carried out at high olefin concentrations, including neat olefin.

References page 44

2.2.4. Experimental Details for Section 2.2

2.2.4.1 General Procedures

Reactions were carried out under inert atmosphere using standard Schlenk and glove-box techniques. Toluene was dried using an Anhydrous Engineering solvent purification system and stored over Linde 4 Å molecular sieves under N_2. Estragole (Sigma-Aldrich, 98%) was degassed by consecutive freeze/pump/thaw cycles and filtered through neutral alumina under N_2. Decane (Sigma-Aldrich, anhydrous, 99%) and potassium trispyrazolylborate (KTp; TCI Chemicals, 97%) were used as received. Complexes **GII**,[48] **Ru-H6**,[33] **Ru-H4**,[49] **Ru-H5**,[49] **Ru-H2**,[50] and **Ru-H1**[51] were prepared by literature methods: see below for an improved procedure for **Ru-H3**. Yields in catalytic runs were measured on an Agilent 7890A Series GC equipped with a flame ionization detector (FID) and Agilent HP-5 polysiloxane column, at an inlet split ratio of 10:1, and inlet temperature of 250 ˚C. Retention times for estragole **1a**, anethole **2a**, and homo-coupled estragole **7a** were confirmed by comparison with authentic samples. Yields were determined from integrated peak areas vs. decane, corrected for the response factors for decane and analyte. Calibration curves (peak areas vs. concentration) were constructed in the relevant concentration regime to account for the dependence on detector response for all analytes.

2.2.4.2 Representative Procedure for Cross Metathesis.

A Schlenk tube was loaded with estragole (270 mg, 1.8 mmol), decane (259 mg, 1.8 mmol; internal standard) and toluene (9.4 mL). An aliquot was removed and assessed by GC-FID to establish the starting ratio of **1a**:decane. Catalyst **GII** (15.5 mg, 0.018 mmol, 1 mol%) was then added. The Schlenk tube was immediately removed from the glovebox, attached to the

Schlenk line. The cap was replaced with a septum for sampling using a syringe. The Schlenk tube was then submerged in a thermostatted oil bath at 40 ˚C. Aliquots were taken at specific time intervals, quenched with KTp (solution in THF, 10 mg/1mL, 10 equiv),[52] diluted with CH_2Cl_2 and analysed by GC-FID.

2.2.4.3 Representative Procedure for Isomerization.

A Schlenk tube was charged with **1a,** decane, and toluene as above, after which an aliquot was removed to establish initial GC-FID integrations. Catalyst **Ru-H4** was then added (14.1 mg, 0.018 mmol, 1 mol%), and the reaction was heated at 80 ˚C. Aliquots removed at specific time intervals were quenched by exposure to air, diluted with CH_2Cl_2, and analysed by GC-FID.

2.2.4.4 Improved Synthesis of Ru-H3

In an earlier report, Beach and Fogg described the synthesis of **Ru-H3** by reaction of $RuHCl(CO)(PPh_3)_3$ **Ru-H2** (as a 2.6 mM solution in benzene) with 3 equiv PCy_3.[49] Problems were encountered, however, in repeating this procedure in the present work: i.e., treating a solution of **Ru-H2** (0.500 g, 0.525 mmol) in 200 mL benzene with solid PCy_3 (0.450 g, 1.61 mmol). Reaction was incomplete after the reported time interval (3 h at 40 °C), owing to the low solubility of **Ru-H2** in benzene. Indeed, unreacted **Ru-H2** remained even on use of 4 equiv PCy_3 and 5 h reaction time. Diluting the reaction by twofold (using 800-1000 mL benzene per gram of **Ru-H2**) was found to be essential to obtain a homogeneous solution. The solution was stirred for 3 h at 40 °C, at which point an aliquot removed for ^{31}P NMR analysis confirmed complete conversion of **Ru-H2** into the desired **Ru-H3**. The solvent was removed under vacuum, and diethyl ether (15 mL) was added to extract free PPh_3. The

reaction mixture was cooled to –35 °C to precipitate the bright yellow product, which was filtered off and washed with ethanol (2 × 5 mL) and diethyl ether (2 × 5 mL), and dried under vacuum. NMR data agree with values previously reported. $^{31}P\{^{1}H\}$ NMR (C_6D_6): δ 46.9 (s); ^{1}H NMR (C_6D_6): δ 2.72–1.15 (m, 66H, Cy), –24.21 (t, 1H, $^{2}J_{H\text{-}P}$ = 18.0 Hz).

2.3. References

(1) Alcaide, B.; Almendros, P.; Luna, A. *Chem. Rev.* **2009**, *109*, 3817–3858.

(2) van Lierop, B. J.; Lummiss, J. A. M.; Fogg, D. E., Ring-Closing Metathesis. In *Olefin Metathesis-Theory and Practice*, Grela, K., Ed. Wiley: Hoboken, NJ, 2014; pp 85–152.

(3) Schmidt, B. *Eur. J. Org. Chem.* **2004**, 1865–1880.

(4) Nam, Y. H.; Snapper, M. L., Ruthenium-Catalyzed Tandem Metathesis/Non-Metathesis Processes. In *Handbook of Metathesis*, Grubbs, R. H.; Wenzel, A. G., Eds. Wiley-VCH: Weinheim, 2015; pp 311–380.

(5) Lehman, S. E.; Schwendeman, J. E.; O'Donnell, P. M.; Wagener, K. B. *Inorg. Chim. Acta* **2003**, *345*, 190–198.

(6) Kuźnik, N.; Krompiec, S. *Coord. Chem. Rev.* **2007**, *251*, 222–233.

(7) Krompiec, S.; Krompiec, M.; Penczek, R.; Ignasiak, H. *Coord. Chem. Rev.* **2008**, *252*, 1819–1841.

(8) Bourgeois, D.; Pancrazi, A.; Nolan, S. P.; Prunet, J. *J. Organomet. Chem.* **2002**, *643-644*, 247–252.

(9) Petkovska, V. I.; Hopkins, T. E.; Powell, D. H.; Wagener, K. B. *Macromolecules* **2005**, *38*, 5878–5885.

(10) Courchay, F. C.; Sworen, J. C.; Wagener, K. B. *Macromolecules* **2003**, *36*, 8231–8239.

(11) Kong, J.; Chen, C.-Y.; Balsells-Padros, J.; Cao, Y.; Dunn, R. F.; Dolman, S. J.; Janey, J.; Li, H.; Zacuto, M. J. *J. Org. Chem.* **2012**, *77*, 3820–3828.

(12) Clark, J. S.; Kettle, J. G. *Tetrahedron* **1999**, *55*, 8231–8248.

(13) Joe, D.; Overman, L. E. *Tetrahedron Lett.* **1997**, *38*, 8635–8638.

(14) Chuchuryukin, A. V.; Chase, P. A.; Dijkstra, H. P.; Suijkerbuijk, B.; Mills, A. M.; Spek, A. L.; van Klink, G. P. M.; van Koten, G. *Adv. Synth. Catal.* **2005**, *347*, 447–462.

(15) Ahuja, R.; Kundu, S.; Goldman, A. S.; Brookhart, M.; Vicente, B. C.; Scott, S. L. *Chem. Commun.* **2008**, 253–255.

(16) Hoye, T. R.; Promo, M. A. *Tetrahedron Lett.* **1999**, *40*, 1429–1432.

(17) van Gerven, P. C. M.; Elemans, J. A. A. W.; Gerritsen, J. W.; Speller, S.; Nolte, R. J. M.; Rowan, A. E. *Chem. Commun.* **2005**, 3535–3537.

(18) Edwards, S. D.; Lewis, T.; Taylor, R. J. K. *Tetrahedron Lett.* **1999**, *40*, 4267–4270.

(19) Kamau, S. D.; Hodge, P.; Hall, A. J.; Dad, S.; Ben-Haida, A. *Polymer* **2007**, *48*, 6808–6822.

(20) Fürstner, A.; Thiel, O. R.; Ackermann, L.; Schanz, H.-J.; Nolan, S. P. *J. Org. Chem.* **2000**, *65*, 2204–2207.

(21) Ivin, K. J.; Mol, J. C., *Olefin Metathesis and Metathesis Polymerization*. Academic Press: New York, 1997.

(22) Courchay, F. C.; Sworen, J. C.; Ghiviriga, I.; Abboud, K. A.; Wagener, K. B. *Organometallics* **2006**, *25*, 6074–6086.

(23) Krompiec, S.; Krompiec, M.; Penczek, R.; Ignasiak, H. *Coord. Chem. Rev.* **2008**, *252*, 1819–1841.

(24) Bilel, H.; Hamdi, N.; Zagrouba, F.; Fischmeister, C.; Bruneau, C. *RSC Adv.* **2012**, *2*, 9584–9589.

(25) Moïse, J.; Arseniyadis, S.; Cossy, J. *Org. Lett.* **2007**, *9*, 1695–1698.

(26) Hong, S. H.; Sanders, D. P.; Lee, C. W.; Grubbs, R. H. *J. Am. Chem. Soc.* **2005**, *127*, 17160–17161.

(27) Endo, K.; Herbert, M. B.; Grubbs, R. H. *Organometallics* **2013**, *32*, 5128-5135.

(28) Selected examples: (a) A. Fürstner, O. R. Thiel, L. Ackermann, H.-J. Schanz, S. P. Nolan, *J. Org. Chem.* **2000**, *65*, 2204–2207. (b) F. C. Courchay, J. C. Sworen, K. B. Wagener, *Macromolecules* **2003**, *36*, 8231–8239. (c) S. D. Kamau, P. Hodge, A. J. Hall, S. Dad, A. Ben-Haida, *Polymer* **2007**, *48*, 6808–6822. (d) P. C. M. van Gerven, J. A. A. W. Elemans, J. W. Gerritsen, S. Speller, R. J. M. Nolte, A. E. Rowan, *Chem. Commun.* **2005**, 3535–3537. (e) A. V. Chuchuryukin, P. A. Chase, H. P. Dijkstra, B. Suijkerbuijk, A. M. Mills, A. L. Spek, G. P. M. van Klink, G. van Koten, *Adv. Synth. Catal.* **2005**, *347*, 447–462. (f) T. R. Hoye, M. A. Promo, *Tetrahedron Lett.* **1999**, *40*, 1429–1432. (g) R. Ahuja, S. Kundu, A. S. Goldman, M. Brookhart, B. C. Vicente, S. L. Scott, *Chem. Commun.* **2008**, 253–255. (h) S. D. Edwards, T. Lewis, R. J. K. Taylor, *Tetrahedron Lett.* **1999**, *40*, 4267–4270.

(29) Sutton, A. E.; Seigal, B. A.; Finnegan, D. F.; Snapper, M. L. *J. Am. Chem. Soc.* **2002**, *124*, 13390–13391.

(30) Hekking, K. F. W.; van Delft, F. L.; Rutjes, F. *Tetrahedron* **2003**, *59*, 6751–6758.

(31) Nicola, T.; Brenner, M.; Donsbach, K.; Kreye, P. *Org. Process Res. Dev.* **2005**, *9*, 513–515.

(32) van Rensburg, W. J.; Steynberg, P. J.; Meyer, W. H.; Kirk, M. M.; Forman, G. S. *J. Am. Chem. Soc.* **2004**, *126*, 14332–14333.

(33) a) S. H. Hong, M. W. Day, R. H. Grubbs, *J. Am. Chem. Soc.* **2004**, *126*, 7414–7415; b) S. H. Hong, D. P. Sanders, C. W. Lee, R. H. Grubbs, *J. Am. Chem. Soc.* **2005**, *129*, 7961–7968.

(34) Hong and Grubbs reported 76% conversion of allylbenzene following treatment with 1.5 mol% **Ru-H6** for 24 h in refluxing CD_2Cl_2. See Ref. 16. For reports invoking the involvement of **Ru-H6** in isomerization, see: a) S. Shahane, L. Toupet, C. Fischmeister, C. Bruneau, *Eur. J. Inorg. Chem.* **2013**, 54-60; b) G. B. Djigoué, M. A. R. Meier, *Applied Catal. A* **2009**, *368*, 158-162; c) R. Hemelaere, F. Carreaux, B. Carboni, *J. Org. Chem.* **2013**, *78*, 6786-6792. For isomerization reactions invoking **Ru-H4** see: Ref. 8; d) S. Hanessian, S. Giroux, A. Larsson, *Org. Lett.* **2006**, *8*, 5481-5484; e) B. Schmidt, *J. Org. Chem.* **2004**, *69*, 7672–7687; f) M. B. Dinger, J. C. Mol, *Organometallics* **2003**, *22*, 1089–1095; g) D. Banti, J. C. Mol, *J. Organomet. Chem.* **2004**, *689*, 3113–3116; h) T. M. Trnka, J. P. Morgan, M. S. Sanford, T. E. Wilhelm, M. Scholl, T.-L. Choi, S. Ding, M. W. Day, R. H. Grubbs, *J. Am. Chem. Soc.* **2003**, *125*, 2546–2558.

(35) Beach, N. J.; Lummiss, J. A. M.; Bates, J. M.; Fogg, D. E. *Organometallics* **2012**, *31*, 2349–2356.

(36) Dinger, M. B.; Mol, J. C. *Eur. J. Inorg. Chem.* **2003**, 2827–2833.

(37) Ashworth, I. W.; Hillier, I. H.; Nelson, D. J.; Percy, J. M.; Vincent, M. A. *Eur. J. Org. Chem.* **2012**, 5673-5677.

(38) Arisawa, M.; Terada, Y.; Takahashi, K.; Nakagawa, M.; Nishida, A. *J. Org. Chem.* **2006**, *71*, 4255–4261.

(39) Clark, J. R.; Griffiths, J. R.; Diver, S. T. *J. Am. Chem. Soc.* **2013**, *135*, 3327–3330.

(40) de Espinosa, L. M.; Meier, M. A. R. *Top. Organomet. Chem.* **2012**, *39*, 1-44.

(41) Manzini, S.; Nelson, D. J.; Nolan, S. P. *ChemCatChem* **2013**, *5*, 2848–2851.

(42) Lummiss, J. A. M.; Oliveira, K. C.; Pranckevicius, A.; Santos, A.; dos Santos, E. N.; Fogg, D. E. *J. Am. Chem. Soc.* **2012**, *134*, 18889–18891.

References page 44

(43) Larsen, C. R.; Grotjahn, D. B. *J. Am. Chem. Soc.* **2012**, *134*, 10357–10360.

(44) **GII** has been shown to effect metathesis of unhindered terminal olefins with internal olefins related to **2**. See, for example: a) J. Czaban, B. M. Schertzer, K. Grela, *Adv. Synth. Catal.* **2013**, *355*, 1997-2006; b) A. Fürstner, O. R. Thiel, L. Ackermann, *Org. Lett.* **2001**, *3*, 449–451.

(45) Krompiec, S.; Kuznik, N.; Krompiec, M.; Penczek, R.; Mrzigod, J.; Torz, A. *J. Mol. Catal. A* **2006**, *253*, 132–146.

(46) Grotjahn, D. B.; Larsen, C. R.; Gustafson, J. L.; Nair, R.; Sharma, A. *J. Am. Chem. Soc.* **2007**, *129*, 9592–9593.

(47) Komiya, S.; Yamamoto, A. *J. Mol. Catal.* **1979**, *5*, 279-292.

(48) Schwab, P.; Grubbs, R. H.; Ziller, J. W. *J. Am. Chem. Soc.* **1996**, *118*, 100–110.

(49) Beach, N. J.; Dharmasena, U. L.; Drouin, S. D.; Fogg, D. E. *Adv. Synth. Catal.* **2008**, *350*, 773–777.

(50) Schunn, R. A.; Wonchoba, E. R.; Wilkinson, G. *Inorg. Synth.* **1971**, *13*, 131–134.

(51) Ahmad, N.; Levison, J. J.; Robinson, S. D.; Uttley, M. F. *Inorg. Synth.* **1974**, *15*, 45–64.

(52) Blacquiere, J. M.; Jurca, T.; Weiss, J.; Fogg, D. E. *Adv. Synth. Catal.* **2008**, *350*, 2849–2855.

Chapter 3. Ruthenium Nanoparticles as Unsuspected Triggers for Olefin Isomerization

3.1. Context and Objectives

The findings of Chapter 2 demonstrated that the catalysts long thought to be responsible for isomerization during olefin metathesis are not in fact kinetically competent to effect this reaction. The work in the present Chapter puts forward a new class of potential candidates. These studies build on parallel work, from this research group and others, aimed at understanding the mechanisms by which metathesis catalysts of the Grubbs and Hoveyda types decompose during catalysis. A common feature of these pathways is the progressive stripping of ligands from the Ru centre, as highlighted in Chapter 1. Most of the mechanistic proposals to date, however, are based on the observation of specific organic products, or Ru byproducts formed under non-catalytic conditions. Our understanding of the fate of the metal under catalytic conditions is remarkably underdeveloped, given the importance of ruthenium-catalyzed olefin metathesis and its decades-long study. The work described below constitutes an important first step toward addressing this deficiency.

3.1.1. Published Contributions

Ruthenium Nanoparticles as Unsuspected Triggers for Olefin Isomerization during Olefin Metathesis. Carolyn S. Higman, Anabel E. Lanterna, M. Luisa Marin, Juan C. Scaiano and Deryn E. Fogg **2016**; submitted.

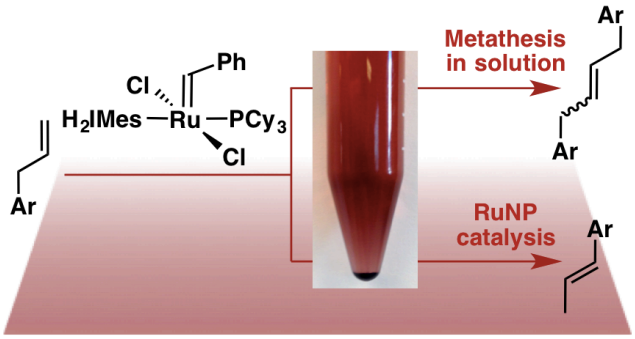

The nature and non-innocence of the inorganic species formed by catalyst decomposition during Ru-catalyzed olefin metathesis are reported. Decomposition of the second-generation Grubbs catalyst **GII** during metathesis is shown to generate Ru nanoparticles (RuNPs), which function as potent olefin isomerization catalysts. These RuNPs are the first catalyst species shown to be kinetically competent to account for the long-standing problem of competing isomerization during olefin metathesis. NPs are also present in **GII** and its precursors, but these exhibit modest isomerization activity once isolated. The previously unsuspected formation of NPs from well-defined molecular ruthenium catalysts has potentially broad relevance in homogeneous catalysis, with implications for both deactivation, and tandem catalysis.

Author Contributions: The concept and story for the paper were conceived, refined, and developed by CSH and DEF. The manuscript was written by CSH, DEF, and JCS. AEL aided in writing the SI. NP synthesis was carried out by CSH, AEL, and MLM. SEM/TEM, XPS, and EDX analyses were completed by AEL. All catalytic reactions were performed by CSH. Methods for preperation of NP-depleted **GII** were developed by CSH.

References page 68

3.2. Ruthenium Nanoparticles as Unsuspected Triggers for Olefin Isomerization during Olefin Metathesis

3.2.1. Introduction

Olefin metathesis is now a core tool in organic synthesis, owing in large part to the development of readily-handled ruthenium catalysts.[1-3] Such catalysts have transformed organic synthesis, and are now emerging in pharmaceutical and specialty chemicals manufacturing.[4-7] Notwithstanding these important advances, a number of reports cite challenges associated with competing olefin isomerization,[8] the dominant non-metathetical side reaction found in these systems.[9] Isomerization is particularly pronounced for the second-generation Grubbs catalyst **GII**, relative to its predecessor **GI** (Chart 3.1).[6,10]

Chart 3.1. Olefin Metathesis Catalysts Discussed.

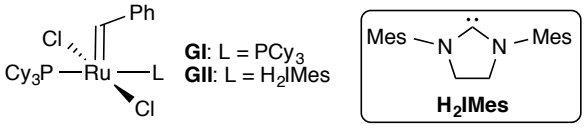

Tandem metathesis–isomerization, employed as a deliberate synthetic strategy, can enable access to targets that are otherwise challenging or inaccessible.[11] More commonly, isomerization is an unintended side-reaction, which undermines the integrity of metathesis reagents and reaction products.[12-14] High-profile examples of such problematic behavior were encountered in metathesis routes to active pharmaceutical ingredients,[5] including the HCV protease inhibitors Vaniprevir (Merck;[12] see Introduction Chapter) and BILN2061 (Boehringer-Ingelheim).[15]

References page 68

Molecular ruthenium hydrides generated by catalyst decomposition are widely viewed as responsible for this behavior, despite their low isomerization activity.[8,16] Until now, the potential contribution of nanoparticles (NPs) had gone overlooked. Here we demonstrate that unintended isomerization is promoted by ruthenium nanoparticles (RuNPs). While RuNPs or colloids are present in commercial samples of **GII**, we show that removing them does not inhibit isomerization, because new, much more active RuNPs are generated by catalyst decomposition during metathesis. These findings give new insight into a long-standing challenge in metathesis catalysis. Further, the discovery that RuNPs from a variety of sources can exhibit high isomerization activity opens the door to development of potent new isomerization catalysts, intentionally optimized for this purpose.

3.2.2. Results and Discussion

Olefin isomerization by RuNPs has not, to our knowledge, previously been reported. Given the activity of such species in other catalytic contexts,[17] however, we speculated that they might function as viable isomerization catalysts. This proved to be the case. RuNPs prepared by a range of methods,[18-20] including strategies adapted from other metals,[21,22] were assayed in the isomerization of estragole (**1a**, Table 3.1). Estragole and related allylbenzenes represent renewable platform chemicals for the billion-dollar perfumery and cosmetics industries.[23] By far most active of the RuNPs examined were the Chaudret-Philippot NPs, prepared under H_2 and stabilized by *N*-heterocyclic carbene (NHC) ligands. These materials effected quantitative isomerization of **1a** within 90 min under the conditions shown. While the other nanostructures in Table 3.1 are insufficiently isomerization-active to compete with

References page 68

metathesis (vide infra), they offer a useful proof of principle demonstrating that RuNPs from diverse sources can contribute to isomerization.

Table 3.1. Isomerization activity of RuNPs prepared by the methods indicated.[a]

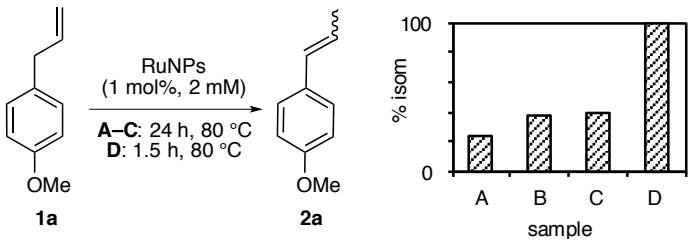

Sample	RuNP preparation method	Ref.
A	$RuCl_3$ + silica-APTES, H_2O, 1 h	19
B	$RuCl_3$ + carbon nanodiamonds, Irgacure 907, EtOH-H_2O, UVA, 1 h	This work
C	$RuCl_3$ + 3 NaOAc, ETG, 165 ˚C, 15 min	20
D	Ru(COD)(COT) + IPr, H_2 (10 bar), RT, 14 h	Adapted from 18

Ananikov and co-workers recently reported that PdNPs are present in commercial sources of $Pd_2(dba)_3$,[24] while the Corma group described the spontaneous formation of catalytically active CuNPs on heating soluble precursors.[25] Given these precedents, we queried whether RuNPs might be present in the Ru metathesis catalysts, and whether these could trigger non-metathetical reactions.

We find that NPs are indeed present in commercial samples of **GII**, albeit in minor amounts. Thus, 4–6 mg of a black solid deposited upon centrifuging solutions of **GII** (200 mg in

References page 68

toluene), an amount that corresponds to <30 mg/g.[†] Scanning electron microscopy (SEM) analysis of the sediment revealed large, polydisperse NPs (60-420 nm; see Appendix, Figure A1).

While the commercial method used to prepare **GII** is proprietary, the classic route to this complex employs strong base at 80 °C to generate the free NHC ligand in situ.[26] As the combination of high temperatures and base is a standard means of generating NPs, this synthetic procedure could plausibly promote NP formation. Indeed, no visible sediment deposited on centrifuging samples of **GII** prepared at room temperature, using free H_2IMes.[27] However, SEM analysis revealed NPs in these samples, as well as the precursors **GI** and $RuCl_2(PPh_3)_3$ (**Ru-1**; see Appendix, Figure A3).

X-ray photoelectron spectroscopy (XPS) and energy-dispersive X-ray spectroscopy (EDX) confirmed that these structures are rich in ruthenium (see Appendices A/B; Figures A2 and B1). XPS analysis on the Ru NPs isolated from **GII** (Appendix B; Figure B1a) revealed the presence of RuO_2, this being inferred from the Ru 3d photoelectron doublet at 282 eV (Ru $3d_{5/2}$) and 286 eV (Ru $3d_{3/2}$).[36] Additional peaks at ca. 284 and 280 eV are assigned to more reduced Ru species, such as Ru(0).[37-39] While the nanostructures isolated from commercial **GII** contain reduced Ru species, their isomerization activity is modest (45% after 24 h, under the conditions of Table 3.1).

[†]Centrifugation of **GII** was carried out on solutions containing 10 mg **GII** per mL of toluene, a concentration well below the limiting solubility observed for this complex (ca. 20 mg/mL).

For Ru@CND (Table 3.1, sample **B**), the high-resolution Ru 3d XPS spectrum also shows peaks at ca. 280 eV (see Appendix; Figure B1b). In contrast, Ru@MCM (Table 3.1, sample **A**), exhibits no peaks at or below 280 eV, suggesting that the Ru species present are more oxidized (see Appendix; Figure B1c). These differences (see Appendix; Figure B1d) may account for the lower isomerization activity of Ru@MCM.

We suspected that the modest isomerization acitivty of the RuNPs isolated from **GII** might be due to agglomeration during the isolation procedure aimed at removing all remaining **GII** (i.e. three cycles of centrifuging, decanting, and resuspending). Indeed, SEM analysis indicated an increase in particle size (from an average of <200 nm to >500 nm), and thus a more limited number of active surface sites.

As an alternative, non-perturbing approach, we examined the proportion of isomerization that occurs during metathesis by NP-rich, vs. NP-depleted, **GII**. The latter was obtained as a free-flowing pink powder by ultracentrifuging **GII** in toluene at 4 °C under N_2, decanting the supernatant, and evaporating the solvent under vacuum. No NPs were observed in this material by SEM and HR-TEM analysis. Isomerization was higher by ca. 15% for NP-rich **GII** (Figure 3.1), indicating that the contaminating NPs indeed promote competing isomerization of both reagents and products during metathesis.

References page 68

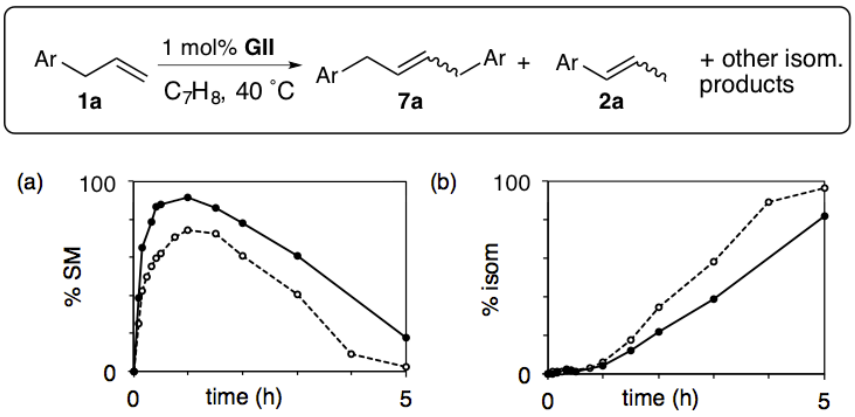

Figure 3.1 Self-metathesis (SM) and isomerization of estragole **1a** by NP-depleted **GII** (solid line) or NP-rich **GII** (dashed line). (a) Formation and loss of the SM product **7a**. (b) Rate of isomerization (sum of reagent and product isomerization). Loss of C_2H_4 was maximized[28] by use of an open vessel. Ar = *p*-methoxyphenyl.

More striking, however, is the fact that the difference is not greater. Clearly, even "NP-depleted" **GII** causes significant isomerization. SEM analysis *following* metathesis explains this behavior: in dramatic contrast with the initial material (Figure 3.2, left), SEM micrographs obtained post-metathesis (Figure 3.2, right) show abundant RuNPs. Decomposition of $RuCl_2(H_2IMes)(PCy_3)(=CH_2)$ **GIIm**, the resting-state species formed from **GII** during metathesis, is now known to liberate $[MePCy_3]Cl$ (see Introduction Chapter).[29] This "ligand stripping" process (i.e. loss of the phosphine, chloride, and methylidene ligands from **GIIm**) is presumably the starting point for the developing Ru-Ru interactions that culminate in NP formation. These results provide the first insight into the fate of the low-coordinate ruthenium products formed during catalysis.

References page 68

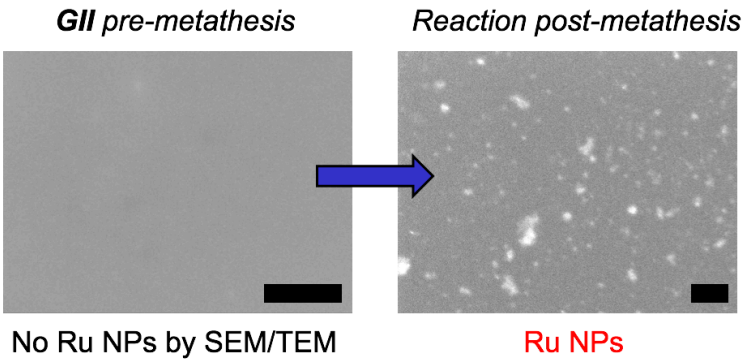

Figure 3.2 Generation of RuNPs from NP-depleted **GII** during styrene (**9**) metathesis[30] (80 °C, 0.5 h; 1 mol% **GII**). Image recorded in SEM composition (COMPO) mode. Scale bar: 1 μm. Particle size (100 ±25) nm.

The mercury test, as the single most widely used test for heterogeneous catalysis, is one of the key criteria used to distinguish homogeneous from NP catalysis. Elemental Hg inhibits the participation of surface-active species in catalysis, by forming an amalgam or adsorbing on the metal surface.[31-34] Isomerization of **1a** using NP-depleted **GII** dropped sharply in the presence of Hg (Figure 3.3), confirming that isomerization-active NPs are generated by catalyst decomposition during metathesis. Control experiments confirmed that added Hg had negligible impact on the isomerization activity of the molecular hydride species $RuHCl(PPh_3)_3$ (**Ru-H1**) and $RuHCl(CO)(H_2IMes)(PCy_3)$ (**Ru-H4**). In fact, the Hg test almost certainly under-reports the contribution of RuNPs in Figure 3.3, as Hg(0) does not form a highly stable amalgam with ruthenium.[35]

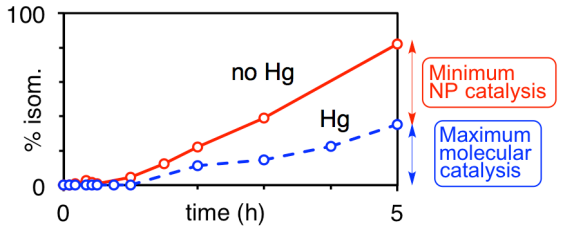

Figure 3.3 The mercury test: confirming the contribution of NP catalysis to isomerization during estragole SM. Starting catalyst: NP-depleted **GII**; conditions as in Figure 3.1.

The NPs formed by decomposition of **GII** during metathesis are evidently much more potent isomerization catalysts than those present in commercial **GII**. We suspect that this reflects faster RuNP formation during metathesis, resulting in smaller particles with less opportunity for agglomeration and surface deactivation. Indeed, the mean particle size is much smaller, at ca. 100 nm. The greater size and polydispersity of the RuNPs in commercial **GII** may be due to their slow formation during catalyst synthesis and storage, and agglomeration during these processes as well as isolation.

3.2.3. Conclusions

The foregoing reveals that RuNPs are present in both **GII** and **GI**, as well as their synthetic precursor **Ru-1**. A common feature in the preparation and use of these complexes is the combination of high temperatures and reducing conditions, the latter being associated with the presence of free Lewis-base ligands. The ubiquity of such conditions in organometallic synthesis and catalysis points toward the potential generality of NPs as spectroscopically unobservable contaminants.

References page 68

Importantly, however, the NPs present in the precatalyst **GII** have a relatively minor impact on product selectivity in metathesis reactions. Much more significant is the impact of fresh NPs generated *during* metathesis, which emerge as key contributors to the extensive isomerization observed during metathesis of estragole. These RuNPs are the first catalyst species shown to trigger competing isomerization during olefin metathesis. More broadly, this discovery represents a previously unrecognized decomposition pathway for **GII**, with potentially broad relevance for the decomposition or deliberate transformation of other molecular transition-metal catalysts. Finally, it should be emphasized that the reaction conditions explored herein were designed to promote metathesis, not to optimize either NP formation or isomerization. Clear potential exists to fine-tune catalysts or catalysis conditions to minimize or to enhance isomerization. In particular, these findings open the opportunity to invent new isomerization catalysts, by optimizing the RuNP synthesis and the isomerization conditions. The high activity of the Chaudret-Philippot NPs, for example, underscores the importance of controlling the nature of the surface sites. Such avenues are presently being pursued, and will be reported in due course.

3.2.4. Experimental Details for Section 3.2

3.2.4.1 General Procedures[‡]

$RuCl_3 \bullet xH_2O$ was purchased from Strem and used as received. **GI**, **GII**, and **Ru-1** were purchased from Sigma-Aldrich. **GII** was also synthesized at room temperature by the reported method, involving ligand exchange of **GI** with free H_2IMes.[27] Estragole **1a** and

[‡] Samples for SEM/TEM, and XPS analyses were prepared by CH, and analyzed by AEL.

styrene (both >99%) were purchased from Sigma-Aldrich, degassed by three freeze-pump-thaw cycles, and thawed under N_2 prior to use. Estragole was passed over neutral alumina after degassing.

Organic species in catalytic experiments were quantified using an Agilent 7890A Series gas chromatograph (GC) equipped with a flame ionization detector (FID), an Agilent 7683B Series autosampler and an Agilent HP-5 polysiloxane column (30 m length, 320 μm diameter), using an inlet split ratio of 10:1, an inlet temperature of 250 °C, and helium (UHP grade) as the carrier gas to maintain column pressure at 11.512 psi. The FID response was maintained between 50-2000 ρA, using analyte concentrations of ca. 5 mM. Calibration curves (peak areas vs. concentration) were constructed in the relevant concentration regime, to account for the dependence on detector response for substrates, products and decane (internal standard in catalytic runs). Conversions and yields in catalytic runs were determined from the integrated peak areas, referenced against decane, and compared to the initial substrate : decane integration ratio.

NP-depleted **GII** was obtained by high-speed centrifugation of toluene solutions at 14,000 rpm (18,407 g, 4 ˚C, N_2 atmosphere) using a Thermo Scientific Sorvall RT1 Centrifuge equipped with an AC 2.14 rotor. The colloids / nanostructures themselves were isolated from **GII** by centrifugation at 3,000 rpm (1,600 g, 23 ˚C, N_2 atmosphere) using a Drucker Diagnostics 653V centrifuge, equipped with the standard horizontal rotor. The sediment was characterized by scanning electron microscopy (SEM), supplemented by dispersive X-ray spectroscopy (EDX) analysis for composition. These experiments were carried out at a

References page 68

magnification of 9,000x, with an electron beam voltage of 20 kV. Backscattered electron (BSE) images with material contrast in composition (COMPO) mode were measured with a typical working distance of 8 mm (required for EDX analysis). EDX spectra were analyzed using the INCA Energy software. Size-distribution histograms were obtained by analyzing several SEM images using ImageJ software. SEM samples were prepared anaerobically by deposition of toluene solutions onto a 200 mesh copper grid coated with a carbon film. The grid was left to dry overnight under N_2, and analyzed immediately after removal from the glovebox using a JEOL JSM-7500F field emission SEM (FESEM). TEM analysis was performed similarly, using a JEOL JEM-2100F FETEM.

The proportion of Ru in the supported RuNPs was determined by inductively coupled plasma emission spectrometry (ICP-ES), using an Agilent Vista Pro ICP emission spectrometer. Approximately 10 mg portions were accurately weighed in triplicate and digested with aqua regia. Solutions were further diluted and measured by ICP-ES. The Ru 267.876 emission line was used for quantification, with verification at six additional Ru emission lines. Elemental analysis of Ru-IPr NPs was carried out by MHW Laboratories, Phoenix, AZ.

X-ray photoelectron spectroscopy (XPS) was recorded using a Kratos analytical model Axis Ultra DLD instrument, using monochromatic aluminum Kα X-rays at 140 W. Samples were prepared by placing the solid samples on a 1 cm x 1 cm silicon wafer. XPS data were analyzed using CasaXPS software (Version 2.3.15). All fittings were obtained using a Gaussian/30% Laurentian analysis with a Shirley baseline.

References page 68

3.2.4.2 Nanoparticle Syntheses

Literature methods were used to prepare Ru nanoparticles according to Methods **A**,[19] **C**,[20] and **D** (see Table 3.1). Method **D** involved a minor modification of the Chaudret-Philippot[18] route in which Ru(COD)(COT) is hydrogenated in the presence of IPr. Specifically, a higher H_2 pressure was employed (10 bar, vs. the original 3 bar) for convenient reproducibility with the available equipment. A new approach (Method **B**) was developed to synthesize RuNPs supported on crystal nanodiamonds (Ru@CND). Representative SEM micrographs for all RuNPs are provided in the Appendix, Figure A4.

3.2.4.3 Synthesis of Crystal Nanodiamond-Supported RuNPs (Ru@CND; Method B)[§]

RuNPs were photodeposited onto crystal nanodiamonds (CND) by suspending 100 mg of CND and 4 mg of $RuCl_3.xH_2O$ in Milli-Q water (40 mL). The slurry was stirred for 10 min, and Irgacure 907 photoinitiator (12 mg) in 10 mL ethanol was added. The mixture was irradiated for 1 h using a Luzchem Research exposure panel equipped with 12 UVA bulbs (65 W/m^2). The gray slurry was centrifuged, washed with ethanol and dried under vacuum overnight. The powder was characterized by ICP-ES, TEM and XPS analysis (see Appendix; Figures A4 and B1).

[§] Synthesis carried out by AEL.

References page 68

3.2.4.4 Observation, Isolation, and Characterization of RuNPs

(a) Observation of NPs in GII and Its Precursors.

In a representative procedure, toluene solutions of commercial **GII** (10 mg **GII** per mL of toluene) were centrifuged under N_2 atmosphere at a g-force of 1,600, causing deposition of a black solid (see Appendix; Figure A3a). While no such deposit was observed for **GII** prepared by the free-carbene method,[27] for **GI**, or for the precursor compound $RuCl_2(PPh_3)_3$ **Ru-1** (see Appendix; Figure A3a), SEM analysis revealed NPs in all compounds analyzed (see Appendix; Figure A3b). The Ru colloids isolated from commercial **GII** exhibit high polydispersity and polymorphism, with sizes in the 60-400 nm range. Figure A1 (see Appendix) shows a particle size distribution for the largest dimension in these very irregular particles. The distribution cannot be treated as a histogram and the numbers are too small for statistical analysis, but it serves to show the general characteristics of the nanoparticle / colloid debris present in commercial **GII**. The images are likely agglomerates, rather than individual particles): organic matter is also still present.

(b) Isolation of RuNPs from GII.

The proportion of NPs present in commercial samples of **GII** is relatively small, and may vary considerably batch-to-batch. The amount in a representative sample of commercial **GII** (200 mg) was assessed by weighing the sediment deposited from a toluene solution (8 mL) by centrifugation at 3,500 rpm for 30 min. Mass: 4 mg (15 mg per gram of **GII**). A comparable figure (6 mg) was determined by difference, by weighing the **GII** sample before and after removal of NPs. All samples were weighed on an analytical balance outside the glovebox.

(c) Characterization of RuNPs Isolated from GII.

RuNPs were isolated free of **GII** by suspension, centrifugation, and decantation, as in 3.2.4.4a. The presence of ruthenium in the isolated RuNPs was confirmed by EDX analysis, which exhibits the characteristic Ru Lα peak at 2.558 KeV (see Appendix; Figure A2). While the presence of P was also confirmed (Kα at 2.013 KeV), detection of N and/or Cl on the NP surfaces is hampered by overlap with C and Ru lines, respectively.

XPS analysis was carried out on the RuNPs isolated from commercial **GII**, Ru@CND, and Ru@MCM, using the C 1s peak (284.0 eV) to calibrate the binding energies. The background signal from the carbon substrate obscures the signals due to the Ru 3d photoelectrons,, complicating analysis. Nevertheless, distinctions are evident between RuNPs obtained by the different methods described. For the Ru NPs isolated from **GII** (see Appendix; Figure B1a), a doublet is observed at 282 eV (Ru $3d_{5/2}$) and 286 eV (Ru $3d_{3/2}$).[36] Additional peaks at ca. 284 and 280 eV are also observed.[37-39] For Ru@CND, the high-resolution Ru 3d XPS spectrum also shows peaks at ca. 280 eV (see Appendix; Figure B1b). In contrast, Ru@MCM exhibits no peaks at or below 280 eV, suggesting that the Ru species present are more oxidized (see above and Appendix B, Figure B1c). These differences may well explain why the first two RuNP samples are able to effect olefin isomerization, while the isomerization activity of Ru@MCM is negligible.

3.2.4.5 Protocol for Preparation of NP-Depleted GII

A solution of commercial **GII** (100 mg) in toluene (6 mL) was divided into six Eppendorf tubes inside the glovebox. Each tube was sealed under N_2, and taped with Parafilm. The

samples were centrifuged at 14,000 rpm (18,407 g), 4 ˚C, for 30 min, after which a black pellet was observable. The tubes were returned to the glovebox, the supernatant removed by pipette, combined, and stripped of solvent to give NP-depleted **GII**. SEM and TEM analysis indicated no observable NPs (Figure 3.2, left).

3.2.4.6 Representative Procedures for Catalysis.

(a) Isomerization of Estragole 1a by Deliberately-Synthesized RuNPs. A 20 mL vial was loaded with estragole (29.6 mg, 0.2 mmol), decane (internal GC standard for GC analysis; 28.5 mg, 0.2 mmol) and toluene (960 μL). An aliquot was removed for GC-FID analysis, to establish the starting ratio of substrate to decane. RuNPs (0.01 equiv Ru) were added as a solution in toluene, affording a final reaction concentration 2 mM (see Appendix; Table A1). The vial was heated for 24 h at 80 ˚C in an oil bath in the glovebox, after which an aliquot was removed and immediately analyzed (GC-FID; see Appendix, Figure C1).

(b) Isomerization of Estragole 1a and Its CM Products During Metathesis. A 20 mL vial was loaded with estragole **1a** (296 mg, 2 mmol), decane (internal standard for GC analysis; 285 mg, 2 mmol) and toluene (9.3 mL). An aliquot was removed and assessed by GC-FID to establish the initial ratio of **1a** to decane. **GII** (17 mg, 0.02 mmol, 1 mol %) was then added, and the solution was heated to 40 ˚C (oil bath) in the glovebox. Aliquots were taken at specific time intervals, quenched with potassium trispyrazolylborate in THF (10 mg/mL, 10 equiv), diluted with CH_2Cl_2 in air, and analyzed by GC-FID (see Appendix, Figure C2). Yields of the primary cross-metathesis product, (*E*)- and (*Z*)-$ArCH_2CH{=}CHCH_2Ar$ **7a** (Ar = *p*-C_6H_4OMe) were quantified against decane, with the appropriate response factor correction.

Isomerization yields were determined from the difference between conversion of **1a** and yield of **7a**. Multiple products are generated by isomerization prior to or following metathesis, or independent of metathesis. These include (*E*)- and (*Z*)-anethole, formed by isomerization of **1a**; (*E*)- and (*Z*)-ArCH=CH_2CHCH_2Ar, formed by isomerization of the primary CM product **7a**, and (*E*)- and (*Z*)-isomers of secondary metathesis products formed by self-metathesis of anethole and by CM of **1a** with anethole **2a**. As well, propylene generated by CM of estragole with anethole may react with any of the aforementioned compounds to yield tertiary CM products, etc., as previously noted.[40]

Self-metathesis of **1a** in the presence of mercury was performed as above, with addition of excess Hg (ca. 0.5 mL, 7 g) immediately following addition of **GII**. The reactions were stirred vigorously to maximize dispersion of Hg droplets. *Caution:* Mercury must be handled using appropriate protection, using standard secondary-containment practices. Wastes and contaminated material must be labelled as hazardous waste and disposed of in accordance with federal regulations.

In some experiments, styrene was used to facilitate SEM imaging post-metathesis. Styrene does not undergo isomerization: instead, it yields stilbene as the sole product. The limited solubility of stilbene in toluene causes it to precipitate, reducing interference by organic products during SEM analysis of the supernatant.

(c) Isomerization of Estragole 1a by Ruthenium Hydrides. Isomerization of estragole by both $RuHCl(PPh_3)_3$ and $RuHCl(CO)(H_2IMes)(PCy_3)$ was carried out as described in 3.2.4.6

References page 68

(a) above. Each catalyst was evaluated in the presence and absence of added mercury. Identical isomerization yields were observed at 5 h, irrespective of the presence of Hg.

3.3. References

(1) For recent books offering comprehensive reviews, see: (a) Grela, K., Ed. *Olefin Metathesis-Theory and Practice*. Wiley: Weinheim, 2014. (b) Grubbs, R. H.; Wenzel, A. G., Eds. *Handbook of Metathesis*. 2nd ed.; Wiley-VCH: Weinheim, 2015. (c) Cossy, J.; Arseniyadis, S.; Meyer, C., Eds. *Metathesis in Natural Product Synthesis: Strategies, Substrates and Catalysts.* Wiley-VCH: Weinheim, 2010.

(2) Vougioukalakis, G. C.; Grubbs, R. H. *Chem. Rev.* **2010**, *110*, 1746–1787.

(3) Astruc, D., Olefin Metathesis Reactions: From a Historical Account to Recent Trends In *Olefin Metathesis-Theory and Practice*, Grela, K., Ed. Wiley: Hoboken, NJ, 2014; pp 5–38.

(4) Higman, C. S.; Lummiss, J. A. M.; Fogg, D. E. *Angew. Chem., Int. Ed.*, in press.

(5) Farina, V.; Horváth, A., Ring-Closing Metathesis in the Large-Scale Synthesis of Pharmaceuticals. In *Handbook of Metathesis*, Wiley-VCH: Weinheim, 2015; Vol. 2, pp 633–658.

(6) van Lierop, B. J.; Lummiss, J. A. M.; Fogg, D. E., Ring-Closing Metathesis. In *Olefin Metathesis-Theory and Practice*, Grela, K., Ed. Wiley: Hoboken, NJ, 2014; pp 85–152.

(7) Chikkali, S.; Mecking, S. *Angew. Chem., Int. Ed.* **2012**, *51*, 5802−5808.

(8) Double-bond isomerization during metathesis is discussed in recent reviews. See Ref. 6 and: Larionov, E.; Li, H.; Mazet, C. *Chem. Commun.* **2014**, *50*, 9816–9826.

(9) Alcaide, B.; Almendros, P.; Luna, A. *Chem. Rev.* **2009**, *109*, 3817–3858.

(10) Selected examples: (a) A. Fürstner, O. R. Thiel, L. Ackermann, H.-J. Schanz, S. P. Nolan, *J. Org. Chem.* **2000**, *65*, 2204–2207. (b) F. C. Courchay, J. C. Sworen, K. B. Wagener, *Macromolecules* **2003**, *36*, 8231–8239. (c) S. D. Kamau, P. Hodge, A. J. Hall, S. Dad, A. Ben-Haida, *Polymer* **2007**, *48*, 6808–6822. (d) P. C. M. van Gerven, J. A. A. W.

Elemans, J. W. Gerritsen, S. Speller, R. J. M. Nolte, A. E. Rowan, *Chem. Commun.* **2005**, 3535–3537. (e) A. V. Chuchuryukin, P. A. Chase, H. P. Dijkstra, B. Suijkerbuijk, A. M. Mills, A. L. Spek, G. P. M. van Klink, G. van Koten, *Adv. Synth. Catal.* **2005**, *347*, 447–462. (f) T. R. Hoye, M. A. Promo, *Tetrahedron Lett.* **1999**, *40*, 1429–1432. (g) R. Ahuja, S. Kundu, A. S. Goldman, M. Brookhart, B. C. Vicente, S. L. Scott, *Chem. Commun.* **2008**, 253–255. (h) S. D. Edwards, T. Lewis, R. J. K. Taylor, *Tetrahedron Lett.* **1999**, *40*, 4267–4270.

(11) For recent examples of tandem catalysis strategies that couple metathesis with isomerization, see: (a) Dobereiner, G. E.; Erdogan, G.; Larsen, C. R.; Grotjahn, D. B.; Schrock, R. R. *ACS Catal.* **2014**, *4*, 3069–3076. (b) Clark, J. R.; Griffiths, J. R.; Diver, S. T. *J. Am. Chem. Soc.* **2013**, *135*, 3327–3330. (c) Schmidt, B.; Hauke, S. *Org. Biomol. Chem.* **2013**, *11*, 4194–4206. (d) Ohlmann, D. M.; Tschauder, N.; Stockis, J.-P.; Gooßen, K.; Dierker, M.; Gooßen, L. J. *J. Am. Chem. Soc.* **2012**, *134*, 13716–13729. (e) Ascic, E.; Jensen, J. F.; Nielsen, T. E. *Angew. Chem. Int. Ed.* **2011**, *50*, 5188–5191. (f) Kobayashi, T.; Arisawa, M.; Shuto, S. *Org. Biomol. Chem.* **2011**, *9*, 1219–1224. (g) Consorti, C. S.; Aydos, G. L. P.; Dupont, J. *Chem. Comm.* **2010**, *46*, 9058–9060. (h) Schmidt, B.; Biernat, A. *Chem. Eur. J.* **2008**, *14*, 6135–6141. For groundbreaking examples, see: (i) Arisawa, M.; Terada, Y.; Nakagawa, M.; Nishida, A. *Angew. Chem. Int. Ed.* **2002**, *41*, 4732–4734. (j) Sutton, A. E.; Seigal, B. A.; Finnegan, D. F.; Snapper, M. L. *J. Am. Chem. Soc.* **2002**, *124*, 13390–13391. For reviews of early work, see: Ref. 9 and: (k) Schmidt, B. *Pure Appl. Chem.* **2006**, *78*, 469–476. (l) Fogg, D. E.; dos Santos, E. N. *Coord. Chem. Rev.* **2004**, *248*, 2365–2379.

(12) Kong, J.; Chen, C.-Y.; Balsells-Padros, J.; Cao, Y.; Dunn, R. F.; Dolman, S. J.; Janey, J.; Li, H.; Zacuto, M. J. *J. Org. Chem.* **2012**, *77*, 3820–3828.

(13) Bilel, H.; Hamdi, N.; Zagrouba, F.; Fischmeister, C.; Bruneau, C. *RSC Adv.* **2012**, *2*, 9584–9589.

(14) Campbell, M. J.; Johnson, J. S. *J. Am. Chem. Soc.* **2009**, *131*, 10370–10371.

(15) Nicola, T.; Brenner, M.; Donsbach, K.; Kreye, P. *Org. Process Res. Dev.* **2005**, *9*, 513–515.

(16) See Ref. 4. For an analysis of the poor kinetic competence of molecular hydride species often regarded as potential culprits, see: (a) Higman, C. S.; Plais, L.; Fogg, D. E. *ChemCatChem* **2013**, *5*, 3548-3551. The four-coordinate species RuHCl(CO)(H_2IMes) has been suggested as a more plausible alternative: see (b) Nelson, D. J.; Percy, J. M., *Dalton Trans*. **2014**, *43*, 4674–4679.

(17) Martínez-Prieto, L. M.; Carenco, S.; Wu, C. H.; Bonnefille, E.; Axnanda, S.; Liu, Z.; Fazzini, P. F.; Philippot, K.; Salmeron, M.; Chaudret, B. *ACS Catal.* **2014**, *4*, 3160−3168.

(18) Lara, P.; Rivada-Wheelaghan, O.; Conejero, S.; Poteau, R.; Philippot, K.; Chaudret, B. *Angew. Chem. Int. Ed. Engl.* **2011**, *50*, 12080–12084.

(19) Carrillo, A. I.; Schmidt, L. C.; Marin, M. L.; Scaiano, J. C. *Catal. Sci. Technol.* **2014**, *4*, 435–440.

(20) Viau, G.; Brayner, R.; Poul, L.; Chakroune, N.; Lacaze, E.; Fiévet-Vincent, F.; Fiévet, F. *Chem. Mater.* **2003**, *15*, 486-494.

(21) Wee, T.-L.; Schmidt, L. C.; Scaiano, J. C. *J. Phys. Chem. C* **2012**, *116*, 24373–24379.

(22) Wee, T.-L.; Sherman, B. D.; Gust, D.; Moore, A. L.; Moore, T. A.; Liu, Y.; Scaiano, J. C. *J. Am. Chem. Soc.* **2011**, *133*, 16742–16745.

(23) de Espinosa, L. M.; Meier, M. A. R. *Top. Organomet. Chem.* **2012**, *39*, 1-44.

(24) Zalesskiy, S. S.; Ananikov, V. P. *Organometallics* **2012**, *31*, 2302–2309.

(25) Oliver-Meseguer, J.; Liu, L.; García-García, S.; Canós-Gimenez, C.; Domínguez, I.; Gavara, R.; Doménech-Carbó, A.; Concepción, P.; Leyva-Perez, A.; Corma, A. *J. Am. Chem. Soc.* **2015**, *137*, 3894−3900.

(26) Scholl, M.; Ding, S.; Lee, C. W.; Grubbs, R. H. *Org. Lett.* **1999**, *1*, 953–956.

(27) van Lierop, B. J.; Reckling, A. M.; Lummiss, J. A. M.; Fogg, D. E. *ChemCatChem* **2012**, *4*, 2020–2025.

(28) Retention of ethylene in solution has long been known to promote catalyst deactivation. See: (a) van Rensburg, W. J.; Steynberg, P. J.; Meyer, W. H.; Kirk, M. M.; Forman, G. S. *J. Am. Chem. Soc.* **2004,** *126*, 14332-14333. (b) Burdett, K. A.; Harris, L. D.; Margl, P.; Maughon, B. R.; Mokhtar-Zadeh, T.; Saucier, P. C.; Wasserman, E. P. *Organometallics* **2004,** *23*, 2027-2047.

(29) Thermolysis of $RuCl_2(H_2IMes)(PCy_3)(=CH_2)$ in the absence of olefin liberates $[MePCy_3]Cl$. See: (a) Hong, S. H.; Wenzel, A. G.; Salguero, T. T.; Day, M. W.; Grubbs, R. H. J. Am. Chem. Soc. 2007, 129, 7961–7968. For formation of $[MePCy_3]Cl$ during metathesis, see: (b) Lummiss, J. A. M.; Ireland, B. J.; Sommers, J. M.; Fogg, D. E. *ChemCatChem* **2014**, *6*, 459–463. For crystallographic and ^{13}C-labelling evidence demonstrating that methylidene abstraction occurs via attack of PCy_3 on the $[Ru]=CH_2$ carbon, see: (c) Lummiss, J. A. M.; McClennan, W. L.; McDonald, R.; Fogg, D. E. *Organometallics* **2014**, *33*, 6738–6741. (d) Lummiss, J. A. M.; Botti, A. G. G.; Fogg, D. E. *Catal. Sci. Technol.* **2014**, *4*, 4210–4218.

(30) These experiments were carried out with styrene (which does not isomerize), to facilitate SEM imaging. The low solubility of the stilbene metathesis product reduces the proportion of occluding organic species present.

(31) Crabtree, R. H. *Chem. Rev.* **2012**, *112*, 1536–1554.

(32) Gómez, M.; Favier, I., Metal Nanoparticles Dispersed in Solution: Tests to Identify the Catalyst Nature. In *Metal Nanoclusters in Catalysis and Materials Science*, Corain, B.; Schmid, G.; Toshima, N., Eds. Elsevier: Amsterdam, 2011; pp 427–436.

(33) Widegren, J. A.; Bennett, M. A.; Finke, R. G. *J. Am. Chem. Soc.* **2003**, *125*, 10301–10310.

(34) Hagen, C. M.; Widegren, J. A.; Maitlis, P. M.; Finke, R. G. *J. Am. Chem. Soc.* **2005**, *127*, 4423–4432.

(35) Whitesides, G. M.; Hackett, M.; Brainard, R. L.; Lavalleye, J. P. P. M.; Sowinski, A. F.; Izumi, A. N.; Moore, S. S.; Brown, D. W.; Staudt, E. M. *Organometallics* **1985**, *4*, 1819–1830.

(36) Wang, W.; Guo, S.; Lee, I.; Ahmed, K.; Zhong, J.; Favors, Z.; Zaera, F.; Ozkan, M.; Ozkan, C. S. *Scientific Reports* **2014**, *4*, 4452–4452.

(37) Elmasides, C.; Kondarides, D. I.; Grünert, W.; Verykios, X. E. *J. Phys. Chem. B* **1999**, *103*, 5227–5239.

(38) García-Peña, N. G.; Redón, R.; Herrera-Gomez, A.; Fernández-Osorio, A. L.; Bravo-Sanchez, M.; Gomez-Sosa, G. *Appl. Surf. Sci.* **2015**, *340*, 25–34.

(39) Shen, X.; Garces, L.-J.; Ding, Y.; Laubernds, K.; Zerger, R. P.; Aindow, M.; Neth, E. J.; Suib, S. L. *Appl. Catal. A* **2008**, *335*, 187–195.

(40) Czaban, J.; Schertzer, B. M.; Grela, K. *Adv. Synth. Catal.* **2013**, *355*, 1997–2006.

Chapter 4. A Truncated N-Heterocyclic Carbene for Olefin Metathesis: A Quest for Improved Catalyst Lifetime and Productivity

4.1. Context and Overview

With the recent uptake of molecular metathesis catalysts in industrial processes, as discussed in Chapter 1, issues of catalyst productivity take on new importance. Studies of deactivation processes in "second-generation" ruthenium metathesis catalysts point toward C-H activation of the mesityl methyl groups in the NHC ligand as a key event. Examined in this Chapter is the impact of replacing the mesityl with a methyl group: that is, truncation of the NHC ligand to IMe4 (IMe4 = 1,3,4,5-tetramethylimidazol-2-ylidene) to inhibit C-H activation. Reaction of the first-generation Grubbs catalyst **GI** with two equivalents of free IMe4 was found to afford a $Ru_2(\mu\text{-}Cl)_3$ dimer **Ru-4**, in which each Ru centre bears a benzylidene and two IMe4 ligands. X-ray analysis revealed a cationic complex with a chloride counterion. In solution, rapid rotation of both the benzylidene and the NHC groups gives rise to three broad ^1H NMR singlets for the benzylidene proton, and eight unique methyl singlets. The dynamic processes involved were explored by EXSY and variable-temperature NMR analysis. Poor metathesis activity results from the stability of the face-bridged structure, but improved performance can be anticipated with minor modification of this novel phosphine-free catalyst.

4.2. A Truncated *N*-Heterocyclic Carbene for Olefin Metathesis: A Quest for Improved Catalyst Lifetime and Productivity

4.2.1. Introduction

Key decomposition pathways for the dominant ruthenium metathesis catalysts were outlined in Chapter 1. The H_2IMes or IMes ligands present are anticipated as a point of vulnerability,

on the basis of precedents for C-H activation of mesityl methyl groups[1-6] and other ortho substituents.[7-11] This Chapter describes first attempts to design a catalyst that cannot readily undergo such C-H activation, but which maintains the high activity associated with the presence of an NHC ligand. Replacing the mesityl substituents with methyl groups was conceived of as a means of inhibiting C-H activation, owing to the spatial placement of the *N*-Me group (compare Figure 4.1a vs. Figure 4.1b), and the very limited orbital overlap with the metal d-orbitals. Such a system (should a mono-NHC species be attainable) could potentially increase overall metathesis productivity by prolonging catalyst lifetime: alternatively, it could afford insight into background decomposition pathways that occur when C-H activation is inhibited. A prior strategy to prevent decomposition via C-H activation pathways was targeted at increasing the bulk on the NHC backbone to inhibit rotation of the aryl groups about the *N*-aryl bond.[12] This strategy is effective in increasing catalyst stability, but it comes at the cost of catalyst activity.[12] An alternative strategy by Grubbs and coworkers introduces fluorines in the ortho positions of N-aryl group to prohibit C-H activation.[13] However, yields were poor and NHC installation proved to be challenging, requiring use of Ag as an NHC transfer agent to prevent dimerization. Additionally, unfavourable Ru-F interactions were found to limit initiation efficiency.

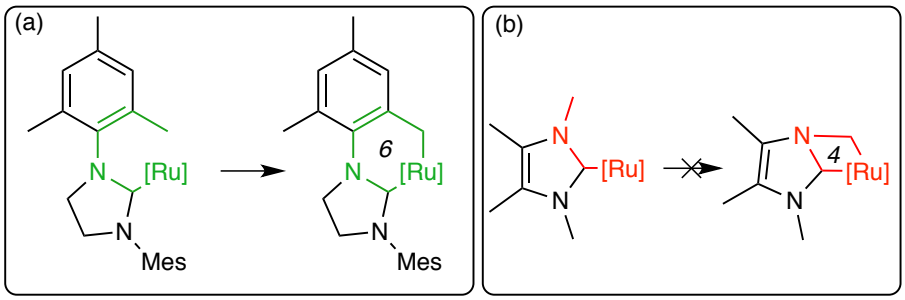

Figure 4.1. Eliminating the opportunity for C-H activation by reducing the ring size of the potential ruthenacycle.

References page 97

The unsaturated NHC IMe4 is known, and is readily accessible. The free carbene is obtained in a reported overall yield of 62% in two steps from commercially available starting materials (Scheme 4.1).[14] Both IMe2 and the corresponding saturated carbenes H_2IMe4 and H_2IMe are accessible by analogous methods. IMe4 was chosen for study in the present work with the idea of maximizing net donicity, although the full implications of backbone unsaturation (see below) emerged only in parallel with the present study.[15]

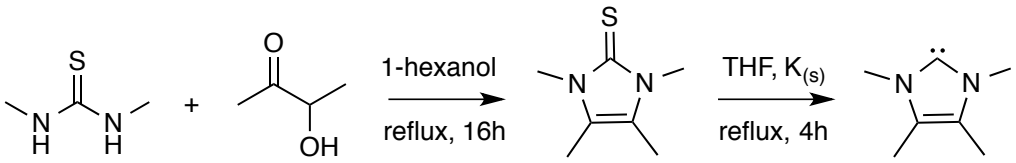

Scheme 4.1. Two-step synthesis of IMe_4.

The electronic parameters of the NHC ligand have a profound influence on metathesis activity and, for phosphine-stabilized precatalysts of the Grubbs class, the ease of initiation.[15] The most widely used metric for NHC donicity is the Tolman Electronic Parameter (TEP), or the frequency of the ν(C–O) stretching band in $Ni(CO)_4$(NHC) complexes. A lower-energy band is thus taken to indicate more backbonding from the metal onto the carbonyl ligands, and hence a more strongly donating NHC ligand. The utility of the TEP is limited, however, by very poor sensitivity, with differences of as little as 2 cm^{-1} for these broad stretching bands being treated as significant. Furthermore, differences in the π-acceptor ability of different NHC ligands limits the validity of the comparison, because back-donation onto the NHC itself will limit back-donation onto the carbonyl ligands.

Recent work from the groups of Bertrand[16] and Ganter[17,18] offer more detailed insight into NHC donor properties. The Bertrand study reported the preparation of various NHC-phosphinidene adducts, and postulated two limiting canonical forms, as shown in Figure 4.2. These range from the phosphinidene extreme, in which the NHC functions solely as a σ-donor, to the phosphaalkene, in which a double bond is present owing to donation from the filled p-orbital on phosphorus to the empty p-orbital on carbon. The ^{31}P NMR chemical shifts for these complexes were therefore proposed to report on the extent of P→C back-donation: more backbonding would result in more extensive deshielding, and hence a more downfield chemical shift. The observed chemical shifts spanned a range of 180 ppm for 16 different NHCs, and thus constitute a more sensitive probe of donicity than the TEP.

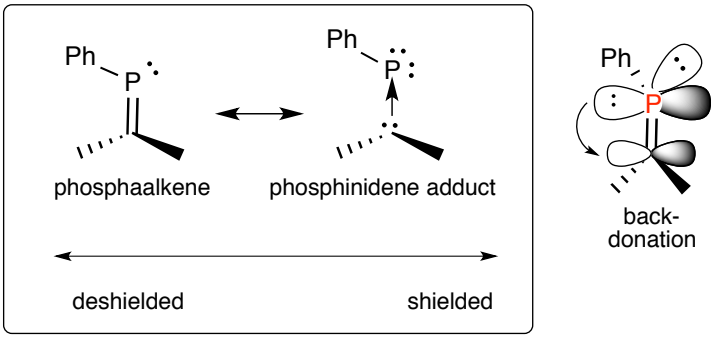

Figure 4.2. The two canonical extremes for RP-NHC binding, and the orbital basis for multiple bonding.

No correlation was found to exist between the TEP for the free NHCs and the ^{31}P NMR chemical shift for the adducts, from which it was inferred that different electronic features dominate the two parameters. Where the TEP was accepted as a reporter on overall donation, the ^{31}P NMR chemical shift was proposed to reflect solely on back-donation. Ganter applied

this analysis to NHC-selenourea adducts, which offer a broader chemical shift window (860 ppm for 22 different NHCs). In a bond energy decomposition analysis of the selenourea adducts,[19] Cavallo and Nolan reported no correlation between shielding and σ-contributions to bonding, but a good correlation with π-contribution, consistent with Bertrand's proposal. In both the selenourea and the phosphinidene scales, therefore, a greater downfield chemical shift is taken to imply a more strongly π-accepting NHC.

On this basis (see Table 4.1), as well as prior computational reports,[16,17,19-29] saturated Arduengo carbenes such as H_2IMes are now widely regarded as being significant π-acceptors, while the π-acidity of IMes is considered to be limited. Consistent with this view are data recently reported by our group, which show restricted rotation (i.e. double-bond character) in the Ru-H_2IMes bond, but not the Ru-IMes bond.[15] This has profound consequences for initiation within the Grubbs class of complexes. The poor π-acceptor capacity of the IMes ligand results in strong Ru→PCy_3 back-donation in the Grubbs methylidene complex $RuCl_2$(IMes)(PCy_3)(=CH_2), resulting in a ca. 8-fold drop in phosphine lability relative to its H_2IMes analogue.

Table 4.1. Electronic parameters for IMe4 and its congener IMe2, relative to IMes and H_2IMes.

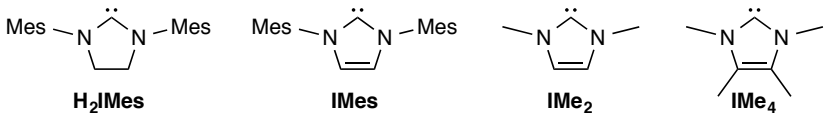

TEP (cm^{-1})	2050.8	2049.6	2051.2	N.R.	[30]
$\delta(^{31}P)$ NHC-PPh	-10.4 ppm	-23.0 ppm	N.R.	-53.5 ppm	[16]
$\delta(^{77}Se)$ NHC-Se	116 ppm	35 ppm	N.R.	3 ppm	[17]

[a] N.R. = not reported.

On the phosphinidene scale, the IMe4 ligand appears to be an even poorer π-acceptor than IMes. Two initial design goals were therefore contemplated: specifically, complexes of the Grubbs and Hoveyda types, containing a single IMe4 ligand (Chart 4.1). Strong σ-donation, coupled with negligible π-acceptor ability, is expected to destabilize binding of the ether donor in the Hoveyda-type complex **Ru-5**. While this should enhance metathesis activity, it may hamper synthesis of the complex. The Grubbs-type complex **Ru-6**, on the other hand, was expected to be considerably more stable, by virtue of enforced π-backbonding onto the phosphine ligand. While this would certainly limit initiation efficiency, it was expected to facilitate initial entry into this class of complexes.

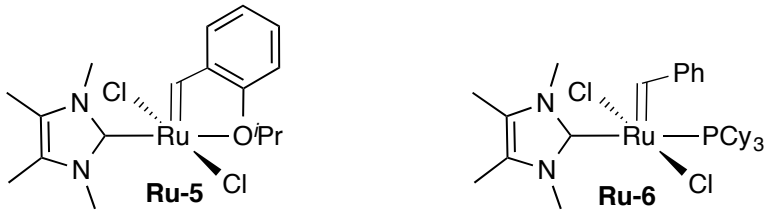

Chart 4.1. Initial design targets.

A survey of the literature reveals few Ru complexes of IMe4. A handful of such complexes have been reported (Chart 4.2, **Ru-7, Ru-H7, Ru-8, Ru-H8**), of which a single example is an alkylidene complex (**Ru-9**).[31] Two IMe_2 alkylidene complexes are also known (**Ru-10, Ru-11**),[32-35] but for both IMe2 and IMe4, examples are limited to mixed-NHC systems in which the second NHC is H_2IMes. Structures of this type, containing two trans-disposed NHC ligands in the basal plane of the square pyramid, require loss of one NHC ligand in order to enter the catalytic cycle. In all cases known to date, such bis-NHC complexes are hampered by slow initiation.[36] The dissociating ligand is generally presumed to be IMe4,[33] based on the appearance of free NHC as observed by time-dependent fluorescence spectroscopy with fluorophore-tagged NHCs.[35] The active species is therefore identical to that generated from **GII**. In short, the mixed H_2IMes-IMe4 (or IMe2) systems **Ru-9–11** suffer not only from slow turnon, but the same limitations of C-H activation as **GII** itself.

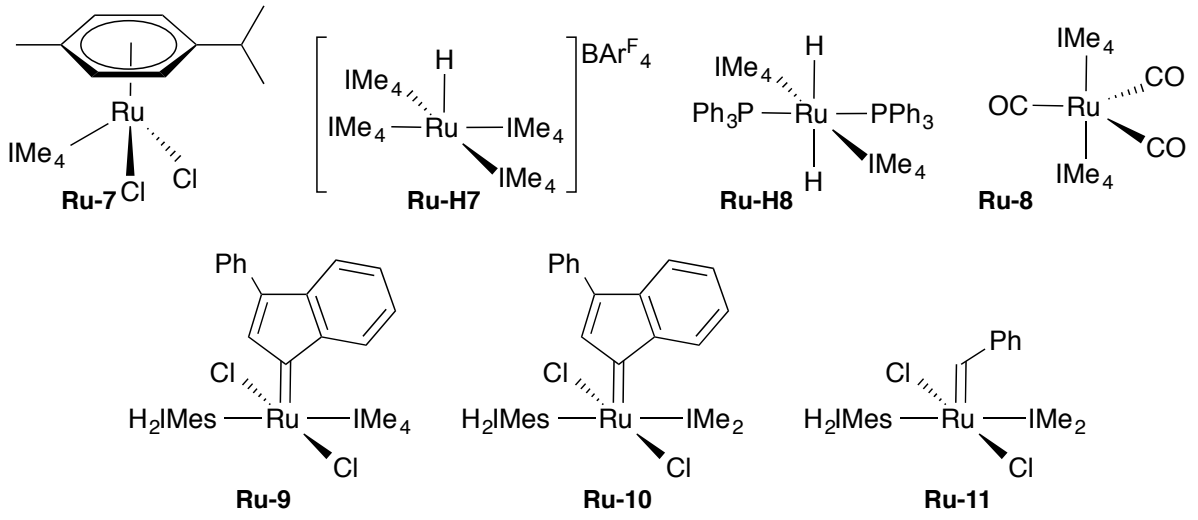

Chart 4.2. Literature complexes of Ru-IMe4 complexes, and known Ru alkylidene complexes bearing the IMe2 or IMe4 ligands.

4.2.2. Results and Discussion

4.2.2.1 Reactions of IMe4 with Ru Precursors

Whittlesey and coworkers have reported that reaction of $RuHCl(PPh_3)_3$ **Ru-H1** with excess NHC, followed by anion exchange with NaBArF, affords the tetra-NHC derivative $[RuH(IMe4)_4]BArF$ **Ru-H7** (Scheme 4.2a).[37] As ruthenium hydrides afford convenient access to alkylidene species by reaction with propargyl chloride, this chemistry was re-examined in the hope of devising access to the mono-derivative. However, treating **Ru-H1** with two equivalents of IMe4 in benzene at RT gave cationic **Ru-H7'** as the sole product (Figure 4.2b). This presumably reflects the strong donor ability and relatively small size[38] of this NHC, although it is striking that the attenuated lability expected for a phosphine ligand trans to NHC is not manifested. Further studies currently being conducted by Ms. Stephanie Rufh of this research group focus on reaction of **Ru-H1** with **Ru-H7**, in the hope that conproportionation will deliver the Ru-hydride complex bearing two IMe4 ligands.

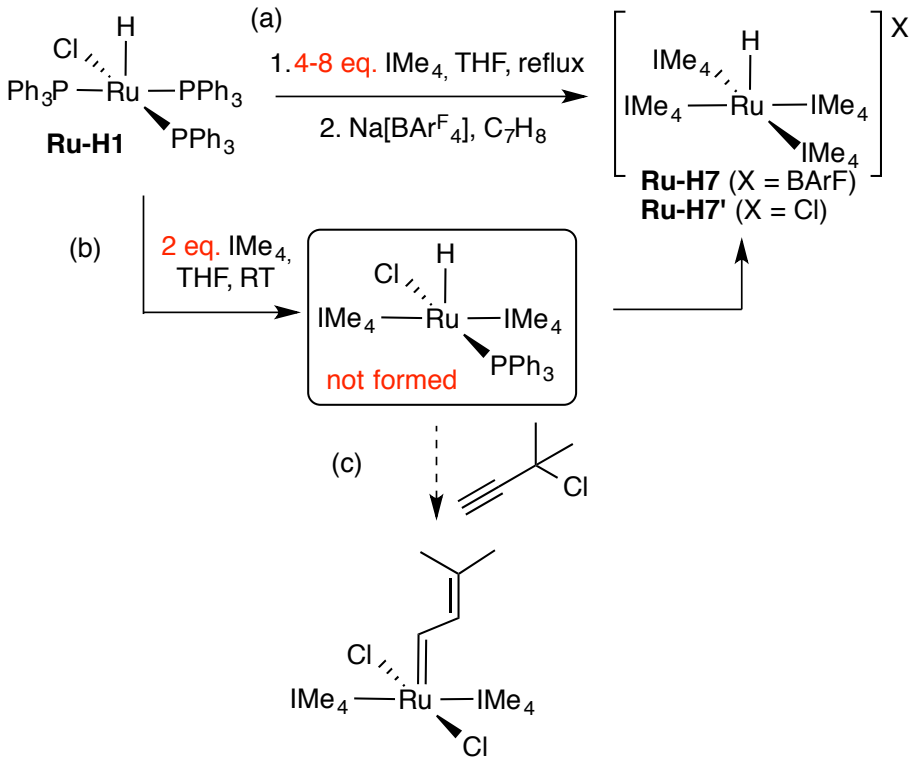

Scheme 4.2. Synthesis of cationic hydride complexes of IMe4. (a) Reaction by Whittlesey and coworkers to form BArF complex **Ru-H7.** (b) Attempted synthesis of bis-IMe_4 complex, leading to formation of cationic **Ru-H7'**. (c) Transformation of a hydride into a vinylidene by reaction with propargyl chloride.

In prior work, Nolan and Plenio independently reported the synthesis of the mono-IMe_2 and IMe_4 alkylidene complexes **Ru-9**,[31] **Ru-10**,[33] and **Ru-11**.[35] All of these complexes are synthesized from the pyridine adducts **GIII** or **GIII-Ind**. Analogously, **GI-py** was treated with 1 equivalent of IMe_4 (Scheme 4.3a). Owing to the increased lability of PCy_3 (cf. H_2IMes used by Plenio and Nolan), selective displacement of the pyridine ligand was not achieved, and up 4–6 different products are observed, depending on the conditions used. The reaction was attempted in toluene, benzene, and pyridine, at RT and -35 °C. In benzene or toluene, three alkylidene signals were observed by ^1H NMR analysis, the $^{31}P\{^1H\}$ NMR spectrum revealed free PCy_3 and two unidentified complexes at 35.2 ppm and 26.7 ppm (integrating at a ratio of 1:0.35:4.3, respectively). The reaction was also attempted in pyridine solvent, as a

means of decreasing the lability of the bound pyridine by pushing the equilibrium toward the starting material. However, multiple products (five alkylidene-containing products) were again observed.

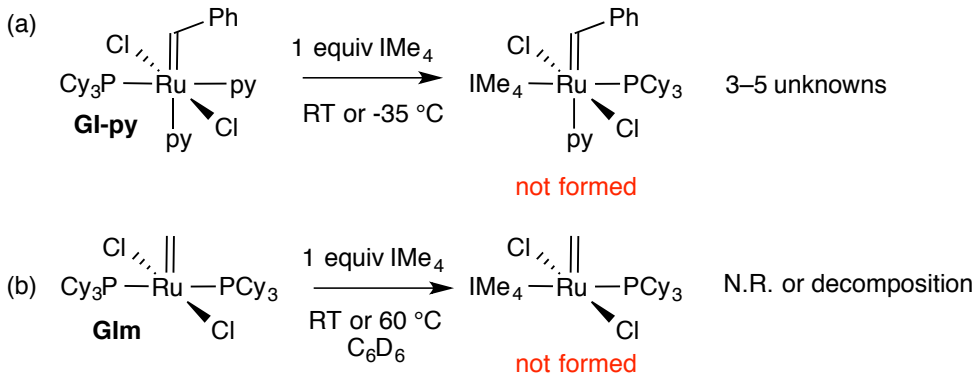

Scheme 4.3. Exploring the reactivity of IMe4 with various Ru=CHR precursors.

In the hope of curbing displacement of the phosphine ligand, **GIm** was employed as an alternative precursor. This methylidene complex is characterized by a significant drop in the lability of the PCy_3 ligand, relative to its benzylidene analogue **GI**.[39] On treating **GIm** with IMe4 at room temperature, the low lability of **GIIm** was manifested in the absence of any discernible reaction over 2 h in C_6D_6 (Scheme 4.3b). At 60 °C, however, decomposition of **GIm** was rapid, and no new alkylidene products were observed.

In another approach, we considered that the bidentate nature of the styrenyl ether ligand of **HI** may help limit the over-addition of IMe4 by increasing the steric constraints at Ru through chelation of the isopropoxy oxygen. **HI** was treated with 1 equivalent of IMe4 (Scheme 4.4). An NMR-scale reaction in C_6D_6 revealed the formation of a new doublet alkylidene at 21.12 ppm (J = 11.5 Hz). A single equivalent of IMe4 was insufficient to

convert all starting **HI,** but retention of the PCy_3 ligand (as judged by the doublet multiplicity of the alkylidene signal) was encouraging. Addition of another equivalent of IMe4 resulted in the formation of two new products by ^1H NMR. Attempts to recoordinate the styrenyl ether by removing the bound PCy_3 using Amberlyst resin[40] or CuCl[41] resulted in non-quantitative reformation of **HI**, implying that the bound IMe_4 ligands are susceptible to protonolysis.

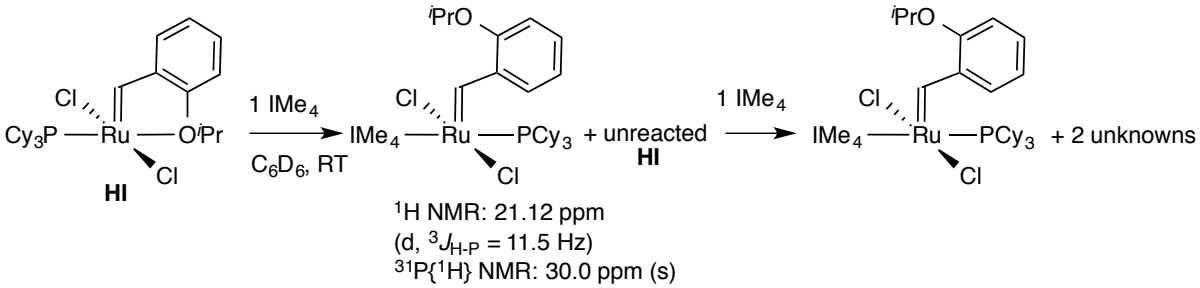

Scheme 4.4. In-situ formation of a mono-IMe4 alkylidene complex by reaction with **HI**.

The reaction of **GI** with one equivalent of free IMe4 was therefore attempted in an NMR-scale reaction (Scheme 4.5). However, the **GI** precursor was only 50% consumed after 3 h at RT in C_6D_6, and three benzylidene singlets were evident in the 20.5-22 ppm region by ^1H NMR analysis. Two new peaks were observed in the $^{31}P\{^1H\}$ NMR, corresponding to free PCy_3 and an unknown species, presumably the mono-IMe4 complex, prior to further displacement of the PCy_3 by another IMe4. By integration against internal standard in the ^1H NMR spectrum, 20% of the total material is missing at 3h, and a green solid is visible as a precipitate in the reaction. The green solid was isolated, and NMR analysis in $CDCl_3$ revealed a single alkylidene peak at 21.0 ppm, but the concentration of the sample was low given the reaction scale. To decrease the rate of ligand substitution the reaction was also

attempted at -35 °C, but the same distribution of species was observed. Similar results were obtained in THF and CH_2Cl_2.

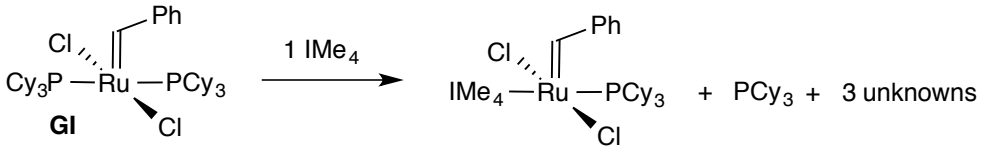

Scheme 4.5. Reaction of **GI** with IMe4.

4.2.2.2 Synthesis and Characterization of Ru-4

Given the difficulty in the installation of a single IMe4 ligand, the synthesis of bis-NHC complexes was re-examined. While a less favoured design target owing to the issue of slow initiation, as discussed above (Section 4.2.1), we considered the possibility that the diminished steric demand of these ligands could enable associative reaction with olefin, which in the Hoveyda catalysts is known to drive loss of a neutral donor.[42] Accordingly, **GI** was treated with 2.1 equiv IMe4 in benzene at room temperature. An immediate colour change from purple to brown occurred, and a green solid precipitated over 18 h. The product was isolated in 66% yield. The immediate colour change upon NHC addition, and the extended reaction time required to get product formation is indicative of a multi-step process occurring. $^{31}P\{^1H\}$ NMR of the isolated solid showed no signals. While ^1H NMR analysis supported a 1:2 ratio of C*H*Ph to I*Me*4, as expected from the reaction stoichiometry, XRD revealed the formation of a dimeric product **Ru-4** (Scheme 4.6).

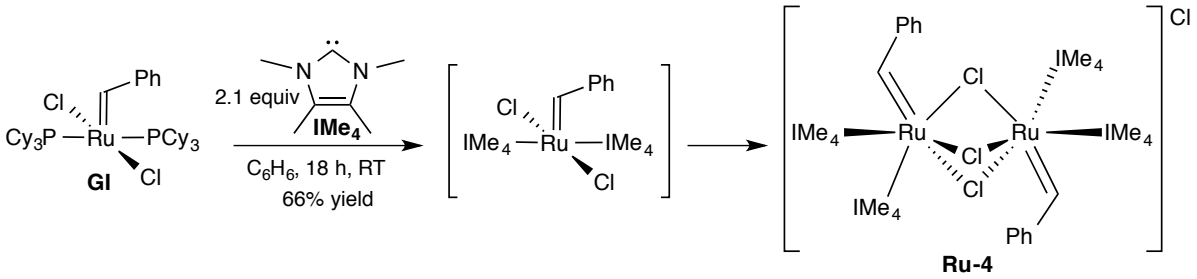

Scheme 4.6. Synthesis of an IMe4 alkylidene complex **Ru-4** from **GI.**

X-ray quality crystals of **Ru-4** were obtained by vapour diffusion of pentane into a saturated dichloroethane solution at ambient temperature over a period of a week. The ORTEP plot is shown in Figure 4.3, with key bond lengths and angles in Tables 4.2 and 4.3. The complex crystallizes as two crystallographically independent, but chemically equivalent dimers containing two Ru(II) centres in slightly distorted octahedral environments. Each consists of a cationic $Ru_2(\mu\text{-}Cl)_3$ dimer, of approximate two-fold symmetry, in which each Ru center additionally bears one benzylidene ligand and two IMe4 ligands.

Given the severely reduced steric bulk of IMe4, as compared to H_2IMes, formation of a dimeric product is unsurprising. This structural motif is very common in Ru complexes bearing small, electron-rich ligands. The challenge for the future is therefore limiting the number of such ligands that originally bind.

References page 97

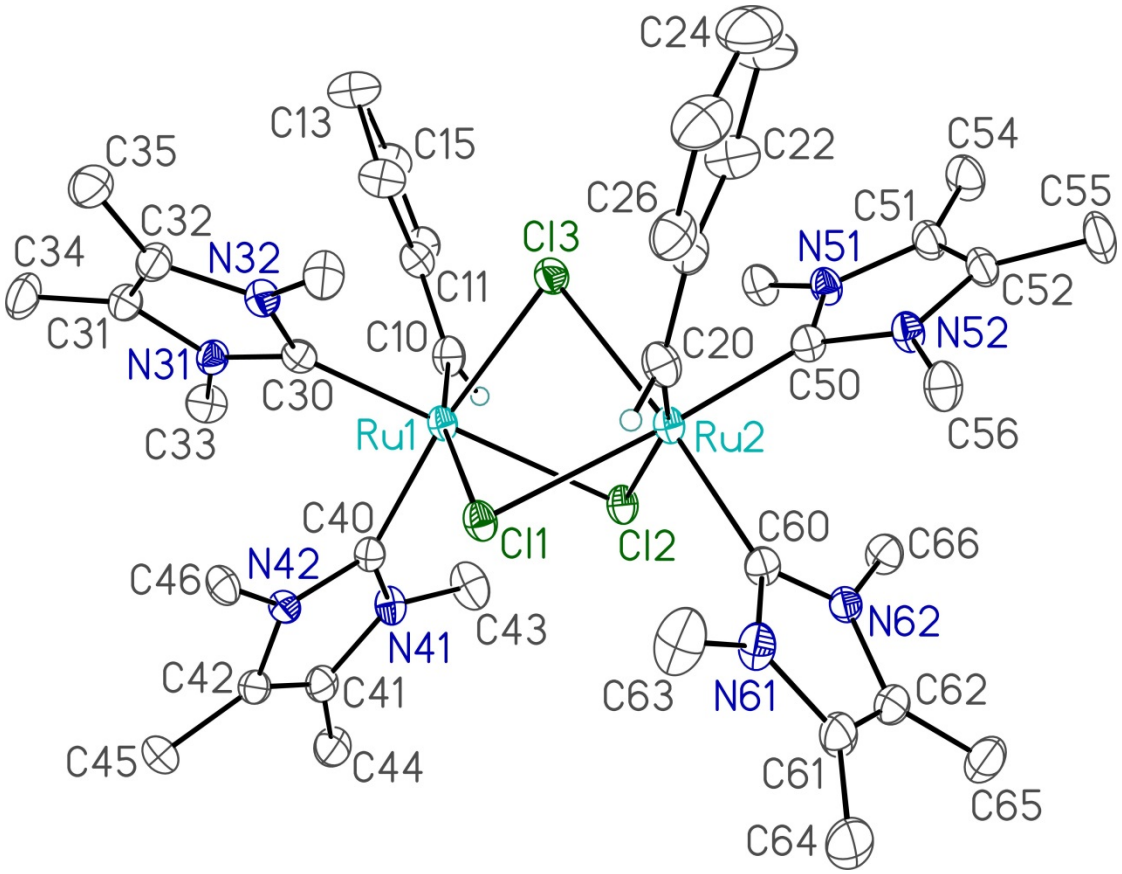

Figure 4.3. Perspective view of one of the two crystallographically-independent **Ru-4** ions (Structure A) showing the atom labelling scheme. Non-hydrogen atoms are represented by Gaussian ellipsoids at the 30% probability level. Hydrogen atoms attached to C10 and C20 are shown with arbitrarily small thermal parameters; all other hydrogens are not shown.

Table 4.2. Selected Interatomic Distances for **Ru-4**.

Structure A			Structure B		
Atom1	Atom2	Distance	Atom1	Atom2	Distance
Ru1	Cl1	2.5926(10)	Ru1	Cl1	2.6535(10)
Ru1	Cl2	2.5497(10)	Ru1	Cl2	2.5622(9)
Ru1	Cl3	2.4967(10)	Ru1	Cl3	2.4825(10)
Ru1	C10	1.870(4)	Ru1	C10	1.864(4)
Ru1	C30	2.024(4)	Ru1	C30	2.018(4)
Ru1	C40	2.046(4)	Ru1	C40	2.050(4)
Ru2	Cl1	2.5601(9)	Ru2	Cl1	2.5576(9)
Ru2	Cl2	2.5952(10)	Ru2	Cl2	2.6410(10)
Ru2	Cl3	2.4812(10)	Ru2	Cl3	2.4891(9)
Ru2	C20	1.860(4)	Ru2	C20	1.860(4)

References page 97

Ru2	C50	2.014(4)	Ru2	C50	2.013(4)
Ru2	C60	2.052(4)	Ru2	C60	2.037(4)

Table 4.3. Selected Interatomic Angles for **Ru-4**.

Structure A				Structure B			
Atom1	Atom2	Atom3	Angle	Atom1	Atom2	Atom3	Angle
Cl1	Ru1	Cl2	77.29(3)	Cl1	Ru1	Cl2	76.47(3)
Cl1	Ru1	Cl3	81.82(3)	Cl1	Ru1	Cl3	81.24(3)
Cl1	Ru1	C10	167.39(13)	Cl1	Ru1	C10	163.59(13)
Cl1	Ru1	C30	98.95(11)	Cl1	Ru1	C30	101.04(11)
Cl1	Ru1	C40	90.28(11)	Cl1	Ru1	C40	91.70(11)
Cl2	Ru1	Cl3	82.45(3)	Cl2	Ru1	Cl3	83.59(3)
Cl2	Ru1	C10	91.91(14)	Cl2	Ru1	C10	91.06(12)
Cl2	Ru1	C30	175.66(12)	Cl2	Ru1	C30	176.85(11)
Cl2	Ru1	C40	91.86(11)	Cl2	Ru1	C40	91.59(11)
Cl3	Ru1	C10	90.40(14)	Cl3	Ru1	C10	86.87(13)
Cl3	Ru1	C30	94.92(12)	Cl3	Ru1	C30	94.15(11)
Cl3	Ru1	C40	171.11(11)	Cl3	Ru1	C40	172.20(11)
C10	Ru1	C30	91.56(17)	C10	Ru1	C30	91.00(16)
C10	Ru1	C40	96.64(18)	C10	Ru1	C40	99.37(17)
C30	Ru1	C40	90.33(16)	C30	Ru1	C40	90.43(15)
Cl1	Ru2	Cl2	77.07(3)	Cl1	Ru2	Cl2	76.77(3)
Cl1	Ru2	Cl3	82.78(3)	Cl1	Ru2	Cl3	83.05(3)
Cl1	Ru2	C20	88.09(14)	Cl1	Ru2	C20	90.70(13)
Cl1	Ru2	C50	175.26(12)	Cl1	Ru2	C50	176.28(11)
Cl1	Ru2	C60	94.46(12)	Cl1	Ru2	C60	93.21(11)
Cl2	Ru2	Cl3	81.83(3)	Cl2	Ru2	Cl3	81.85(3)
Cl2	Ru2	C20	163.99(14)	Cl2	Ru2	C20	163.71(13)
Cl2	Ru2	C50	100.61(12)	Cl2	Ru2	C50	100.48(11)
Cl2	Ru2	C60	88.74(12)	Cl2	Ru2	C60	92.37(11)
Cl3	Ru2	C20	90.49(15)	Cl3	Ru2	C20	86.38(13)
Cl3	Ru2	C50	92.83(12)	Cl3	Ru2	C50	94.11(11)
Cl3	Ru2	C60	170.54(12)	Cl3	Ru2	C60	173.69(11)
C20	Ru2	C50	93.75(18)	C20	Ru2	C50	91.53(16)
C20	Ru2	C60	98.48(19)	C20	Ru2	C60	98.78(17)
C50	Ru2	C60	89.60(16)	C50	Ru2	C60	89.40(15)
Ru1	Cl1	Ru2	82.04(3)	Ru1	Cl1	Ru2	81.59(3)
Ru1	Cl2	Ru2	82.19(3)	Ru1	Cl2	Ru2	81.74(3)

References page 97

Ru1	Cl3	Ru2	85.59(3)	Ru1	Cl3	Ru2	86.46(3)
Ru1	C10	C11	134.6(3)	Ru1	C10	C11	134.1(3)
Ru2	C20	C21	137.1(3)	Ru2	C20	C21	134.4(3)
Ru1	C30	N31	128.0(3)	Ru1	C30	N31	128.3(3)
Ru1	C30	N32	129.3(3)	Ru1	C30	N32	127.6(3)
Ru1	C40	N41	129.3(3)	Ru1	C40	N41	128.2(3)
Ru1	C40	N42	127.4(3)	Ru1	C40	N42	127.4(3)
Ru2	C50	N51	128.4(3)	Ru2	C50	N51	127.7(3)
Ru2	C50	N52	128.5(3)	Ru2	C50	N52	128.5(3)
Ru2	C60	N61	129.7(3)	Ru2	C60	N61	128.6(3)
Ru2	C60	N62	126.7(3)	Ru2	C60	N62	128.6(3)

On comparison of similar angles within a dimer (Table 4.3, Cl1-Ru1-C10 versus Cl2-Ru2-C20 angles) it can be noted that the variability within dimers is similar to the variability between dimers. Differences in the torsional angles between the two dimers point to the effects of packing forces on the geometries of the moieties.

4.2.2.3 Molecular dynamics study: Ru=CHPh and Ru-NHC rotation

The alkylidene region of the ^{1}H NMR spectrum of **Ru-4** revealed three distinct, but broad, singlets, integrating at a ratio of 1: 0.4: 0.1 ($\Delta\nu_{h/2}$ = 6.6, 12.3, and 9.2 Hz, respectively). A molecular dynamics study was undertaken. ^{1}H-^{1}H EXSY experiments revealed chemical exchange between all three alkylidene singlets (Figure 4.4).

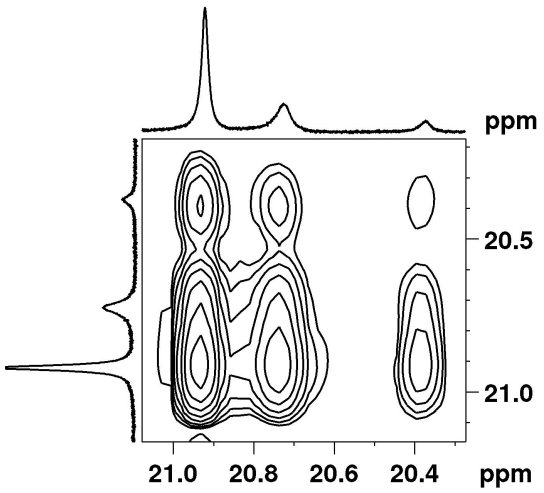

Figure 4.4. ^{1}H-^{1}H EXSY spectrum (300 MHz, CD_2Cl_2) of **Ru-4** demonstrating exchange of all three Ru=C*H*Ph signals.

Generally, EXSY signals arise from the chemical or conformational exchange of two spins. Conformational exchange, in the case of **Ru-4**, is ruled out by the presence of just one set of methyl signals in the ^{1}H NMR spectrum. As shown in Figure 4.5, three unique chemical environments are possible for the alkylidene proton: one where this proton is situated between two NHCs, one where it is between two chlorides, and one where it is between a chloride and an NHC ligand. The IMe_4 ligand is clearly strikingly different from most of the NHCs so far employed in metathesis, in that its reduced bulk affords access to several low-energy rotamers. In comparision, rotation of the benzylidene ligand in **GII** is impeded by unfavourable steric interactions with the PCy_3 ligand,[43] and potentially by favourable π-π interactions between the benzylidene and *N*-mesityl groups.[44]

References page 97

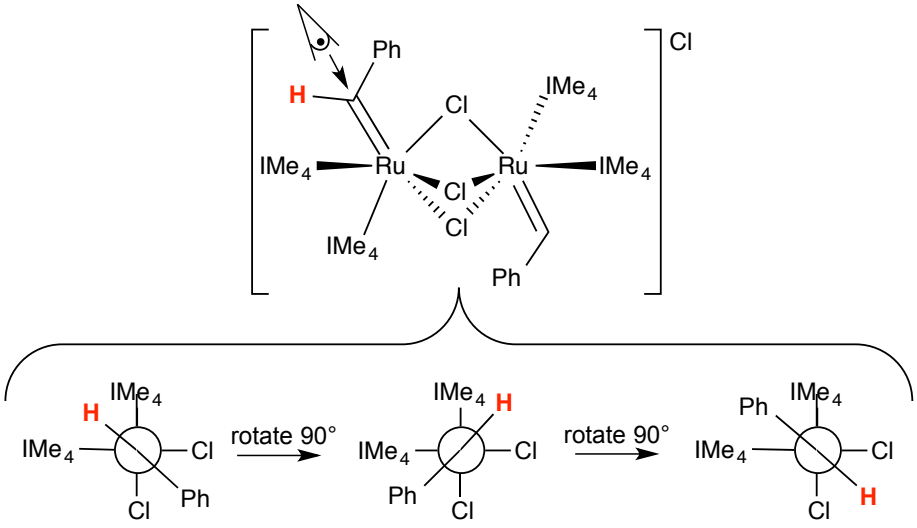

Figure 4.5. Newman projections of **Ru-4**, showing three possible rotational isomers.

Further evidence of alkylidene rotation can be seen in the alkyl region of the ^{1}H-^{1}H EXSY spectrum (Figure 4.6). Correlations are observed between NHCs (dashed arrows, e.g. Me1 with Me8) which are only possible if alkylidene rotation is occurring. Exchange peaks are also observed for all N-*Me* with all C-*Me* signals. Exchange of methyl group Me1 with Me4 (blue arrow), and Me2 with Me3 (red arrow) implies that rotation about the Ru-NHC bond is occurring on the EXSY timescale. Similarly, exchange peaks are observed for Me5 with Me8 (green arrow), and Me6 with Me7 (pink arrow).

As expected, the ^{1}H-^{1}H NOESY spectrum (see Appendix D) revealed through-space interactions of the alkylidene proton with four N-Me groups, as well as the ortho-proton on the benzylidene.

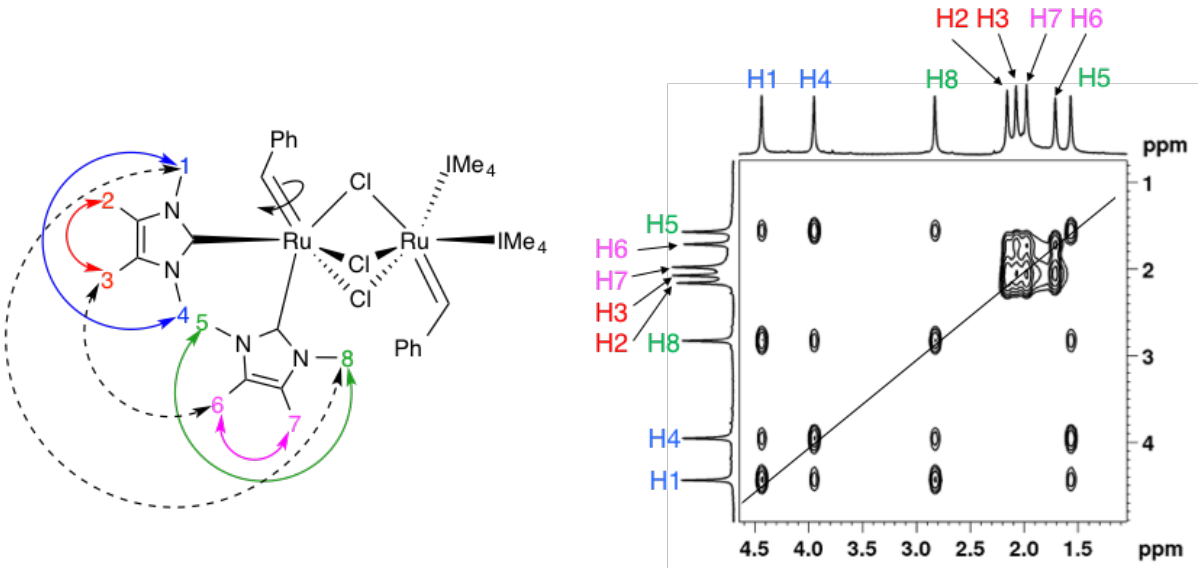

Figure 4.6. ^{1}H-^{1}H EXSY spectrum (300 MHz, CD_2Cl_2) of **Ru-4** demonstrating exchange of all N-*Me* and C-*Me* signals. The diagonal is defined with a line. Select correlations are shown using double-headed arrows.

To further examine the dynamic nature of **Ru-4**, variable temperature NMR was performed. Minor differences are observed up to 60 °C, but coalescence of the alkylidene signals occurs at 70 °C (Figure 4.7). Partial coalescence of the methyl groups is also observed. However, integration of the newly formed broad singlet in the alkyl region vs. integration of the alkylidene proton gives 12:1, accounts for only half the methyl protons. An extremely broad signal in the baseline is assigned to the other four methyl groups (12H) at 70 °C. Low-temperature NOESY experiments should reveal the thermodynamically most stable rotamer, but these have not yet been undertaken.

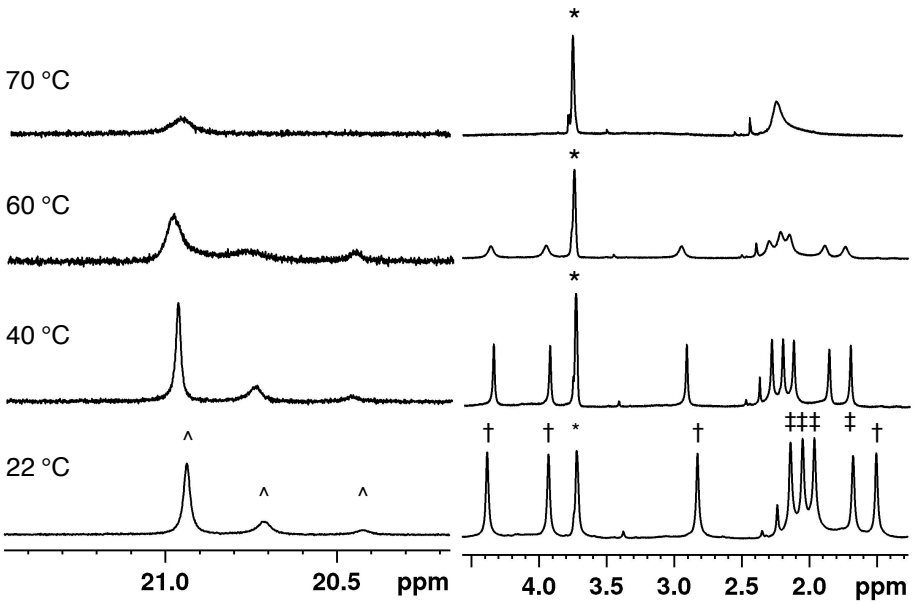

Figure 4.7. Variable-temperature ^{1}H NMR spectrum of dimeric **Ru-4**, demonstrating signal coalescence at 70 °C. For the labels shown in the room-temperature spectrum, ^denotes Ru=C*H*Ph signals; †denotes N*Me* signals; ‡denotes backbone *Me* signals; *denotes residual proton signals due to the NMR solvent.

4.2.2.4 Catalytic Studies

Dimeric **Ru-4** showed limited activity in the RCM of diethyl diallylmalonate in DCE, even at reflux (Figure 4.8a). This is unsurprising, given the coordinative saturation of the two Ru centres in **Ru-4**, which necessitates opening of the thermodynamically stable dimer, or loss of an IMe_4 ligand (Figure 4.8b). Attempts to activate the complex with 2 equivalents of HCl (1 equiv per Ru)[45] resulted in marginal improvement, with 14% RCM after 72 h at 40 °C. Addition of Amberlyst, an acidic ion-exchange resin (8 equiv, 4 equiv per Ru), increased the yield to >50% after 72 h. Acid may aid reactivity by abstracting a IMe4 ligand from the metal centre, as described in Section 4.2.2.1 for the reactions involving **HI**. Controlled access to a reactive edge-bridged, dicationic dimer may be possible by abstracting two chloride ions with, e.g., $NaBAr^{F}$.

References page 97

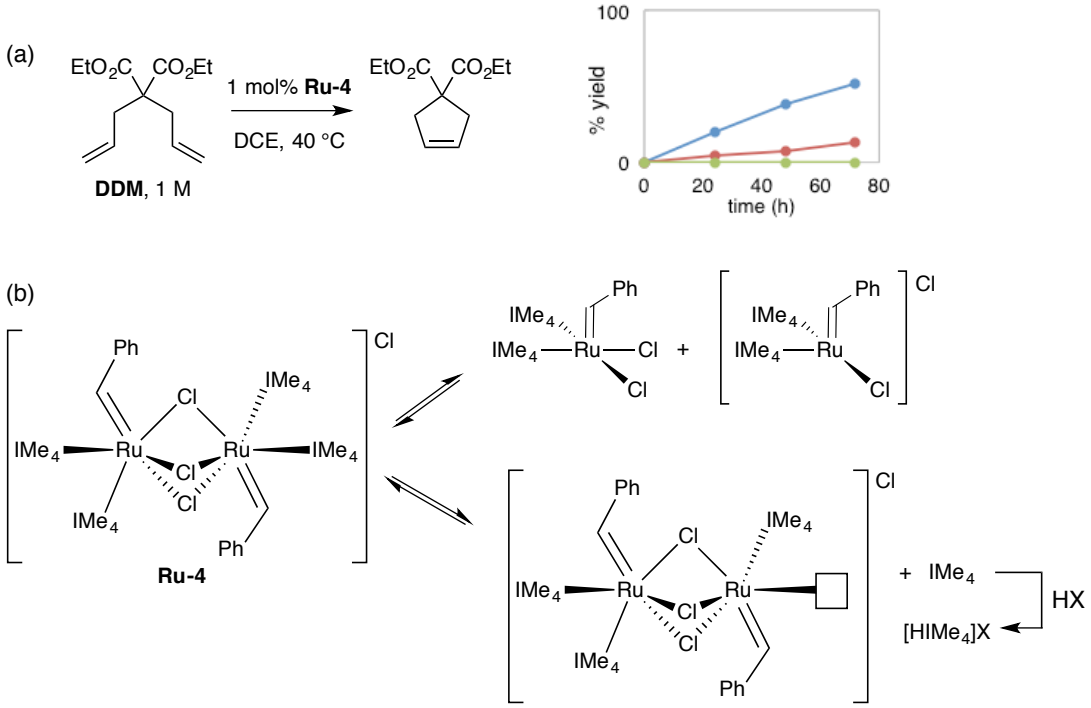

Figure 4.8. (a) RCM of DDM promoted by **Ru-4** without additive (green), with HCl (orange), and with Amberlyst resin (blue). (b) Potential routes into catalytically active derivatives of **Ru-4**.

4.2.3. Conclusions

Despite the difficulties in accessing a monomeric, mono-IMe4 complex, the formation and activity of **Ru-4** highlight key elements of catalyst design. The removal of too much steric bulk at the metal centre can promote deactivation to yield catalytically-inactive face-bridged dimers. Future work will include a systematic variation of the *N*-substituent bulk to determine the minimum requirements to prevent dimerization. The effect of backbone saturation and substitution on reaction chemistry and catalytic activity will also be examined by Ms. Stephanie Rufh of this research group.

References page 97

4.2.4. Experimental Details for Section 4.2.

4.2.4.1 General Procedures

All reactions were carried out in an N_2-filled glovebox. Dry, oxygen-free, C_6H_6, and C_7H_8 were obtained using a Glass Contour solvent purification system. Dichloroethane was dried over Ca_SO_4 for 12 h under N_2, then heated to reflux over P_2O_5 for 6 h prior to distillation. Pentane was dried similarly over Mg_2SO_4 then P_2O_5. NMR solvents ($CDCl_3$, CD_2Cl_2, DCE-d4 and C_6D_6) were degassed by five freeze-pump-thaw cycles. All solvents were stored in the glovebox over 4 Å molecular sieves, with the exception of DCE and DCE-d4, which were stored over 5 Å molecular sieves.

All reagents were purchased from Sigma-Aldrich unless otherwise specified. Anhydrous *n*-decane (>99% purity; internal standard for gas chromatography) was used as received. Diethyl diallylmalonate (98%; Sigma-Aldrich) was degassed by five freeze-pump-thaw cycles, and stored under N_2 in the glovebox. Potassium hydrotris(1-pyrazolyl)borate (KTp; >97%) was purchased from TCI and used as received. IMe_4,[14] **GI**,[46] **HI**,[40] **GI-py**,[47] **GIm**,[48] and **Ru-H1**[49] were synthesized by literature methods.

NMR spectra were recorded on a Bruker Avance 300 or 500 MHz spectrometer at spectrometers at 23 °C, unless otherwise noted, and referenced to the residual proton or carbon signals of the deuterated solvent. Signals are reported in ppm relative to TMS (^1H, ^{13}C) at 0 ppm. NOESY / EXSY experiments were collected using a mixing time of 0.06 s.

References page 97

GC quantification was performed on samples diluted with CH_2Cl_2 (ACS reagent grade) on an Agilent 7890A Series GC equipped with a flame ionization detector (FID), an Agilent 7683B Series autosampler and an Agilent HP-5 polysiloxane column (30 m length, 320 μm diameter), using an inlet split ratio of 10:1, an inlet temperature of 250 °C, and helium (UHP grade) as the carrier gas to maintain column pressure at 11.512 psi. The FID response was maintained between 50-2000 ρA, using analyte concentrations of ca. 5 mM. Calibration curves (peak areas vs. concentration) were constructed in the relevant concentration regime, to account for the dependence on detector response for substrates, products and decane (internal standard in catalytic runs). Conversions and yields in catalytic runs were determined from the integrated peak areas, referenced against decane, and compared to the initial substrate : decane integration ratio.

4.2.4.2 Representative Procedure for Metathesis.

A 4 mL vial was loaded with diethyl diallylmalonate (481 mg, 2 mmol), decane (285 mg, 2 mmol) and DCE (0.62 mL). A ca. 10 μL aliquot was removed for GC-FID analysis to establish the starting ratio of substrate to decane. **Ru-4** (10.2 mg, 0.01 mmol, 1 mol% Ru) was then added, and the reaction was stirred open to the well-purged glovebox atmosphere for 24 h. Aliquots were taken from the stirred reaction at specific time intervals, quenched with KTp, diluted with CH_2Cl_2 on the bench, and analyzed by GC-FID.

4.2.4.3 Synthesis and Characterization of Ru-4, $[Ru_2(\mu\text{-}Cl)_3(CHPh)_2(IMe_4)_4]Cl$

In the glovebox, purple **GI** (120 mg, 0.15 mmol) was dissolved in 15 mL C_6H_6 in a 20 mL vial. Free IMe_4 (38 mg, 0.3 mmol, 2.1 equiv) was added as a white powder, upon which the solution immediately changed colour from purple to brown. The solution was stirred for 18 h at 23 °C, over which time a green solid deposited. The green solid was collected on a fine frit, and washed with benzene (3 × 2 mL) and pentane (3 × 2 mL) to yield **Ru-4** as an emerald-green powder, which proved soluble in chlorinated solvents (CH_2Cl_2, $CHCl_3$, DCE), sparingly soluble in THF, and completely insoluble in diethyl ether, benzene, toluene, hexanes, and pentane. The insolubility of the complex in the latter solvents enabled purification without reprecipitation. ^{1}H NMR analysis of brown filtrate / washings revealed multiple alkylidene-containing products. Yield of pure **Ru-4**: 50 mg (66%). X-ray quality crystals were grown by vapour diffusion of pentane into DCE at 298 K (glovebox, 1 week). ^{1}H NMR (DCE-d_4, 500 MHz, 298 K) δ 20.93, 20.71, 20.43 (3 × br s, 1H, H^{15}), 7.48 (t, $^3J_{H\text{-}H}$ = 7.0 Hz, 1H, H^{19}), 7.41 (d, $^3J_{H\text{-}H}$ = 7.4 Hz, 2H, H^{17}), 7.29 – 7.04 (overlapping multiplet, 2H, H^{18}), 4.39 (s, 3H, H^1), 3.93 (s, 3H, H^4), 2.83 (s, 3H, H^8), 2.14 (s, 3H, H^2), 2.05 (s, 3H, H^3), 1.96 (s, 3H, H^7), 1.68 (s, 3H, H^6), 1.51 (s, 3H, H^5). ^{13}C NMR (DCE-d_4, 125.7 MHz, 298 K) δ 322.7 (C^{16}, located via the ^{1}H-^{13}C HMQC correlation with H^{15}), 172.6 (C^9 or C^{10}), 171.6 (C^{10} or C^9), 154.8 (C^{16}), 130.3–128.3 (overlap; C^{17}, C^{18}, C^{19}), 126.7 (C^{11}), 126.3 (two overlapping s, C^{12}, C^{14}), 125.1 (C^{13}), 36.4 (C^4), 35.4 (C^1), 34.6 (C^8), 32.5 (C^5), 9.9 – 8.9 (4 overlapping s, C^2, C^3, C^6, C^7). Anal. Calcd. for $C_{21}H_{30}Cl_2N_4Ru$: C, 49.41%; H, 5.92%; N, 10.98%. Found: pending.

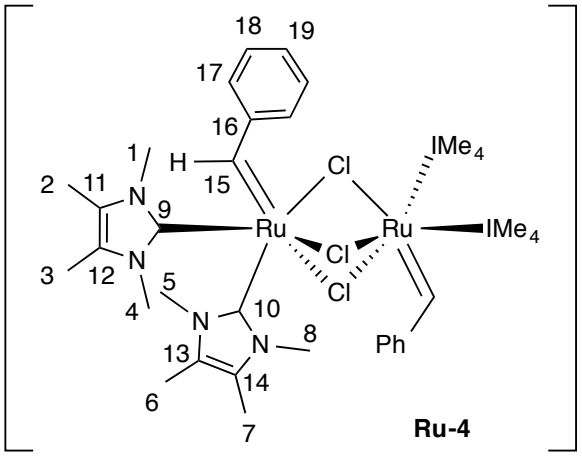

Ru-4

4.3. References

(1) Poater, A.; Ragone, F.; Correa, A.; Cavallo, L. *J. Am. Chem. Soc.* **2009**, *131*, 9000-9006.

(2) Hong, S. H.; Wenzel, A. G.; Salguero, T. T.; Day, M. W.; Grubbs, R. H. *J. Am. Chem. Soc.* **2007**, *129*, 7961–7968.

(3) Leitao, E. M.; Dubberley, S. R.; Piers, W. E.; Wu, Q.; McDonald, R. *Chem. Eur. J.* **2008**, *14*, 11565–11572.

(4) Burling, S.; Paine, B. M.; Nama, D.; Brown, V. S.; Mahon, M. F.; Prior, T. J.; Pregosin, P. S.; Whittlesey, M. K.; Williams, J. M. J. *J. Am. Chem. Soc.* **2007**, *129*, 1987–1995.

(5) Abdur-Rashid, K.; Fedorkiw, T.; Lough, A. J.; Morris, R. H. *Organometallics* **2004**, *23*, 86–94.

(6) Trnka, T. M.; Morgan, J. P.; Sanford, M. S.; Wilhelm, T. E.; Scholl, M.; Choi, T.-L.; Ding, S.; Day, M. W.; Grubbs, R. H. *J. Am. Chem. Soc.* **2003**, *125*, 2546–2558.

(7) Hong, S. H.; Chlenov, A.; Day, M. W.; Grubbs, R. H. *Angew. Chem. Int. Ed.* **2007**, *46*, 5148–5151.

(8) Mathew, J.; Koga, N.; Suresh, C. H. *Organometallics* **2008**, *27*, 4666–4670.

(9) Vieille-Petit, L.; Luan, X.; Gatti, M.; Blumentritt, S.; Linden, A.; Clavier, H.; Nolan, S. P.; Dorta, R. *Chem. Commun.* **2009**, 3783–3785.

(10) Vehlow, K.; Gessler, S.; Blechert, S. *Angew. Chem. Int. Ed.* **2007**, *46*, 8082–8085.

(11) Herbert, M. B.; Lan, Y.; Keitz, B. K.; Liu, P.; Endo, K.; Day, M. W.; Houk, K. N.; Grubbs, R. H. *J. Am. Chem. Soc.* **2012**, *134*, 7861–7866.

(12) Chung, C. K.; Grubbs, R. H. *Org. Lett.* **2008**, *10*, 2693–2696.

(13) Ritter, T.; Day, M. W.; Grubbs, R. H. *J. Am. Chem. Soc.* **2006**, *128*, 11768–11769.

(14) Kuhn, N.; Kratz, T. *Synthesis* **1993**, 561–562.

(15) Lummiss, J. A. M.; Higman, C. S.; Fyson, D. L.; McDonald, R.; Fogg, D. E. *Chem. Sci.* **2015**, *6*, 6739–6746.

(16) Back, O.; Henry-Ellinger, M.; Martin, C. D.; Martin, D.; Bertrand, G. *Angew. Chem. Int. Ed.* **2013**, *52*, 2939 –2943.

(17) Liske, A.; Verlinden, K.; Buhl, H.; Schaper, K.; Ganter, C. *Organometallics* **2013**, *32*, 5269−5272.

(18) Verlinden, K.; Buhl, H.; Frank, W.; Ganter, C. *Eur. J. Inorg. Chem.* **2015**, *2015*, 2416–2425.

(19) Vummaleti, S. V. C.; Nelson, D. J.; Poater, A.; Gomez-Suarez, A.; Cordes, D. B.; Slawin, A. M. Z.; Nolan, S. P.; Cavallo, L. *Chem. Sci.* **2015**, *8*, 1895–1904.

(20) Minenkov, Y.; Occhipinti, G.; Heyndrickx, W.; Jensen, V. R. *Eur. J. Inorg. Chem.* **2012**, 1507–1516

(21) Comas-Vives, A.; Harvey, J. N. *Eur. J. Inorg. Chem.* **2011**, 5025-5035.

(22) Antonova, N. S.; Carbo, J. J.; Poblet, J. M. *Organometallics* **2009**, *28*, 4283–4287. As DFT calculations were carried out on a model $RuCl_2(NHC)(PH_3)(=CH_2)$ system, the computed Ru–NHC back-donation should be regarded as a lower limit.

(23) Ciancaleoni, G.; Scafuri, N.; Bistoni, G.; Macchioni, A.; Tarantelli, F.; Zuccaccia, D.; Belpassi, L. *Inorg. Chem.* **2014**, *53*, 9907−9916.

(24) Getty, K.; Delgado-Jaime, M. U.; Kennepohl, P. *J. Am. Chem. Soc.* **2007**, *129*, 15774–15776.

(25) , For early computational or integrated experimental/computational studies showing evidence of backbonding onto NHC ligands, see: (a) M. Tafipolsky, W. Scherer, K. Öfele, G.

Artus, B. Pedersen, W. A. Herrmann and G. S. McGrady, *J. Am. Chem. Soc.*, 2002, **124**, 5865–5880. (b) D. Nemcsok, K. Wichmann and G. Frenking, *Organometallics* 2004, **23**, 3640–3646. (c) X. Hu, I. Castro-Rodriguez, K. Olsen and K. Meyer, *Organometallics*, 2004, **23**, 755–764. (d) G. Occhipinti, H.-R. Bjorsvik and V. R. Jensen, *J. Am. Chem. Soc.*, 2006, **128**, 6952–6964. (e) H. Jacobsen, A. Correa, C. Costabile and L. Cavallo, *J. Organomet. Chem.*, 2006, **691**, 4350–4358. (f) E. F. Penka, C. W. Schlapfer, M. Atanasov, M. Albrecht and C. Daul, *J. Organomet. Chem.*, 2007, **692**, 5709–5716.

(26) For early experimental evidence of the π-acceptor ability of NHC ligands, see: (a) A. A. D. Tulloch, A. A. Danopoulos, S. Kleinhenz, M. E. Light, M. B. Hursthouse and G. Eastham, *Organometallics*, 2001, **20**, 2027–2031. (b) L. Mercs, G. Labat, A. Neels, A. Ehlers and M. Albrecht, *Organometallics*, 2006, **25**, 5648-5656. (c) M. D. Sanderson, J. W. Kamplain and C. W. Bielawski, *J. Am. Chem. Soc.*, 2006, **128**, 16514-16515. (d) S. Fantasia, J. L. Petersen, H. Jacobsen, L. Cavallo and S. P. Nolan, *Organometallics*, 2007, **26**, 5880–5889. (e) D. M. Khramov, V. M. Lynch and C. W. Bielawski, *Organometallics*, 2007, **26**, 6042–6049.

(27) Diez-Gonzalez, S.; Nolan, S. P. *Coord. Chem. Rev.* **2007**, *251*, 874–883.

(28) Jacobsen, H.; Correa, A.; Poater, A.; Costabile, C.; Cavallo, L. *Coord. Chem. Rev.* **2009**, *253*, 687–703.

(29) Marchione, D.; Belpassi, L.; Bistoni, G.; Macchioni, A.; Tarantelli, F.; Zuccaccia, D. *Organometallics* **2014**, *33*, 4200−4208.

(30) Nelson, D. J.; Nolan, S. P. *Chem. Soc. Rev.* **2013**, *42*, 6723–6753.

(31) Bantreil, X.; Randall, R. A. M.; Slawin, A. M. Z.; Nolan, S. P. *Organometallics* **2010**, *29*, 3007–3011.

(32) Wolf, S.; Plenio, H. *Green Chem.* **2011**, *13*, 2008–2012.

(33) Peeck, L. H.; Plenio, H. *Organometallics* **2010**, *29*, 2761–2766.

(34) Lujan, C.; Nolan, S. P. *Catal. Sci. Technol.* **2012**, *2*, 1027-1032.

(35) Sashuk, V.; Peeck, L. H.; Plenio, H. *Chem. Eur. J.* **2010**, *16*, 3983–3993.

(36) Weskamp, T.; Schattenmann, W. C.; Spiegler, M.; Herrmann, W. A. *Angew. Chem. Int. Ed.* **1998**, *37*, 2490–2493.

(37) Davies, C. J. E.; Lowe, J. P.; Mahon, M. F.; Poulten, R. C.; Whittlesey, M. K. *Organometallics* **2013**, *32*, 4927–4937.

(38) Clavier, H.; Nolan, S. P. *Chem. Commun.* **2010**, *46*, 841–861.

(39) Ulman, M.; Grubbs, R. H. *J. Org. Chem.* **1999**, *64*, 7202–7207.

(40) van Lierop, B. J.; Reckling, A. M.; Lummiss, J. A. M.; Fogg, D. E. *ChemCatChem* **2012**, *4*, 2020–2025.

(41) Garber, S. B.; Kingsbury, J. S.; Gray, B. L.; Hoveyda, A. H. *J. Am. Chem. Soc.* **2000**, *122*, 8168–8179.

(42) Thiel, V.; Hendann, M.; Wannowius, K.-J.; Plenio, H. *J. Am. Chem. Soc.* **2012**, *134*, 1104–1114.

(43) Straub, B. F. *Angew. Chem. Int. Ed.* **2005**, *44*, 5974–5978.

(44) Fürstner, A.; Ackermann, L.; Gabor, B.; Goddard, R.; Lehmann, C. W.; Mynott, R.; Stelzer, F.; Thiel, O. R. *Chem. Eur. J.* **2001**, *7*, 3236–3253.

(45) Rouen, M.; Queval, P.; Falivene, L.; Allard, J.; Toupet, L.; Crévisy, C.; Caijo, F.; Baslé, O.; Cavallo, L.; Mauduit, M. *Chem. Eur. J.* **2014**, *20*, 13716–13721.

(46) Schwab, P.; Grubbs, R. H.; Ziller, J. W. *J. Am. Chem. Soc.* **1996**, *118*, 100–110.

(47) Trnka, T. M.; Dias, E. L.; Day, M. W.; Grubbs, R. H. *ARKIVOC* **2002**, 28–41.

(48) Lummiss, J. A. M.; Beach, N. J.; Smith, J. C.; Fogg, D. E. *Catal. Sci. Technol.* **2012**, *2*, 1630–1632.

(49) Schunn, R. A.; Wonchoba, E. R.; Wilkinson, G. *Inorg. Synth.* **1971**, *13*, 131–134.

Chapter 5. Transformation of Essential-Oil Phenylpropenoids into High-Value Products

5.1. Context and Objectives

Much of the work discussed in preceding Chapters focuses on double-bond isomerization as a challenge in metathesis. A particular emphasis was placed on identifying the origin of such behaviour, as a first step in developing potential means of circumventing it. The present Chapter instead focuses on synthetic opportunities created by isomerization. The combination of metathetical and non-metathetical catalytic transformations in tandem catalysis has captured much attention.[1] Interest in deliberately combining metathesis with isomerization is of long standing. While this interest may be due in part to the simple ubiquity of isomerization as a side-reaction, there is no question that such tandem methodologies can offer significant advantages in terms of synthetic scope and convenience. Most widely explored is the tandem metathesis–isomerization, in which both transformations are effected using a single precatalyst. Such processes are now well established, and can proceed with good yields and selectivities.[2] More challenging is the reverse approach: that is, isomerization followed by metathesis. This Chapter explores the feasibility of isomerization-metathesis protocols for the transformation of naturally-occurring essential oils into high-value cinnamates and ferulates.

5.1.1. Published Contributions

Tandem catalysis versus One-Pot Catalysis: Ensuring Process Orthogonality in the Transformation of Essential-Oil Phenylpropenoids into High-Value Products via Olefin Isomerization-Metathesis

Carolyn S. Higman, Marcio P. de Araujo, and Deryn E. Fogg *Catal. Sci. Tech.* **2016,** Advance Article, DOI: 10.1039/c5cy02038g (selected as Cover Article).

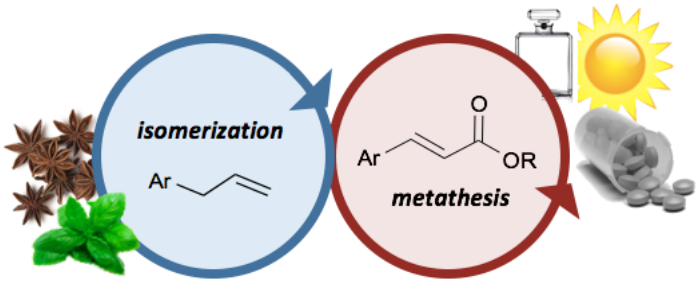

Conversion of essential-oil allylbenzenes (phenylpropenoids) to high-value fine chemicals via isomerization-metathesis is reported. The target reaction sequence involves isomerization of $ArCH_2CH=CH_2$ **1** into the corresponding conjugated olefins **2**, and ensuing cross-metathesis with acrylates to generate $ArCH=CHCO_2R$ **3**. The second-generation Hoveyda catalyst **HII** was chosen for the metathesis step. A range of lead candidates was assessed for the isomerization step, of which most active was the Grotjahn catalyst $[CpRu(PN)(MeCN)]PF_6$ (**Ru-2**; PN = 2-P^{i}Pr$_2$-4-^{t}Bu-1-Me-imidazole). The following order of isomerization activity was determined, using the isomerization of estragole **1a** to anethole **2a** (Ar = *p*-$MeOC_6H_4$) as a probe reaction: $[CpRu(PN)(MeCN)]PF_6$ > $RuHCl(CO)(PPh_3)_3$ > $Ru(Me\text{-}allyl)_2(COD)$ > $Pd_2Br_2(P^tBu_3)_2$ > $RuHCl(PPh_3)_3$ > $RuCl_3(\mu_2\text{-}C)(\kappa^1\text{-}C,\mu_2,\eta^6\text{-}Mes\text{-}H_2IMes)Ru(H)(H_2IMes)$ (the "Grubbs hydride") > $RuHCl(CO)(H_2IMes)(PCy_3)$ > $RuHCl(CO)(IMes)(PCy_3)$ > $RuHCl(CO)(PCy_3)_2$. To maximize process efficiency, a systematic comparison of orthogonal tandem catalysis versus sequential catalyst addition was undertaken, using catalysts **Ru-2** and **HII**. The impact of each process type on product selectivity and catalyst compatibility was assessed. Selectivity was undermined in tandem isomerization-metathesis by competing metathesis of **1**. Sequential catalyst addition

References page 122

eliminated this problem. The isomerization catalyst **Ru-2** adversely affected metathesis yields when equimolar with **HII**, an effect traced to the imidazole functionality in **Ru-2**. However, at the low catalyst loadings required for efficient isomerization (0.1 mol% **Ru-2**), negligible impact on metathesis yields was evident. The target cinnamates and ferrulates were obtained in quantitative yields by coupling these steps in a one-pot isomerization-metathesis protocol.

Author Contributions: The manuscript was written by CSH and DEF. CSH performed all experiments presented in the paper. Initial experiments were performed by MPA.

5.2. Tandem catalysis versus One-Pot Catalysis: Ensuring Process Orthogonality in the Transformation of Essential-Oil Phenylpropenoids into High-Value Products via Olefin Isomerization-Metathesis

5.2.1. Introduction

Notwithstanding recent advances in the discovery and exploitation of fossil-fuel reserves,[3] the long-term prospect is one of dwindling supplies at increasing cost. Development of synthetic methodologies based on renewable resources thus remains an imperative.[4,5] Among such resources, essential oils stand out for the high proportion of functionalized, readily modified aromatic compounds more typically available from petrochemicals.[6] Of particular note for their abundance are functionalized allylbenzenes **1** (Fig. 1a), which serve as important precursors to the conjugated phenylpropenoids **2**. We recently described the metathetical transformation of **2** into high-value antioxidants for the personal-care market (see, e.g., **4a**; Figure 5.1b).[7] More generally, conjugated arylpropenes of type **2** are of interest as renewable feedstocks that can be elaborated into polyfunctional aromatic targets via olefin

References page 122

metathesis.[6-12] This approach can be seen as complementary to strategies focused on metathetical degradation of biomass into simple building-blocks for commodity chemicals manufacturing.[13-15]

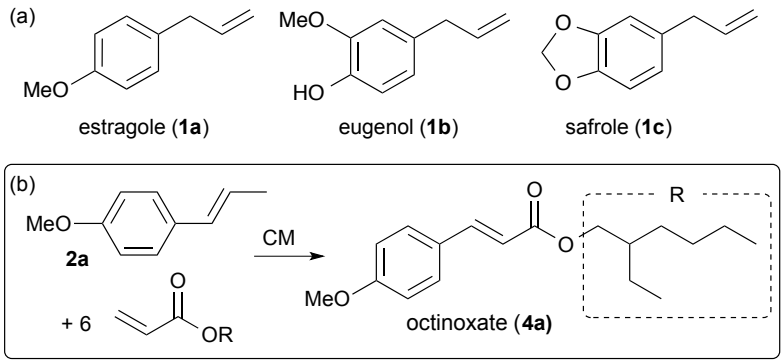

Figure 5.1. (a) Functionalized allylbenzenes (phenylpropenoids; 2-propenylbenzenes). (b) Transformation of conjugated phenylpropenoids (1-propenylbenzenes) to high-value cinnamates and ferulates.

In the present study, we sought to expand the scope of this chemistry by coupling the metathesis step with a prior isomerization reaction, in order to harness the more abundant 1-arylpropene feedstocks. Industrially, isomerization of estragole **1a** to its conjugated isomer anethole **2a** is reportedly effected by treatment with excess KOH at 200 °C.[16,17] Much interest has focused on the development of alternative, catalytic routes, and a wide range of catalysts has now been reported.[18]

In considering routes from **1** to **3**/**4** (methyl- and ethylhexyl-acrylate cross products, respectively), we were particularly interested in one-pot processes, which eliminate the inefficiency and materials waste associated with the intervening workup to isolate **2**. Tandem catalysis, as a specific embodiment of this approach, is of added interest in moving beyond stoichiometric methodologies.[19] Tandem metathesis-isomerization is now well established,

and has recently been reviewed.[2,20] Such processes typically rely on "assisted tandem catalysis",[17b] involving the induced decomposition of a ruthenium metathesis catalyst into isomerization-active species. Isomerization can be highly efficient, ambiguities in the identity of the active catalyst notwithstanding.[21]

Required here is the opposite sequence: that is, tandem isomerization-metathesis. Early examples of success in such methodologies were largely substrate-specific, in that ring strain or steric constraints precluded metathesis prior to the isomerization step.[22-24] In the absence of such constraints, tandem isomerization-metathesis is commonly hampered by poor process orthogonality. Product selectivity is limited by both premature metathesis, and isomerization of the product. In an elegant example of orthogonal tandem catalysis[19b] applied to olefin homologation, Grotjahn and Schrock resolved this issue by deploying a metathesis catalyst that is unreactive toward internal olefins, and an isomerization catalyst that is remarkably selective for reaction with trans-olefinic linkages (see Scheme 5.1).[25]

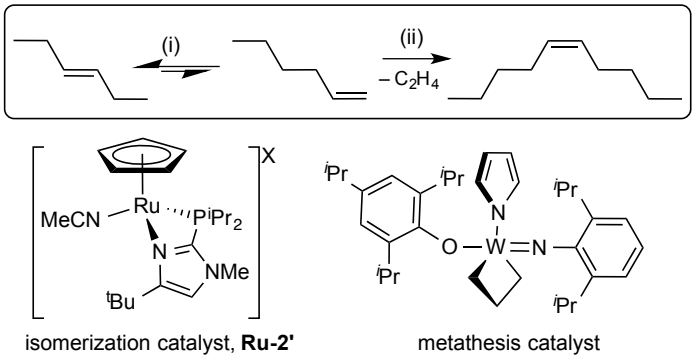

Scheme 5.1. Selective homologation of C_n (*E*)-olefins into C_{2n-2} (*Z*)-olefins via orthogonal tandem catalysis, involving concurrent processes of (i) isomerization; (ii) metathesis.

In related work, Consorti, Dupont, and co-workers achieved selectivity by immobilizing the metathesis catalyst in an ionic liquid phase, with an isomerization catalyst in the organic phase. Preferential solubility of the olefinic substrates in the organic layer accelerated isomerization relative to metathesis.[26] Finally, Mauduit and Carreaux employed a system in which isomerization is promoted by choosing a Ru-IPr metathesis catalyst, for which the onset of decomposition to isomerization-active species is rapid (IPr = 1,3-bis(2,6-diisopropylphenyl)imidazol-2-ylidene).[27]

Gooβen's synthesis of functionalized styrenes via "isomerizing metathesis" embodies an alternative strategy, again based on orthogonal tandem catalysis.[28,29] Here the terminal olefin in the phenolic precursor is isomerized toward the more thermodynamically stable, conjugated site, following which the styrenyl target is generated by cross-metathesis with ethylene (CM "ethenolysis"; Scheme 5.2, top). Any incidence of metathesis prior to complete isomerization is immaterial, as this simply results in stepwise shortening of the side-chain by ethenolysis, prior to another isomerization step (Scheme 5.2, bottom). Gooβen and Cole-Hamilton recently applied this strategy to the synthesis of tsetse fly attractants,[28] while Nolan and co-workers utilized the same approach to convert **1** into the corresponding styrenes.[30]

References page 122

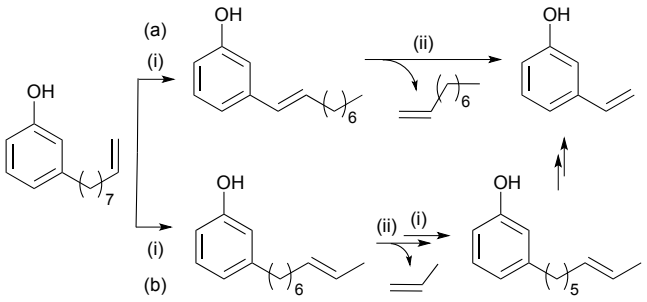

Scheme 5.2. Example of selectivity in isomerization-metathesis, achieved by metathetical excision of the extraneous alkyl chain. Shown are two extremes: (a) Multi-site isomerization to the conjugated position, followed by ethenolysis. (b) Stepwise isomerization-CM. (i) $Pd_2Br(P^tBu_3)_2$ **Pd-1**; (ii) C_2H_4 + Ru metathesis catalyst.

More generally, however, poor orthogonality between the two processes can limit selectivity, and sequential catalyst addition is used to control the process. Sequential addition has been extensively deployed for the assembly of heterocyclic compounds, including indoles and other benzo-fused heterocycles.[31,32] In a modified approach, the Hulea group recently demonstrated the utility of serially linked, differentially packed catalyst beds to effect the transformation of ethylene to propylene via dimerization-isomerization-metathesis.[33]

Anticipated as a challenge in the present work is the higher metathesis reactivity of the terminal olefin, relative to the internal olefin generated in the isomerization step. Nevertheless, selectivity can be envisaged if the isomerization catalyst is sufficiently reactive to promote initial isomerization relative to metathesis. We therefore explored both tandem and one-pot transformations in developing a methodology for the transformation of essential-oil allylbenzenes into high-value cinnamate and ferulate targets.

References page 122

5.2.2. Results and Discussion

Initial experiments focused on the isomerization of estragole **1a**, as a representative, abundant 1-phenylpropenoid. In developing methodologies for transformation of **1a** into cinnamate **3a**, we considered a range of candidates for the isomerization step, as discussed below. For the metathesis step, however, we selected the second-generation Hoveyda catalyst **HII**, on the basis of prior work.[7,13,34,35] The dominant Grubbs-class catalysts (that is, phosphine-stabilized pre-catalysts, of which **GII** is the exemplar) were rejected on the basis of their incompatibility with acrylates.[36] The incompatibility arises from Michael reactions between the electron-deficient olefin and the PCy_3 ligand liberated from **GII** during catalyst initiation. Such reactions yield reactive[37] that were shown to trigger rapid catalyst decomposition.[34]

5.2.2.1 Attempted tandem catalysis

The first question explored was that of process efficiency: specifically, the viability of orthogonal tandem catalysis. Prior work aimed at the self-metathesis of estragole **1a** using **HII** demonstrated that unintended isomerization of **1a** can compete with metathesis,[9] as indeed noted more broadly elsewhere.[38] We therefore considered it possible that deliberate use of a highly reactive isomerization catalyst (e.g. the Grotjahn catalyst **Ru-2**),[39,40] in conjunction with **HII**, could promote initial isomerization relative to metathesis, and enable selectivity for the target cinnamates. This proved unsuccessful. As shown in Scheme 5.3, very poor selectivities were observed under conditions previously established as optimal for the CM reaction, when estragole and methyl acrylate were present simultaneously with **HII** and **Ru-2**. Competing metathesis of **1a** afforded homocoupled and cross-products, among a

multiplicity of other products (see Appendix C), and yields of the target **3a** were limited to 55%.

While competing metathesis of **1** could potentially be overcome by using higher loadings of **Ru-2**, or a less reactive metathesis catalyst, either comes at a price: that is, the requirement for excess catalyst (with attendant issues of cost and Ru removal), or slow throughput. We therefore accepted the necessity of sequential catalytic processes, in which the metathesis catalyst and acrylate coupling partner are added only once isomerization is complete.

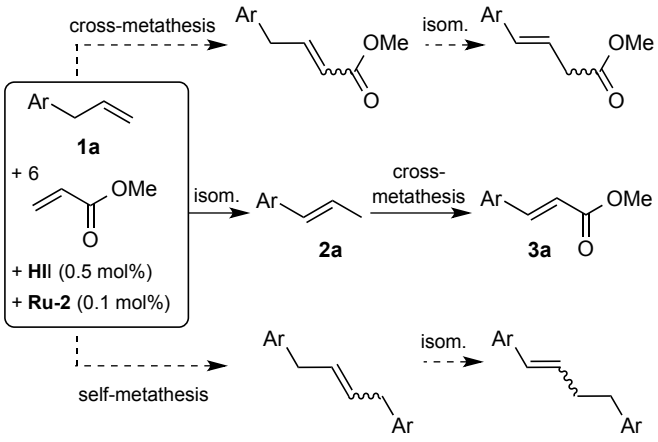

Scheme 5.3. Target tandem isomerization-metathesis reaction (solid arrows; Ar = *p*-$MeOC_6H_4$). Dashed arrows show representative, competing metathesis and metathesis-isomerization processes. Conditions: C_7H_8, 70 °C, 6 h. Catalyst loadings are based on literature precedents for both **HII**[7] and **Ru-2**,[39,40] and validated below.

5.2.2.2 Isomerization of estragole

In the next phase of the study, we screened a range of known isomerization catalysts (Figure 5.2) for maximum activity in the transformation of **1a** to anethole **2a.** Leading reviews have described the isomerization activity of a large number of potential catalysts, with a particular

focus on the impact of substrate functional groups on activity.[41-43] Additional candidates were identified from the recent literature.[18,43] As well as the Grotjahn catalyst **Ru-2**,[40] which has previously shown exceptional activity for isomerization of estragole and eugenol to the (*E*)-olefins,[39] we examined $RuHCl(CO)(PPh_3)_3$ **Ru-H2** and $RuHCl(PPh_3)_3$ **Ru-H1**, the highest-performing isomerization catalysts among several comparators recently examined.[21] Other candidates emerge from the tandem catalysis studies described in the Introduction, including dimeric $Pd_2Br(PtBu_3)_2$ **Pd-1**,[28,29] and $Ru(COD)(methallyl)_2$ **Ru-3**.

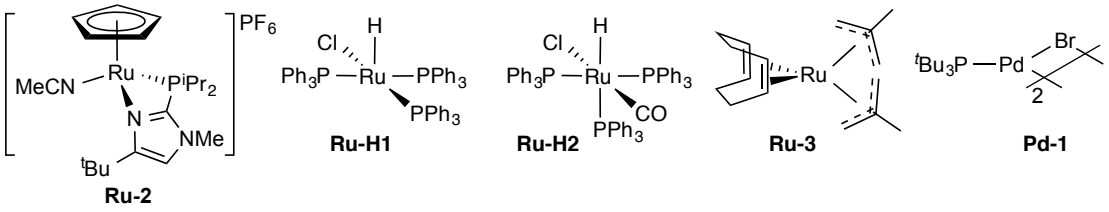

Figure 5.2. Candidate complexes screened for isomerization activity in this work.

Isomerization experiments were carried out at 40 °C in toluene, at a catalyst loading of 1 mol% (Figure 5.3). Under these conditions, the Grotjahn catalyst **Ru-2** exhibited highest activity, delivering quantitative yields of **2a** within 5 min. Hydridochlorocarbonyl complex **Ru-H2** and bis-allyl catalyst **Ru-3** were also highly active, while dimeric **Pd-1** (at 0.5 mol%, i.e. 1 mol% Pd) required 1 h for complete reaction. In comparison, $RuHCl(PPh_3)_3$ **Ru-H1** reached only ca. 50% conversion at 1 h. All catalysts showed >95% selectivity for (*E*)-anethole **2a** by 1 h, with the sole exception of **Ru-H2**, for which 10% of (*Z*)-**2a** was present at 100% yield. However, the proportion of (*E*)-**2a** increases if reaction is continued after conversion to **2a** is complete.

References page 122

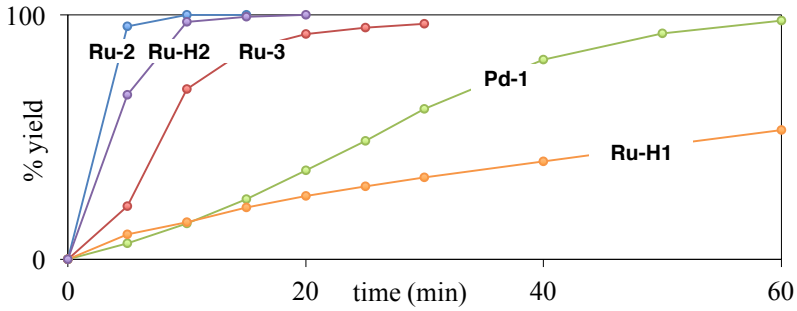

Catalyst	%*E* at 0.5 h*	%*E* at 1 h
Ru-2	99	ND
Ru-H2	90	96
Ru-H1	96	96
Pd-1	94	97
Ru-3	97	97

* %*E* at 100% yield for **Ru-2** and **Ru-H2** (ca. 15 min).

Figure 5.3. Assessing the activity of the candidate catalysts in isomerization of estragole. Conditions: 1 mol% Ru or Pd, 40 °C, C_7H_8.

The relatively low isomerization activity of **Ru-H1** is particularly striking, given that in related work,[21] this catalyst significantly out-performed others that have been regarded as potentially potent isomerization catalysts, including RuHCl(CO)(L)(PCy_3) (L = PCy_3 **Ru-H3**, H_2IMes **Ru-H4**, IMes **Ru-H5**),[44] and the "Grubbs hydride" **Ru-H6**.[45] All were tested under the conditions shown in Figure 5.2,[21] permitting extraction of the order of isomerization activity depicted in Figure 5.4.

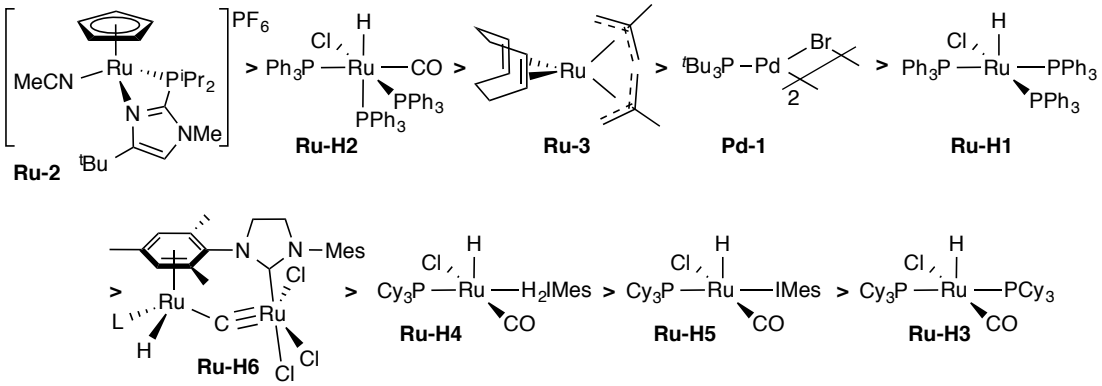

Figure 5.4. Order of isomerization activity (from highest to lowest) for catalysts surveyed in the reaction of Figure 5.3.

5.2.2.3 Solvent compatibility

Isomerization using cationic **Ru-2** is normally carried out in acetone.[46] While a range of solvents is feasible for metathesis, toluene and dichloromethane are generally most favourable.[38] Acetone and other polar solvents can limit catalyst productivity.[47] Moreover, a relatively high-boiling solvent is required for efficiency in the targeted metathesis step, in which formation of cinnamate **3a** is retarded by the intermediate formation of stilbenes, which are slowly consumed even at 70 °C.[7] To identify a reaction medium that balances the requirements for each reaction type, we examined the solvent dependence for isomerization of **1a** and metathesis of **2a**, in THF, toluene, and dichloroethane (DCE; Figure 5.5). Given the high activity of **Ru-2**, isomerization was undertaken at RT, with the metathesis step being carried out at a bath temperature of 70 °C. As noted previously,[7] efficient volatilization of the propylene and ethylene byproducts from metathesis is essential to promote selectivity for the desired CM reaction. Metathesis reactions were therefore carried out with efficient stirring in open vessels in a well-purged glovebox.

While isomerization was marginally faster in the polar solvent THF (declining in the order THF > DCE > toluene; Figure 5.5a), reaction was complete in all cases within 0.5 h at RT. In comparison, metathesis of **2a** was considerably slower in THF (Figure 5.5b). Given the equivalent performance of DCE and toluene, the latter was adopted as the less toxic, environmentally less undesirable[48] alternative, and used as a good compromise solvent for both reactions.[49]

References page 122

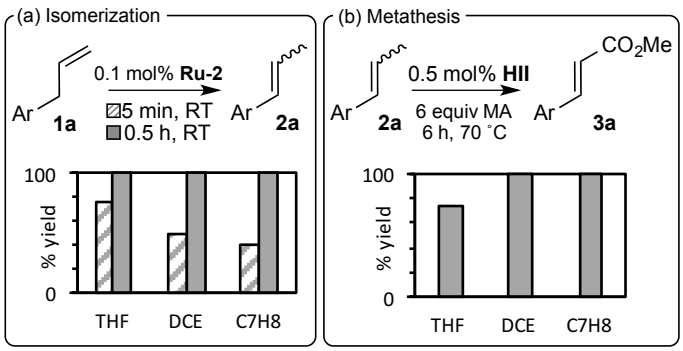

Figure 5.5. Evaluating the impact of solvent on the isomerization and cross-metathesis steps. Ar = *p*-methoxyphenyl.

5.2.2.4 Compatibility of metathesis and isomerization catalysts

A final question in developing the one-pot / dual catalyst methodology lay in the potential sensitivity of the metathesis step to the isomerization catalyst **Ru-2**. To dissect out this effect, we focused on metathesis of anethole **2a**, the intended product of estragole isomerization, and examined the impact on yields of added **Ru-2**. Metathesis yields suffered when **Ru-2** is present in amounts equimolar with **HII** (Table 5.1, entries 1 vs. 2). The detrimental effect was traced to the imidazole moiety by experiments in which free MeCN or imidazole were added to the metathesis reaction, in molar amounts equivalent to **HII**, in the absence of **Ru-2**. Added MeCN had essentially no effect, while added imidazole strongly depressed CM yields (entry 3, 4). This behaviour is consistent with the proposed hemilability of the phosphine-imidazole ligand.[50]

References page 122

Table 5.1. Evaluating the robustness of anethole–acrylate CM toward isomerization catalyst **Ru-2** and its constituent ligands. Ar = *p*-methoxyphenyl.

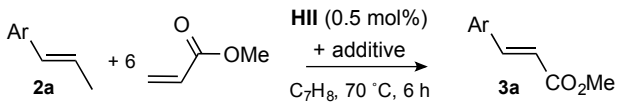

Entry	Additive	mol% additive	% conv	% yield
1	none	---	100	100
2	**Ru-2**	0.5	100	73[a]
3	MeCN	0.5	100	100
4	imidazole	0.5	81	48[a]
5	**Ru-2**	0.1	100	100

GC-FID analysis. [a]Stilbenes resulting from self-metathesis constitute the balance of material.

The negative impact of free imidazole is unsurprising. Not only do imidazole[51] and methyl imidazole[52] function as effective quenching agents in metathesis, but the metallacyclobutane intermediate that carries metathesis was recently shown to be highly sensitive to deprotonation by Brønsted base.[53] Importantly, however, the relative rates of metathesis and deactivation can be tuned by adjusting the ratios of **HII** and **Ru-2**. Thus, quantitative metathesis could be achieved by reducing the proportion of **Ru-2** fivefold (to 0.1 mol%; Entry 5). The impact on isomerization rates is minor, as the transformation of **1a** to **2a** was shown above to be complete within 30 min at this catalyst loading, even at RT.

References page 122

5.2.2.5 One-pot isomerization-metathesis.

Sequential isomerization-metathesis was carried out using the optimized conditions identified above. Accordingly, a toluene solution of estragole **1a** and catalyst **Ru-2** (0.1 mol%) was stirred for 0.5 h at RT under N_2, following which methyl acrylate and the metathesis catalyst **HII** (0.5 mol%) were added, and the reaction was heated at 70 °C for 6 h. ^{1}H NMR analysis indicated quantitative yields of the desired cinnamate **3a** (Table 5.2, entry 1).

This sequential isomerization-metathesis methodology shows excellent tolerance for the unprotected phenolic functionality in eugenol **1b**, affording the ferulate target **3b** in quantitative yields (entry 2). Similar performance was also found for safrole **1c** (entry 3). Likewise successful was the transformation of estragole by isomerization and cross-metathesis with 2-ethylhexyl acrylate (Table 5.2, entry 4). This reaction is of particular interest, given the high value of the octinoxate product **4a**, an important sunscreen agent. CM of eugenol **1b** and safrole **1c** proceeded correspondingly well (entries 5, 6). In all cases, quantitative yields were achieved, irrespective of the phenylpropenoid / acrylate combination.

References page 122

Table 5.2. One-pot isomerization-cross-metathesis of phenylpropenes with acrylates to yield high-value cinnamates and ferulates.[a]

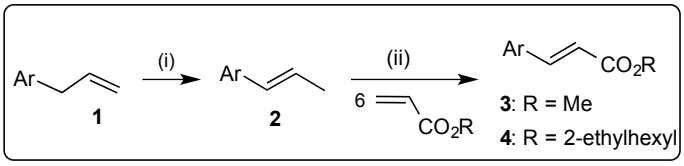

entry	substrate	product	% conv	% yield
methyl acrylate				
1	**1a**	**3a**	100	100
2	**1b**	**3b**	100	>99
3	**1c**	**3c**	100	>99
2-ethylhexyl acrylate				
4	**1a**	**4a**	100	>99
5	**1b**	**4b**	100	>99
6	**1c**	**4c**	100	>99

Conditions. (i) Isomerization: **Ru-2** (0.1 mol%), C_7H_8, RT, 0.5 h. Quantitative formation of **2** confirmed prior to adding reagents for next step. (ii) Metathesis: Addition of **HII** (0.5 mol%), acrylate (6 equiv); 70 °C, 6 h. Conversions of **2** assessed by GC-FID, yields of **3** by GC-FID or ^{1}H NMR analysis; see section 5.2.4.1. Ar = *p*-methoxyphenyl. *Note:* While no other products were evident, NMR yields are indicated as >99% to reflect analytical limits on the accuracy of NMR integration.

5.2.3. Conclusions

The foregoing highlights the potential of olefin metathesis to elaborate the conjugated phenolic structures that represent key chemical motifs in naturally-occurring essential oils, and expands the available pool of such resources by coupling isomerization with metathesis catalysis. Thus, the renewable phenylpropenoids estragole, eugenol, and safrole are

References page 122

converted into cinnamate and ferulate products relevant to fine-chemicals markets, via sequential processes of isomerization and acrylate cross-metathesis.

The high propensity of the terminal olefins toward metathesis, in competition with isomerization, hampered development of orthogonal tandem catalysis methodologies. Such processes are attractive for their operational simplicity; specifically, "walk-away" operation, but are frequently constrained by such imperfect orthogonality. Process efficiency was nevertheless achieved by identifying conditions suitable for performing the two reactions in a single vessel. Addition of the metathesis catalyst following isomerization reduces waste by eliminating the need for intervening workup and purification. Key to overcoming the incomplete tolerance of the metathesis process for the isomerization catalyst is the high activity of the latter, which permits use of catalyst loadings sufficiently low that metathesis proceeds unimpeded.

5.2.4. Experimental Details for Section 5.2

5.2.4.1 General Procedures

All reactions were carried out in an N_2-filled glove-box. Dry, oxygen-free C_7H_8 and THF were obtained using a Glass Contour solvent purification system and stored in the glovebox in amber bottles over 4 Å molecular sieves. Dichloroethane was dried over Ca_SO_4 for 12 h under N_2, then refluxed over P_2O_5 for 6 h prior to distillation, and stored as above, over 5 Å molecular sieves. Anhydrous *n*-decane (internal standard for gas chromatography) was purchased from Sigma-Aldrich.

Substrates **1a** (98%), **1b** (99%), **1c** (>97%), and **2a** (99%) were purchased from Sigma-Aldrich, and passed over neutral alumina prior to use. Acrylates (Sigma-Aldrich; 99% (methyl) or 98% (2-ethylhexyl)) were used without removing the phenolic stabilizers. Acrylates and phenylpropenes were degassed by five freeze-pump-thaw cycles, and stored protected from light under N_2 in the glovebox freezer (–35 °C). Catalysts **Pd-1**, **Ru-2**, and **Ru-3** were purchased from Strem and used as received. Catalysts **HII**,[54] **Ru-H2**,[55] and **Ru-H1**[56] were synthesized by literature methods. Potassium hydrotris(1-pyrazolyl)borate (KTp; >97%) was purchased from TCI and used as received.

NMR spectra were recorded on a Bruker Avance 300 or 500 MHz spectrometer at 298 K, and referenced to the residual proton or carbon signals of the deuterated solvent (^{1}H, ^{13}C(^{1}H) NMR). Signals are reported in ppm, relative to TMS (^{1}H, ^{13}C) at 0 ppm.

GC quantification was performed on samples diluted with CH_2Cl_2 (ACS reagent grade) on an Agilent 7890A Series GC equipped with a flame ionization detector (FID), an Agilent 7683B Series autosampler and an Agilent HP-5 polysiloxane column (30 m length, 320 μm diameter), using an inlet split ratio of 10:1, an inlet temperature of 250 °C, and helium (UHP grade) as the carrier gas to maintain column pressure at 11.512 psi. The FID response was maintained between 50-2000 ρA, using analyte concentrations of ca. 5 mM. Calibration curves (peak areas vs. concentration) were constructed in the relevant concentration regime, to account for the dependence on detector response for substrates, products and decane (internal standard in catalytic runs). Conversions and yields in catalytic runs were determined from the integrated peak areas, referenced against decane, and compared to the initial

substrate : decane integration ratio. Conversions of **1** and **2**, and yields of products **2** and **3a**, were assessed by GC-FID. Other product yields (**3b**, **3c**, **4a**, **4b**, **4c**) were assessed by ^{1}H NMR analysis, as poor peak shapes hampered GC quantification. The NMR data for these compounds are provided in Appendix D.

5.2.4.2 Representative Procedure for Isomerization.

A 20 mL vial was loaded with estragole **1a** (59 mg, 0.40 mmol), decane (GC internal standard; 57 mg, 0.40 mmol) and toluene (1.9 mL). An aliquot was removed for GC-FID analysis to establish the starting ratio of substrate to decane. Catalyst was added from a stock solution of **Ru-2** (11 μL, 0.40 μmol, 0.1 mol%); stock solution 11 mg in 0.50 mL toluene; 40 mM). Aliquots were taken from the stirred reaction at specific time intervals, quenched with air, diluted with CH_2Cl_2 on the bench, and analyzed by GC-FID.

5.2.4.3 Representative Procedure for Cross-Metathesis.

Reaction carried out as above, with the following changes: anethole (59 mg, 0.40 mmol), in 1.6 mL toluene, with the addition of methyl acrylate (207 mg, 2.40 mmol, 6 equiv), and **HII** as catalyst (63 μL, 2.0 μmol, 0.5 mol%); stock solution 10 mg in 0.50 mL toluene (36 mM). The reaction was heated in a thermostatted oil bath open to the glovebox atmosphere, and analyzed as above.

References page 122

5.2.4.4 Attempted Tandem Isomerization / Cross-Metathesis.

Reaction carried out as for estragole **1a** above, with methyl acrylate (207 mg, 2.40 mmol, 6 equiv) in 1.6 mL toluene, and addition of both **Ru-2** (0.40 μmol, 0.1 mol%) and **HII** (2.0 μmol, 0.5 mol%) from stock solutions. The reaction was heated in a thermostatted oil bath at 70 °C, open to the glovebox atmosphere, and analyzed as above after quenching with KTp (glovebox; solution in THF, 10 mg/1 mL, 10 equiv vs. **HII**) then air.

5.2.4.5 Representative Procedure for One-Pot Isomerization / Cross-Metathesis.

Reaction carried out as above, using 20 mg estragole (0.20 mmol), decane (29 mg, 0.20 mmol) and toluene (0.80 mL). An aliquot taken after 30 min confirmed complete conversion to anethole **2a**. Methyl acrylate (103 mg, 1.20 mmol, 6 equiv) and **HII** (1.0 μmol from stock solution, 0.5 mol%) were then added. The reaction was heated as above for 6 h, after which an aliquot was quenched with KTp, then air, and analyzed.

References page 122

5.3. References

(1) Nam, Y. H.; Snapper, M. L., Ruthenium-Catalyzed Tandem Metathesis/Non-Metathesis Processes. In *Handbook of Metathesis*, Grubbs, R. H.; Wenzel, A. G., Eds. Wiley-VCH: Weinheim, 2015; pp 311–380.

(2) For selected examples of tandem metathesis-isomerization, see: (a) J. R. Clark, J. R. Griffiths and S. T. Diver, *J. Am. Chem. Soc.*, 2013, **135**, 3327–3330; (b) B. Schmidt and S. Hauke, *Org. Biomol. Chem.*, 2013, **11**, 4194–4206; (c) B. Schmidt and O. Kunz, *Synlett*, 2012, **23**, 851–854; (d) A. D. Wadsworth, D. P. Furkert, J. Sperry and M. A. Brimble, *Org. Lett.*, 2012, **14**, 5374–5377; (e) Ascic, J. F. Jensen and T. E. Nielsen, *Angew. Chem. Int. Ed.*, 2011, **50**, 5188 –5191; (f) B. Schmidt, R. Berger and F. Holter, *Org. Biomol. Chem.*, 2010, **8**, 1406–1414; (g) A. Mallagaray, G. Dominguez, A. Gradillas and J. Perez-Castells, *Org. Lett.*, 2008, **10**, 597–600; (h) D. Finnegan, B. A. Seigal and M. L. Snapper, *Org. Lett.*, 2006, **8**, 2603–2606.

(3) British Petroleum Company. *BP Statistical Review of World Energy*, 64th Ed. BP, London, 2015.

(4) Imhof, P.; Cornelis van der Waal, J., *Catalytic Process Development for Renewable Materials*. Wiley: Weinheim, Germany, 2013.

(5) Ulber, R.; Sell, D.; Hirth, T., *Renewable Raw Materials*. Wiley: Weinheim, Germany, 2011.

(6) de Espinosa, L. M.; Meier, M. A. R. *Top. Organomet. Chem.* **2012**, *39*, 1-44.

(7) Lummiss, J. A. M.; Oliveira, K. C.; Pranckevicius, A.; Santos, A.; dos Santos, E. N.; Fogg, D. E. *J. Am. Chem. Soc.* **2012**, *134*, 18889–18891.

(8) Hitce, J.; Crutizat, M.; Bourdon, C.; Vivès, A.; Marat, X.; Dalko-Csiba, M. *Green Chem.* **2015**, *17*, 3756–3761.

(9) Bilel, H.; Hamdi, N.; Zagrouba, F.; Fischmeister, C.; Bruneau, C. *RSC Adv.* **2012**, *2*, 9584–9589.

(10) Vieille-Petit, L.; Clavier, H.; Linden, A.; Blumentritt, S.; Nolan, S. P.; Dorta, R. *Organometallics* **2010**, *29*, 775–788.

(11) Moïse, J.; Arseniyadis, S.; Cossy, J. *Org. Lett.* **2007**, *9*, 1695–1698.

(12) Ferré-Filmon, K.; Delaude, L.; Demonceau, A.; Noels, A. F. *Eur. J. Org. Chem.* **2005**, 3319–3325.

(13) Biermann, U.; Bornscheuer, U.; Meier, M. A. R.; Metzger, J. O.; Schafer, H. J. *Angew. Chem. Int. Ed.* **2011**, *50*, 3854–3871.

(14) Chikkali, S.; Mecking, S. *Angew. Chem., Int. Ed.* **2012**, *51*, 5802−5808.

(15) Winkler, M.; Meier, M. A. R. *Green Chem.* **2014**, *16*, 3335–3340.

(16) Fahlbusch, K.-G.; Hammerschmidt, F.-J.; Panten, J.; Pickenhagen, W.; Schatkowski, D., Flavors and Fragrances. In *Ullmann's Encyclopedia of Industrial Chemistry (Electronic Release)*, Wiley-VCH: Weinheim, Germany, 2012.

(17) Sharma, S. K.; Srivastava, V. K.; Jasra, R. V. *J. Mol. Catal. A* **2006**, *245*, 200–209.

(18) Hassam, M.; Taher, A.; Arnott, G. E.; Green, I. R.; van Otterlo, W. A. L. *Chem. Rev.* **2015**, *115*, 5462–5569.

(19) Reviews of tandem catalysis: (a) T. L. Lohr and T. J. Marks, *Nat. Chem.*, **2015**, *7*, 477–482; (b) J.-C. Wasilke, S. J. Obrey, R. T. Baker and G. C. Bazan, *Chem. Rev.*, **2005**, *105*, 1001–1020; (c) D. E. Fogg and E. N. dos Santos, *Coord. Chem. Rev*., **2004**, *248*, 2365–2379.

(20) For reviews of tandem catalysis strategies that couple metathesis with isomerization, see: (a) B. Schmidt and S. Krehl, in *Olefin Metathesis-Theory and Practice*, ed. K. Grela, Wiley, Hoboken, NJ, 2014, ch. 5, pp. 187–232; (b) Y. H. Nam and M. L. Snapper, in *Handbook of Metathesis*, eds. R. H. Grubbs and A. G. Wenzel, Wiley-VCH, Weinheim, Germany, 2015, Vol. 2, ch. 4, pp 311–380; (c) B. Schmidt, *Pure Appl. Chem.*, **2006**, *78*, 469–476. (d) B. Alcaide, P. Almendros and A. Luna, *Chem. Rev.*, **2009**, *109*, 3817–3858. For tactics in orthogonal tandem catalysis, see: (c) and Refs. 19a and 19c.

(21) Higman, C. S.; Plais, L.; Fogg, D. E. *ChemCatChem* **2013**, *5*, 3548-3551.

(22) Braddock, D. C.; Matsuno, A. *Tetrahedron Lett.* **2002**, *43*, 3305–3308.

(23) Michalak, K.; Michalak, M.; Wicha, J. *Tetrahedron Lett.* **2005**, *46*, 1149–1153.

(24) Michalak, M.; Wicha, J. *Synlett* **2005**, 2277–2280.

(25) Dobereiner, G. E.; Erdogan, G.; Larsen, C. R.; Grotjahn, D. B.; Schrock, R. R. *ACS Catal.* **2014**, *4*, 3069–3076.

(26) Consorti, C. S.; Aydos, G. L. P.; Dupont, J. *Chem. Comm.* **2010**, *46*, 9058–9060.

(27) Hemelaere, R.; Caijo, F.; Mauduit, M.; Carreaux, F.; Carboni, B. *Eur. J. Org. Chem.* **2014**, 3328–3333.

(28) Baader, S.; Podsiadly, P. E.; Cole-Hamilton, D. J.; Gooßen, L. J. *Green Chem.* **2014**, *16*, 4885–4890.

(29) Ohlmann, D. M.; Tschauder, N.; Stockis, J.-P.; Gooßen, K.; Dierker, M.; Gooßen, L. J. *J. Am. Chem. Soc.* **2012**, *134*, 13716–13729.

(30) Manzini, S.; Nelson, D. J.; Nolan, S. P. *ChemCatChem* **2013**, *5*, 2848–2851.

(31) (a) T. Kobayashi, M. Arisawa and S. Shuto, *Org. Biomol. Chem.*, 2011, **9**, 1219–1224; (b) Y. Kasaya, K. Hoshi, Y. Terada, A. Nishida, S. Shuto and M. Arisawa, *Eur. J. Org.*

Chem., 2009, 4606–4613; (c) M. Arisawa, Y. Terada, K. Takahashi, M. Nakagawa and A. Nishida, *J. Org. Chem.*, 2006, **71**, 4255–4261; (d) M. Arisawa, Y. Terada, M. Nakagawa and A. Nishida, *Angew. Chem. Int. Ed.*, 2002, **41**, 4732–4734.

(32) (a) W. A. L. van Otterlo, G. L. Morgans, L. G. Madeley, S. Kuzvidza, S. S. Moleele, N. Thornton and C. B. de Koning, *Tetrahedron*, 2005, **61**, 7746–7755; (b) W. A. L. van Otterlo, E. L. Ngidi and C. B. de Koning, *Tetrahedron Lett.*, 2003, **44**, 6483–6486; (c) W. A. L. van Otterlo, R. Pathak and C. B. de Koning, *Synlett*, 2003, 1859–1861.

(33) Andrei, R. D.; Popa, M. I.; Fajula, F.; Cammarano, C.; Khudhair, A. A.; Bouchmella, K.; Mutin, P. H.; Hulea, V. *ACS Catal.* **2015**, *5*, 2774–2777.

(34) Miao, X.; Malacea, R.; Fischmeister, C.; Bruneau, C.; Dixneuf, P. H. *Green Chem.* **2011**, *13*, 2911–2919.

(35) Ho, T. T.; Jacobs, T.; Meier, M. A. R. *ChemSusChem* **2009**, *2*, 749–754.

(36) Bailey, G. A.; Fogg, D. E. *J. Am. Chem. Soc.* **2015**, *137*, 7318–7321.

(37) Fan, Y. C.; Kwon, O. *Chem. Commun.* **2013**, *49*, 11588–11619.

(38) van Lierop, B. J.; Lummiss, J. A. M.; Fogg, D. E., Ring-Closing Metathesis. In *Olefin Metathesis-Theory and Practice*, Grela, K., Ed. Wiley: Hoboken, NJ, 2014; pp 85–152.

(39) Larsen, C. R.; Grotjahn, D. B. *J. Am. Chem. Soc.* **2012**, *134*, 10357–10360.

(40) Grotjahn, D. B.; Larsen, C. R.; Gustafson, J. L.; Nair, R.; Sharma, A. *J. Am. Chem. Soc.* **2007**, *129*, 9592–9593.

(41) Schmidt, B. *Eur. J. Org. Chem.* **2004**, 1865–1880.

(42) Krompiec, S.; Kuznik, N.; Krompiec, M.; Penczek, R.; Mrzigod, J.; Torz, A. *J. Mol. Catal. A* **2006**, *253*, 132–146.

(43) Larionov, E.; Li, H.; Mazet, C. *Chem. Commun.* **2014**, *50*, 9816–9826.

References page 122

(44) Dharmasena, U. L.; Foucault, H. M.; dos Santos, E. N.; Fogg, D. E.; Nolan, S. P. *Organometallics* **2005**, *24*, 1056–1058.

(45) Hong, S. H.; Day, M. W.; Grubbs, R. H. *J. Am. Chem. Soc.* **2004**, *126*, 7414–7415.

(46) Larsen, C. R.; Erdogan, G.; Grotjahn, D. B. *J. Am. Chem. Soc.* **2014**, *136*, 1226–1229.

(47) Bai, C.-X.; Lu, X.-B.; He, R.; Zhang, W.-Z.; Feng, X.-J. *Org. Biomol. Chem.* **2005**, *3*, 4139–4142.

(48) ACS GCI Pharmaceutical Roundtable Solvent Selection Guide, Version 2.0, 2011. http://www.acs.org/content/dam/acsorg/greenchemistry/industriainnovation/roundtable/acs-gci-pr-solvent-selection-guide.pdf. Accessed Nov. 18, 2015.

(49) In extreme cases, solvent incompatibility between sequential processes can be addressed by modifying the solvent system once the first step is complete. The Blechert group described such an approach in developing a one-pot metathesis-dihydroxylation sequence. Because the CH_2Cl_2 solvent used in the metathesis reaction was found to limit dihydroxylation yields, the solvent was evaporated following RCM, and the residue was redissolved in acetonitrile-ethyl acetate-water, to which the oxidation catalyst was added. See: S. Beligny, S. Eibauer, S. . Beligny, S. Eibauer, S. Maechling and S. Blechert, *Angew. Chem. Int. Ed.*, **2006**, ***45***, 1900–1903. In subsequent work, Snapper and coworkers carried out the metathesis step in ethyl acetate, obviating the need for an intervening evaporation step. See: A. A. Scholte, M. H. An and M. L. Snapper, *Org. Lett*., **2006**, *8*, 4759–4762.

(50) Erdogan, G.; Grotjahn, D. B. *J. Am. Chem. Soc.* **2009**, *131*, 10354–10355.

(51) Wei, X.; Shu, C.; Haddad, N.; Zeng, X.; Patel, N. D.; Tan, Z.; Liu, J.; Lee, H.; Shen, S.; Campbell, S.; Varsolona, R. J.; Busacca, C. A.; Hossain, A.; Yee, N. K.; Senanayake, C. H. *Org. Lett.* **2013**, *15*, 1016–1019.

(52) Blacquiere, J. M.; Jurca, T.; Weiss, J.; Fogg, D. E. *Adv. Synth. Catal.* **2008**, *350*, 2849–2855.

(53) Ireland, B. J.; Dobigny, B. T.; Fogg, D. E. *ACS Catal.* **2015**, *5*, 4690−4698.

(54) van Lierop, B. J.; Reckling, A. M.; Lummiss, J. A. M.; Fogg, D. E. *ChemCatChem* **2012**, *4*, 2020–2025.

(55) Ahmad, N.; Levison, J. J.; Robinson, S. D.; Uttley, M. F. *Inorg. Synth.* **1974**, *15*, 45–64.

(56) Schunn, R. A.; Wonchoba, E. R.; Wilkinson, G. *Inorg. Synth.* **1971**, *13*, 131–134.

Chapter 6. Conclusions and Future Directions

Ruthenium metathesis catalysts have transformed approaches to the assembly of new carbon skeletons – in academia. They are now, after two decades, finally beginning to see applications in process chemistry. In the past two years, the first examples of chemical processes using these catalysts in pharmaceutical and specialty-chemicals manufacturing have come online. For improved process efficiency and expanded uptake, however, outstanding issues of catalyst productivity and selectivity remain to be addressed. Deeper fundamental understanding of the catalyst life-cycle, and particularly deactivation pathways, offers opportunities to limit side-reactions and increase turnover numbers, by providing guidelines that can aid in the development of more active, more robust catalyst systems. This thesis work was aimed at understanding the origin of common side-reactions that erode yields and selectivity, to the detriment of process costs and efficiency.

Double-bond isomerization is the most prevalent side-reaction in olefin metathesis. Adventitious isomerization during metathesis constitutes a major challenge in target-directed synthesis, in both academic and industrial contexts. A considerable body of research has focused on this issue, and attempts have been made to pinpoint the species responsible. Two known catalyst decomposition products are widely viewed as responsible for adventitious isomerization, although their performance remained untested at the outset of this thesis work. Chapter 2 rectified this gap by examining the isomerization activity of these complexes, in comparison to the levels of isomerization observed during metathesis under the same conditions. This study led to the conclusion that these commonly invoked catalyst systems

are not in fact kinetically competent to account for competing isomerization during metathesis.

While a number of reviews now document isomerization activity for a host of metal complexes, few studies to date report on the important question of *relative* activity. In the course of this work, a selected set of metal hydride complexes was surveyed for isomerization activity. A correlation was established between the lability of an ancillary ligand and increased isomerization activity. Such structure-activity relationships are not only important in considering alternative candidates for the species responsible for isomerization during metathesis, but also, more broadly, when carrying out isomerization reactions as part of a deliberate synthetic strategy. These studies ultimately led to consideration of the possibility of more extensive decomposition of the Grubbs catalyst during metathesis, leading to ruthenium products in which low substitution increased isomerization activity, and also hampered identification of discrete products. This query forms the basis for the work described in Chapter 3.

Chapter 3 puts forward an entirely new paradigm in terms of the ruthenium products of decomposition. Ruthenium nanoparticles are identified as major products from decomposition of the second-generation Grubbs catalyst during metathesis. The competence of these RuNPs in promoting undesired isomerization during metathesis is demonstrated. The significance of this work is two-fold. First, the decomposition pathways operative for this important catalyst are of intense interest. Secondly, the identification of highly-active

isomerization catalysts generated during metathesis not only clarifies a puzzle of long standing, but offers new opportunities to inhibit isomerization, or alternatively to deliberately enhance and harness such reactivity for target-directed synthesis by (e.g.) tandem catalysis. More generally, this idea may have broader relevance in others areas of homogeneous catalysis where decomposition occurs via progressive ligand stripping. Mechanistic understanding of the events leading to catalyst death is at the heart of catalyst redesign.

Chapter 4 takes up this challenge, exploring one potential way to circumvent ligand stripping. The original design strategy was simple: to inhibit the C-H activation step that is central to many of the decomposition pathways noted above. Thus, a truncated *N*-methyl NHC was used in place of the standard *N*-mesityl ligand H_2IMes. Synthesis, characterization, and metathesis activity of a new dimeric alkylidene complex bearing this small NHC was discussed in Chapter 4. While the ultimate product exhibited low metathesis activity, the observed dimerization chemistry reveals one consequence of decreasing the steric bulk at the metal centre. The formation and reactivity of this complex offers new insights into key parameters for catalyst redesign.

While Chapters 2–4 focused on the adverse effects of isomerization in metathesis, the work described in Chapter 5 adopts a different perspective, which seeks to deliberately couple isomerization with metathesis. New synthetic strategies are explored for the valorization of biorenewable essential-oil feedstocks for production of high-value chemicals. Analyzed in this chapter are opportunities and limitations associated with orthogonal tandem

isomerization-metathesis, versus sequential catalytic reactions, with a specific focus on control over product selectivity. Issues of process and catalyst compatibility were investigated, and an efficient one-pot, two-catalyst protocol for sequential isomerization-cross metathesis was developed. This protocol was successfully applied to the elaboration of essential oil 1-phenylpropenes into high-value cinnamates and ferulates. This work hence highlights not only the opportunity and power of isomerization in metathesis, but applications in the important field of biorenewables, and strategies in tandem catalysis.

Research building on this thesis work is now under way in the Fogg group, in the hands of Dr. Emma Davey (nanoparticle chemistry) and Ms. Stephanie Rufh (inhibiting isomerization through catalyst design). While clear links exist between these projects, specifics of each will be treated individually below. Many avenues for investigation stem from the nanoparticle chemistry. A primary goal is establishing which ligands are retained, and their density, following decomposition and NP growth. Of keen interest are the early steps in the decomposition mechanism, as well as identification of ligands that maximize or suppress the isomerization activity of the NPs. Further characterization will involve synthesis of metathesis catalysts bearing a ^{13}C-labelled NHC. The fate of the NHC ligand during catalyst decomposition will be tracked by $^{13}C\{^{1}H\}$ NMR analysis. If the NHC remains on the nanoparticle, as currently envisaged, isotopic enrichment will afford a valuable spectroscopic handle for nanoparticle characterization, including by solid-state NMR methods, and will be important in reporting on the number of unique carbene sites.

Both the early stages of NP formation and the nature of the product NPs are the focus of an ongoing collaboration with Prof. Pierre Kennepohl (University of British Columbia), and a France-Canada Fund proposal for work with Prof. Karine Philippot at Toulouse. The challenge in studying these materials lies in their susceptibility to agglomeration during attempted isolation. The NPs will be characterized in situ using synchrotron methods: wide-angle X-ray spectroscopy (WAXS), small-angle X-ray spectroscopy (SAXS), and X-ray absorption spectroscopy (XAS). These experiments will be conducted at the Stanford Synchrotron Radiation Lightsource (SSRL). In preliminary experiments, an experimental setup has already been tested, and design of a new flow cell to accommodate these experiments is currently underway at SSRL. The beamline experiments will give insight into particle shape and size, NP surface properties, and the number of Ru neighbours for a given particle. These experiments will be conducted on both isolated samples and on catalytic experiments to monitor the formation of dimers, trimers, etc. and ultimately nanoparticle formation. Inert-atmosphere MALDI will be carried out in conjunction with these experiments to confirm the presence of dimers and trimers in the early stages of the reaction.

The nanoparticle work will be extended to other catalyst systems, in particular the Hoveyda catalyst **HII**, which is second only to the Grubbs catalyst for its popularity in academia, and is emerging as a privileged design platform for metathesis in industry. A general consensus holds that problems of isomerization are more acute for **HII** than for **GII**: the validity of this dogma will be examined with the possibility of nanoparticle formation and activity in mind. Also of interest is the effect of substrate structure and reaction conditions on NP formation.

A range of substrates, temperatures, concentrations, solvents, additives, and timescales will be screened to determine optimal conditions to promote or inhibit nanoparticle formation. New isomerization catalysts constituting novel Ru-NHC nanoparticles will also be designed, synthesized, and tested for isomerization in collaboration with Prof. Philippot.

As a broader concept, the observation of NP formation during metathesis raises the provocative possibility that such deactivation pathways may in fact be rather general in homogeneous catalysis. Such pathways are now well established in palladium chemistry, where Pd NPs are increasingly viewed as a reservoir that can be drawn on for catalysis, or scavenged by available ligands. It is possible that in other catalyst systems, deactivation likewise leads to the formation of nanoparticles, and indeed that such particles are non-innocent. The key questions are whether (e.g.) β-elimination and HCl elimination pathways afford access to the elemental metals, and whether the ligand-stripping pathways demonstrated for metathesis are more broadly applicable.

The work on catalyst decomposition in this thesis represents only one facet of a larger effort within the Fogg group aimed at understanding mechanisms of decomposition of key metathesis catalysts. Nevertheless, a common element is the need for a strongly-donating NHC to amplify catalyst activity, and the susceptibility of the NHC to C-H activation pathways. The truncated carbene chemistry thus remains an important avenue of study. A primary goal in the IMe4 system is accessing a more reactive catalyst. One simple objective involves halide abstraction to afford a reactive edge-bridged structure, which is expected to

enable access to mononuclear, olefin-bound species. A more ambitious goal targets mono-carbene species of the Hoveyda class: that is, inhibiting the over-substitution chemistry that plagues the truncated *N*-methyl NHC. Potential avenues include use of the Ru(COD)(COT) and Ru(Me-allyl)$_2$(COD) precursors, the relative steric congestion of which could aid in limiting NHC substitution. This represents one approach to ligand redesign to minimize catalyst death.

A. Electron Micrographs

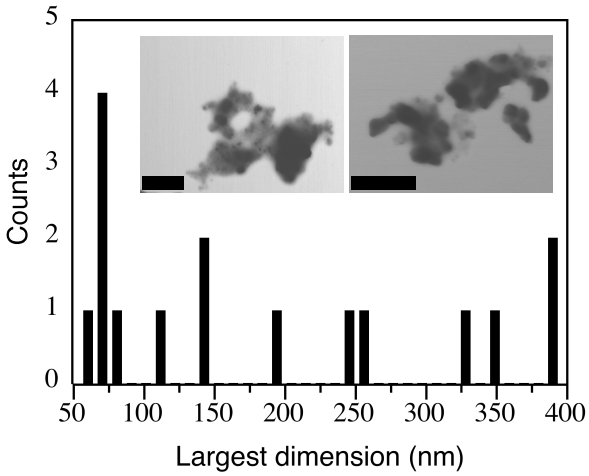

Figure A1. Size distribution for Ru agglomerates isolated from commercial **GII**, observed by SEM. These structures are irregular in shape and size: for the purposes of illustration, the largest dimension for 16 representative particles was measured. Inset shows two of the agglomerates measured (scale bar 1 μm).

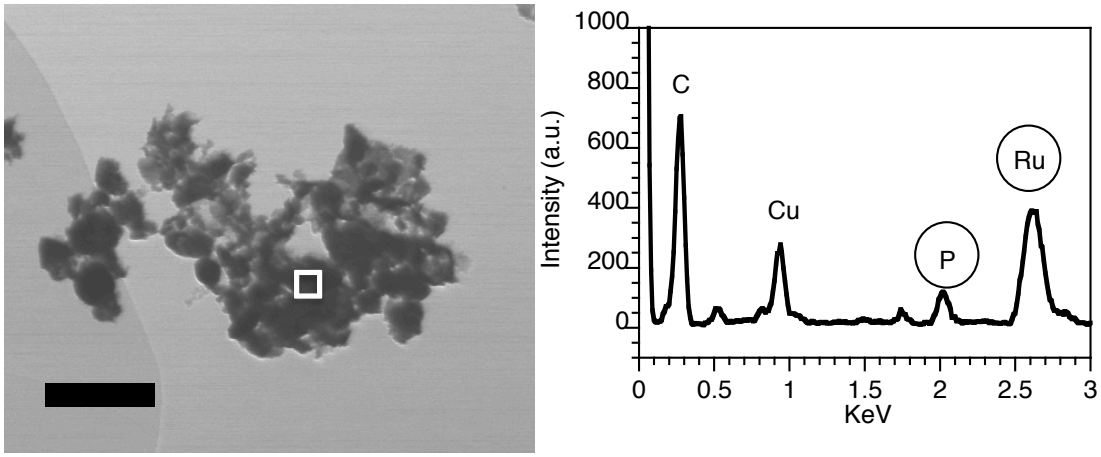

Figure A2. SEM image (transmission mode) of RuNPs isolated from commercial **GII** and EDX spectrum recorded in the area defined by a white square (Scale bar: 1μm). Note: C and Cu signals are attributed to the carbon film on the copper grid used as sample holder.

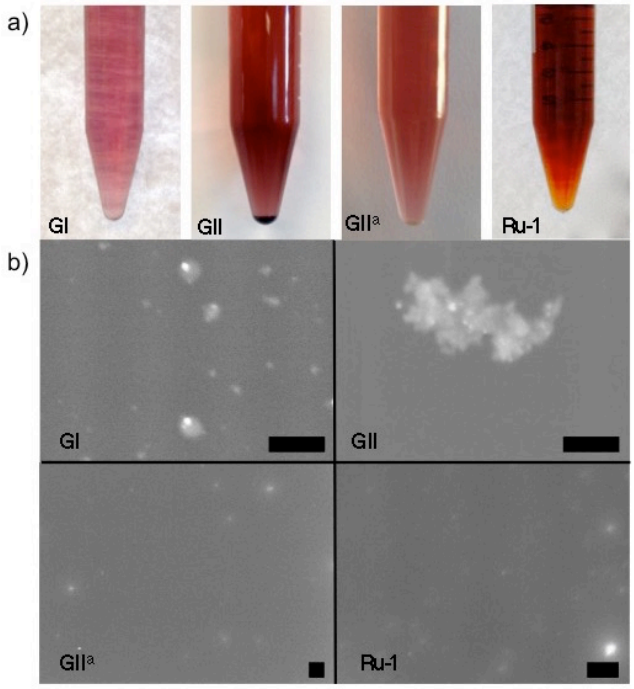

Figure A3. (a) Visual evidence of sediment following centrifugation of toluene solutions of **GII**, but not of other metathesis catalysts. (b) SEM images (scale bar 1 μm). [a] This batch of **GII** was prepared at room temperature, by reaction of **GI** with free H_2IMes.[1]

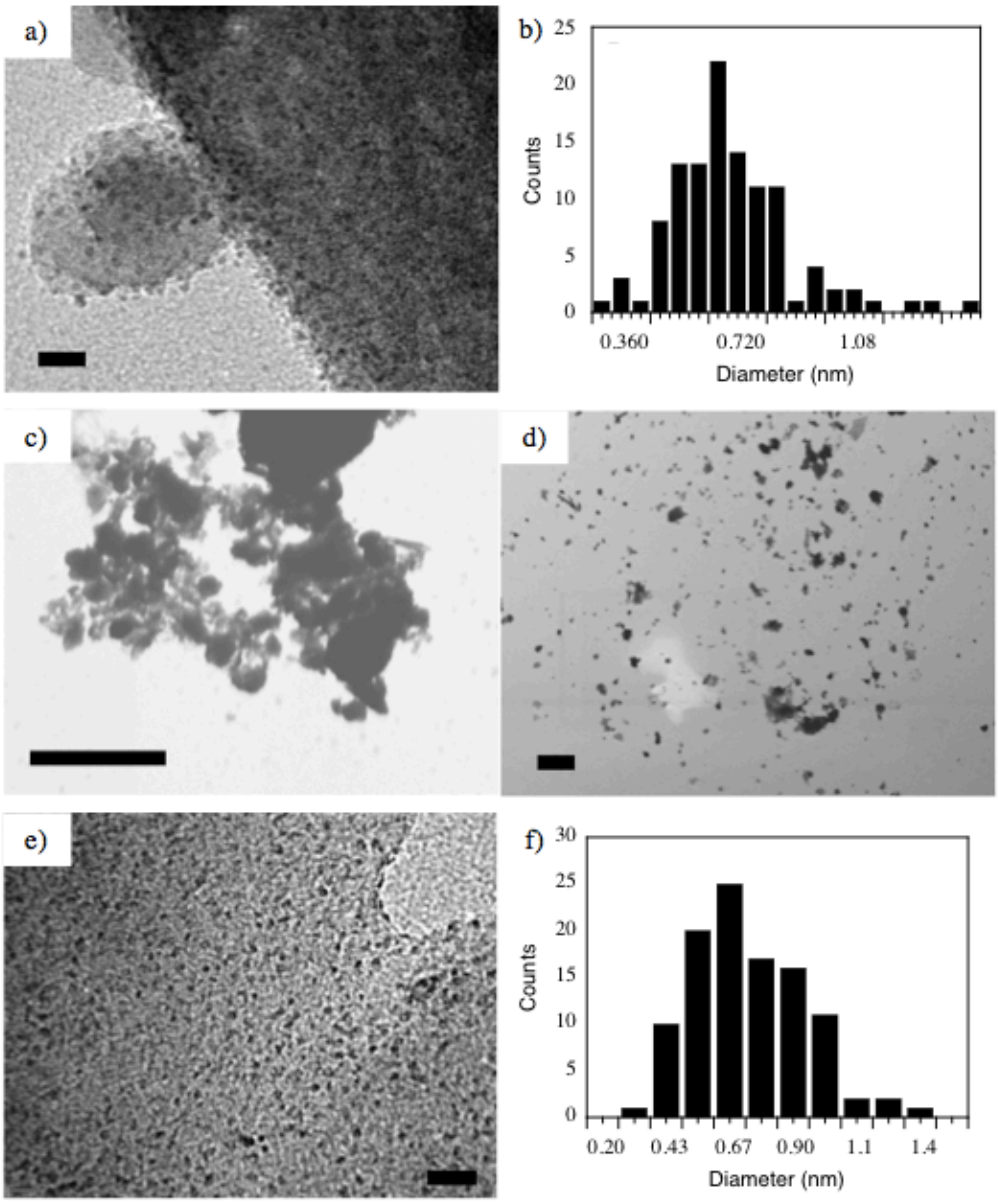

Sample	RuNP preparation method
A	$RuCl_3$ + silica-APTES, H_2O, 1 h
B	$RuCl_3$ + carbon nanodiamonds, Irgacure 907, EtOH-H_2O, UVA, 1 h
C	$RuCl_3$ + 3 NaOAc, ETG, 165 ˚C, 15 min
D	Ru(COD)(COT) + IPr, H_2 (10 bar), RT, 14 h

Figure A4. a) TEM image for Ru@MCM obtained by Method **A** (scale bar: 10 nm); b) particle size distribution for Ru@MCM: average (0.7 ±0.3) nm; c) SEM image (transmission mode) of RuNPs obtained by Method **C** (scale bar: 1 μm); d) SEM image (transmission mode) of RuNPs obtained by Method **D** (scale bar: 1 μm). e) TEM of Ru@CND prepared by new Method **B** (scale bar: 10 nm). f) Size distribution of Ru@CND: average (0.6 ± 0.2) nm.

B. X-ray Photoelectron Spectroscopy

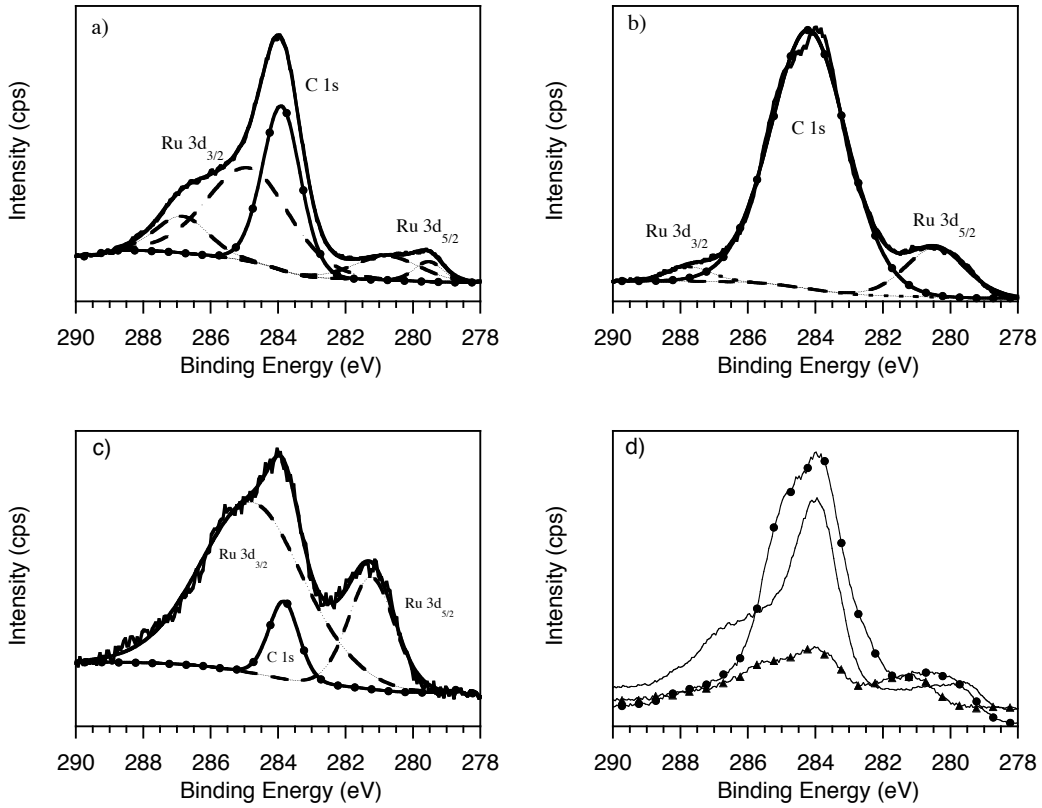

Figure B1. Deconvoluted Ru 3d high-resolution XPS spectra, normalized to 284 eV. a) RuNPs isolated from commercial **GII**; b) Ru@CND; c) Ru@MCM; d) overlay of traces for a–c: RuNPs isolated from commercial **GII** (——), Ru@CND (–●–) and Ru@MCM (–▲–).

Table B1. Proportions of RuNPs used to achieve a standard Ru concentration of 2 mM for isomerization experiments.[a]

Sample	Material	weight % Ru	Proportion
A	Ru@MCM	2.3–2.5[b]	10.1 mg
B	Ru@CND	0.53[b]	10.1 mg
C	Ru in ethylene glycol	3.25 mM	615 μL
D	Ru IPr	33.9[c]	3.0 mg

[a]Ru@MCM = NPs supported on mesoporous silica; Ru@CND = NPs supported on carbon nanodiamond; ETG = ethylene glycol; IPr = 1,3-bis(2,6-diisopropylphenyl)imidazol-2-ylidene; [b]Ru content of supported NPs determined by ICP-ES analysis. [c]Determined by elemental analysis.

C. GC Traces

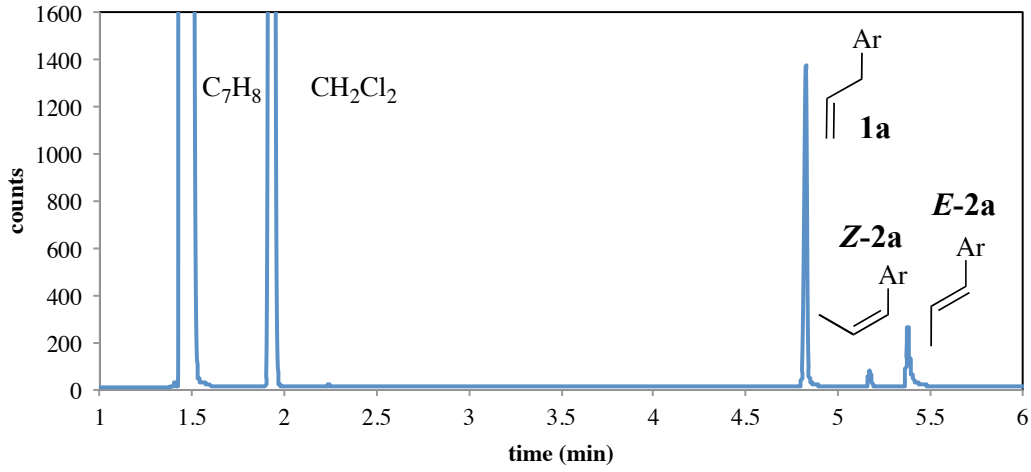

Figure C1. Representative GC-FID trace for isomerization of estragole **1** to *E*- and *Z*-anethole **2a**, ArCH=CHMe (Ar = *p*-C_6H_4-OMe).

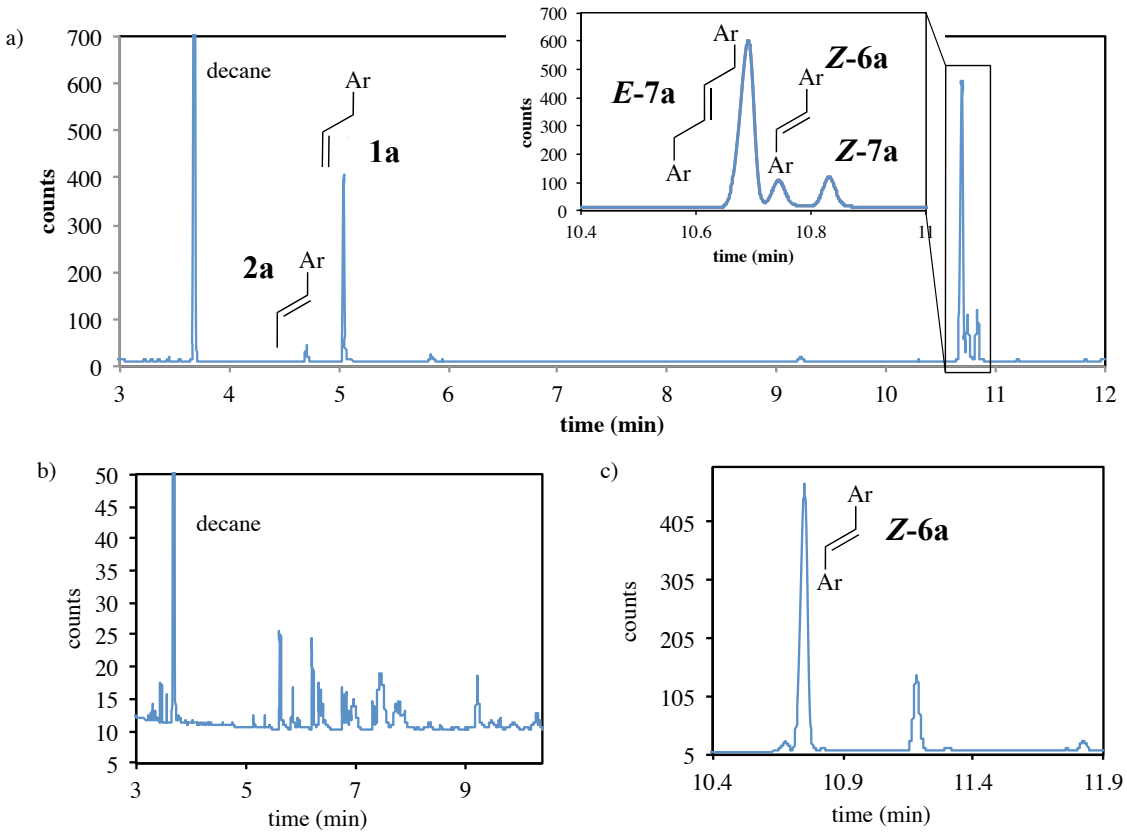

Figure C2. GC-FID traces for self-metathesis of estragole **1a** by Ru@MCM; solvent front omitted. (a) Trace at 1 h. Inset shows expansion of the region in which the primary CM products (*E*)- and (*Z*)-**7a** appear. Also apparent is a signal for one of the isomerization products, ArCH=CHAr (Ar = *p*-C_6H_4OMe). (b) Trace at 5 h showing essentially complete

loss of the primary metathesis product **7a** to isomerization. (c) Expansion of (b) in the region in which signals for **7a** would appear.

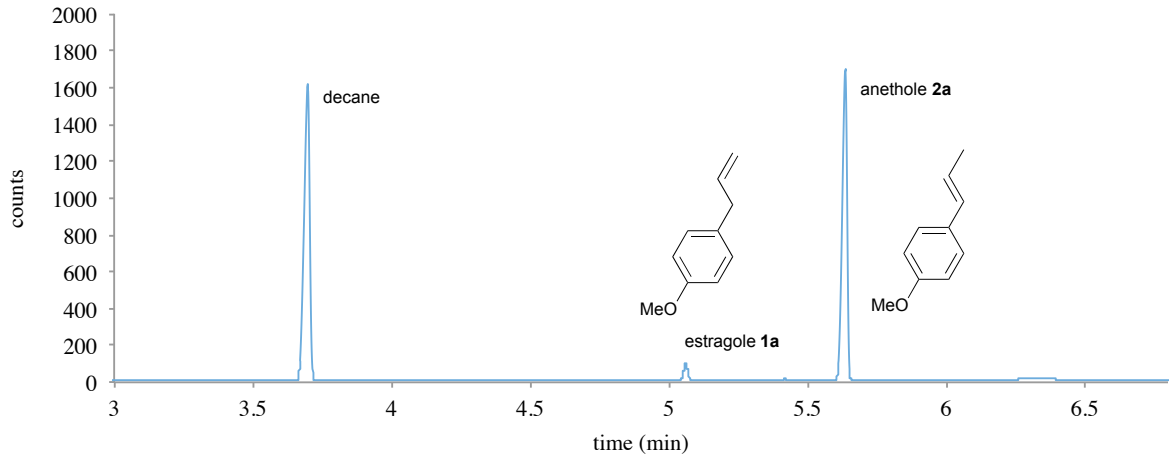

Figure C3. GC-FID trace for isomerization of estragole **1a** to anethole **2a** promoted by the Grotjahn catalyst **Ru-2** at 5 min. Solvent front omitted.

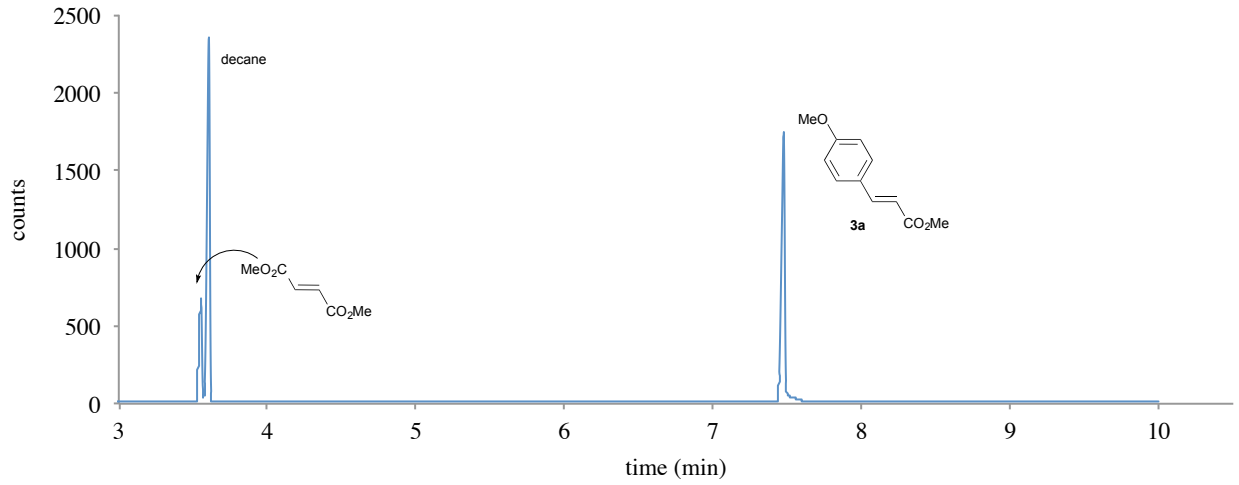

Figure C4. GC-FID trace for sequential isomerization-metathesis of anethole **1a** to cinnamate **3a** using the Grotjahn catalyst **Ru-2** and **HII**, after 6.5 h reaction (0.5 h isomerization, 6 h cross-metathesis). Solvent front omitted.

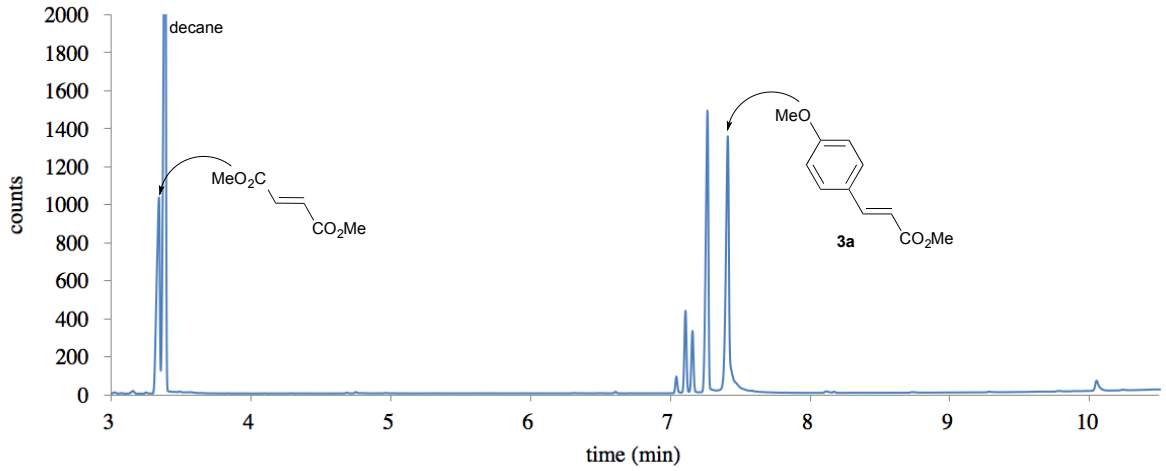

Figure C5. GC-FID trace showing side-products formed during the attempted transformation of **1a** to **3a** by orthogonal tandem catalysis using catalysts **Ru-2** and **HII**. Solvent front omitted.

D. NMR Characterization

D1. Details of 1H NMR Quantification of Cinnamate and Ferrulate Products

Conversions of the 1-allylbenzenes **1a**–**c** and 2-allylbenzenes **2a**–**c**, as well as yields of products **2a**–**c** and **3a**, were assessed by GC-FID. Yields of cinnamate or ferulate products other than **3a** (specifically, **3b**, **3c**, and **3a'**, **3b'**, **3c'**) were assessed by ^{1}H NMR analysis, as the accuracy of GC quantification was hampered by poor peak shapes.

^{1}H NMR signal assignments were confirmed by comparison to the literature values summarized in Tables S1 and S2 below. Quantification was established by integration of well-isolated signals for the desired products against those for the styrene intermediates and the stilbene byproducts, the data for which are shown in Tables S3 and S4, respectively. A representative spectrum for the reaction involving transformation of **1b** to **3b** appears in Figure S1.

Table D1. Literature ^{1}H NMR data for cinnamate and ferulate targets (methyl esters).

Compound	^{1}H NMR chemical shifts ($CDCl_3$)	Ref.
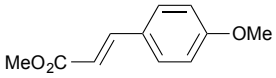 **3a**	7.65 (d, *J* = 16.0 Hz, 1H), 7.47 (m, 2H), 6.93-6.89 (m, 2H), 6.31 (d, *J* = 16.0 Hz, 1H), 3.83 (s, 3H), 3.79 (s, 3H)	[2]
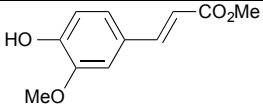 **3b**	7.64 (d, 1H, *J* = 15.9 Hz), 7.09 (dd, 1H, *J* = 1.9 Hz, *J* = 8.2 Hz), 7.04 (d, *J* = 1.9 Hz, 1H), 6.94 (d, *J* = 8.2 Hz, 1H), 6.31 (d, *J* = 15.9 Hz, 1H), 5.89 (s, 1H), 3.95 (s, 3H), 1.61 (s, 1H)	[3]
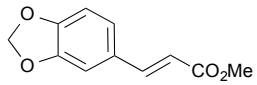 **3c**	7.58 (d, *J* = 15.9 Hz, 1H), 7.02 (s, 1H), 6.99 (dd, *J* = 8.1 Hz, *J* = 1.5 Hz, 1H), 6.80 (d, *J* = 8.1 Hz, 1H), 6.25 (d, *J* = 15.9 Hz, 1H), 6.00 (s, 2H), 3.79 (s, 3H)	[4]

Table D2. Literature ^{1}H NMR data for cinnamate and ferulate targets (2-ethylhexyl esters).

Compound	^{1}H NMR chemical shifts ($CDCl_3$)	Ref.
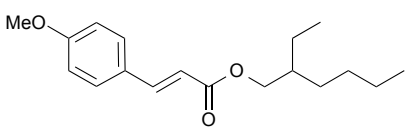 **4a**	7.64–7.56 (d, *J* = 16.0 Hz, 1H), 7.48–7.44 (d, *J* = 8.6 Hz, 2H), 6.90–6.89 (d, *J* = 8.8 Hz, 2H), 6.33–6.25 (d, *J* = 16.0 Hz, 1H), 34.10–4.07 (d, *J* = 5.7 Hz, 2H), 1.63–0.85 (m, 15H)	5
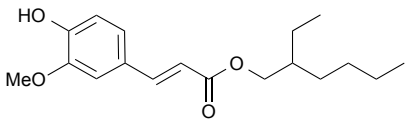 **4b**	7.60 (d, $^{2}J_{HH}$ = 15.8 Hz, 1H), 7.08 (dd, $^{3}J_{HH}$ = 8.1 Hz, $^{4}J_{HH}$ = 2.0 Hz, 1H), 7.04 (d, $^{4}J_{HH}$ = 2.0 Hz, 1H), 6.92 (d, $^{3}J_{HH}$ = 8.1 Hz, 1H), 6.29 (d, $^{2}J_{HH}$ = 15.8 Hz, 1H), 5.88 (s, 1H), 4.11 (dd, $^{3}J_{HH}$ = 6.0 Hz, $^{4}J_{HH}$ = 1.7 Hz, 2H), 3.93 (s, 3H), 1.65 (m, 1H), 1.48-1.24 (m, 8H), 0.96-0.86 (m, 6H)	6
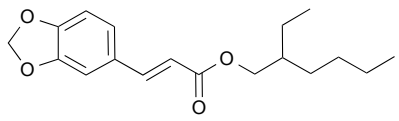 **4c**	7.58 (d, $^{2}J_{HH}$ = 15.9 Hz, 1H), 7.04 (d, $^{4}J_{HH}$ = 1.7 Hz, 1H), 7.00 (dd, $^{3}J_{HH}$ = 8.0 Hz, $^{4}J_{HH}$ = 1.7 Hz, 1H), 6.81 (d, $^{3}J_{HH}$ = 8.0 Hz, 1H), 6.27 (d, $^{2}J_{HH}$ = 15.9 Hz, 1H), 6.00 (s, 2H), 4.10 (dd, $^{3}J_{HH}$ = 5.9 Hz, $^{4}J_{HH}$ = 1.5 Hz, 2H), 1.64 (m, 1H), 1.49-1.22 (m, 8H), 0.97-0.84 (m, 6H)	6

Table D3. Literature ^{1}H NMR data for styrene intermediates.

Compound	^{1}H NMR values ($CDCl_3$)	Ref.
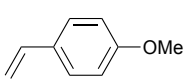 **5a**	7.35 (d, *J* = 9.0, 2 H), 6.86 (d, *J* = 8.9, 2 H), 6.66 (dd, *J* = 17.6 and 10.9, 1 H), 5.62 (dd, *J* = 17.6, *J* = 0.6 Hz, 1 H), 5.12 (dd, *J* = 10.9, *J* = 0.6 Hz, 1 H), 3.81 (s, 3 H)	7
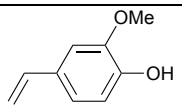 **5b**	6.88-6.81 (m, 3H), 6.63-6.54 (m, 1H), 5.68 (s, 1H), 5.71 (d, *J* = 17.56 Hz, 1H), 5.09 (d, *J* = 10.92 Hz, 1H), 3.84 (3H, s)	8
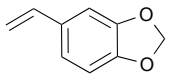 **5c**	6.97 (s, 1H), 6.84 (dd, *J* = 8, 2 Hz, 1H), 6.77 (d, *J* = 7 Hz, 1H), 6.63 (dd, *J* = 18, 10 Hz, 1H), 5.96 (s, 2H), 5.58 (d, *J* = 18 Hz, 1H), 5.13 (d, *J* = 10 Hz, 1H)	9

Table D4. Literature ^{1}H NMR data for stilbene byproducts.

Compound	^{1}H NMR values ($CDCl_3$)	Ref.
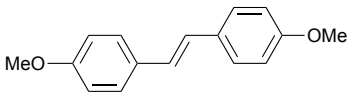 **6a**	7.41 (d, $^3J_{HH}$ = 8.9 Hz, 4H), 6.92 (s, 2H), 6.87 (d, $^3J_{HH}$ = 8.6 Hz, 4H), 3.81 (s, 6H)	10
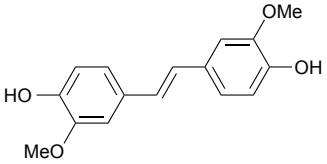 **6b**	7.02 (d, *J* = 2 Hz, 1H), 7.00 (dd, *J* = 8 Hz, *J* = 2 Hz, 1H), 6.90 (d, *J* = 8 Hz, 1H), 6.89 (s, 1H), 5.61 (s, 1H), 3.95 (s, 3H)	11
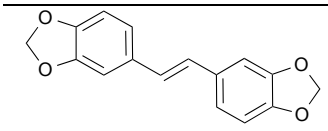 **6c**	7.01 (s, 2H), 6.87 (d, $^3J_{HH}$ = 8.2 Hz, 2H), 6.83 (s, 2H), 6.76 (d, $^3J_{HH}$ = 8.2 Hz, 2H), 5.96 (s, 4H)	12

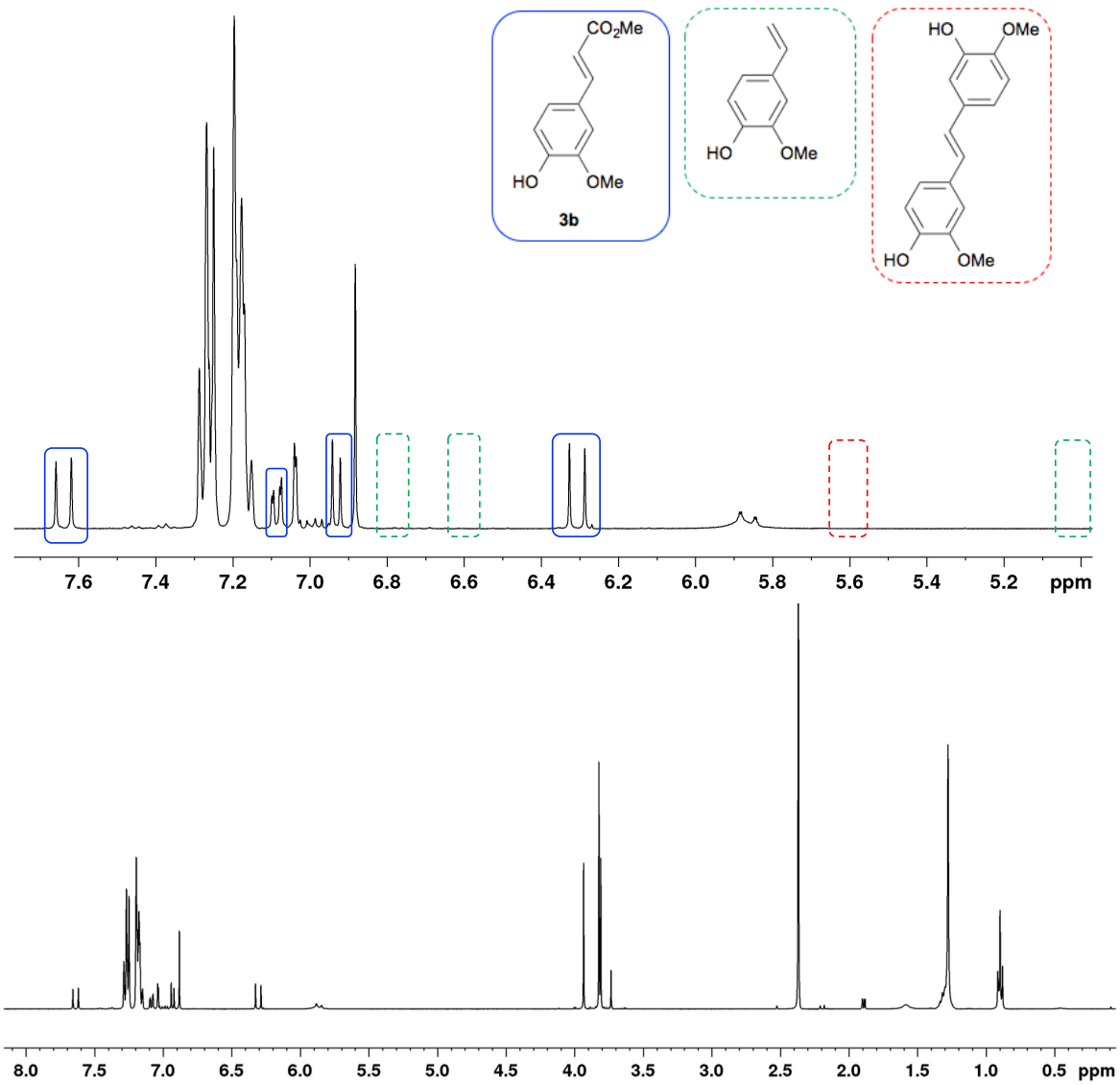

Figure D1. ^{1}H NMR spectrum ($CDCl_3$, 300 MHz) for the sequential isomerization-metathesis of anethole **1a** to cinnamate **3a** using the Grotjahn catalyst **Ru-2** and metathesis catalyst **HII**, after a total of 6.5 h reaction (0.5 h isomerization, 6 h cross-metathesis). Inset shows the diagnostic olefinic region used for quantification. Peaks for **3b** are outlined in blue; locations for the styrene and stilbene intermediates are outlined in green and red, respectively.

D2. NMR Characterization of **Ru-4**.

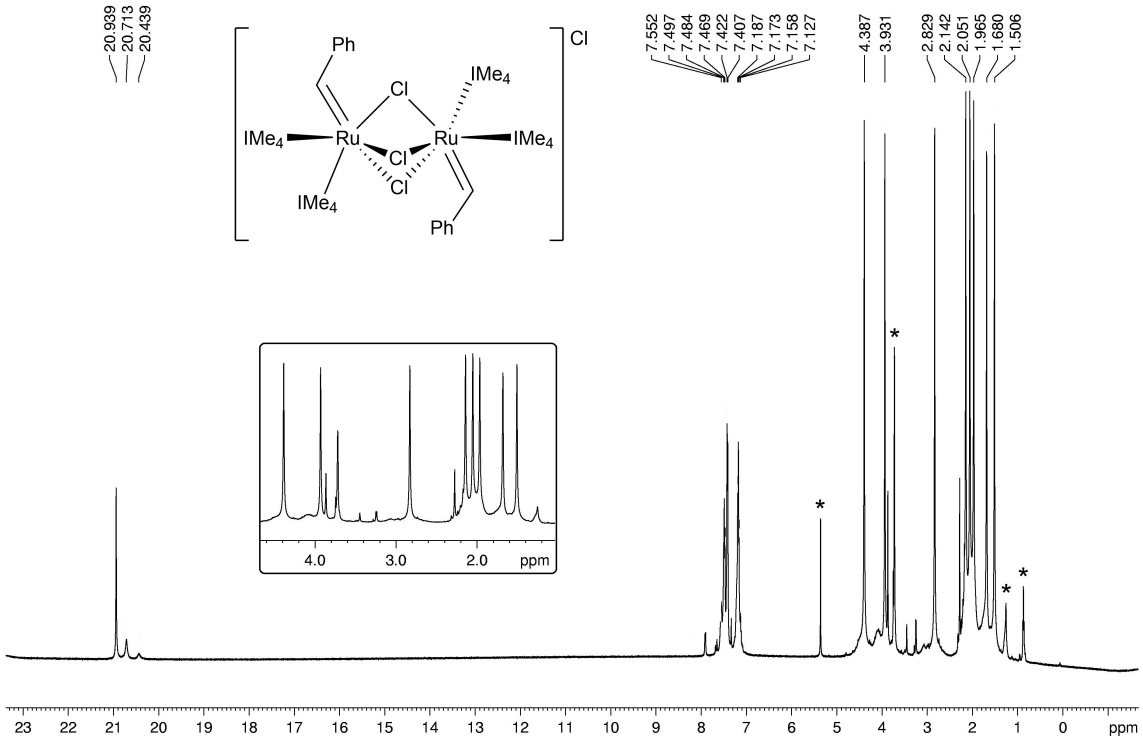

Figure D2. ^{1}H NMR spectrum of **Ru-4** (DCE-d4, 500 MHz).

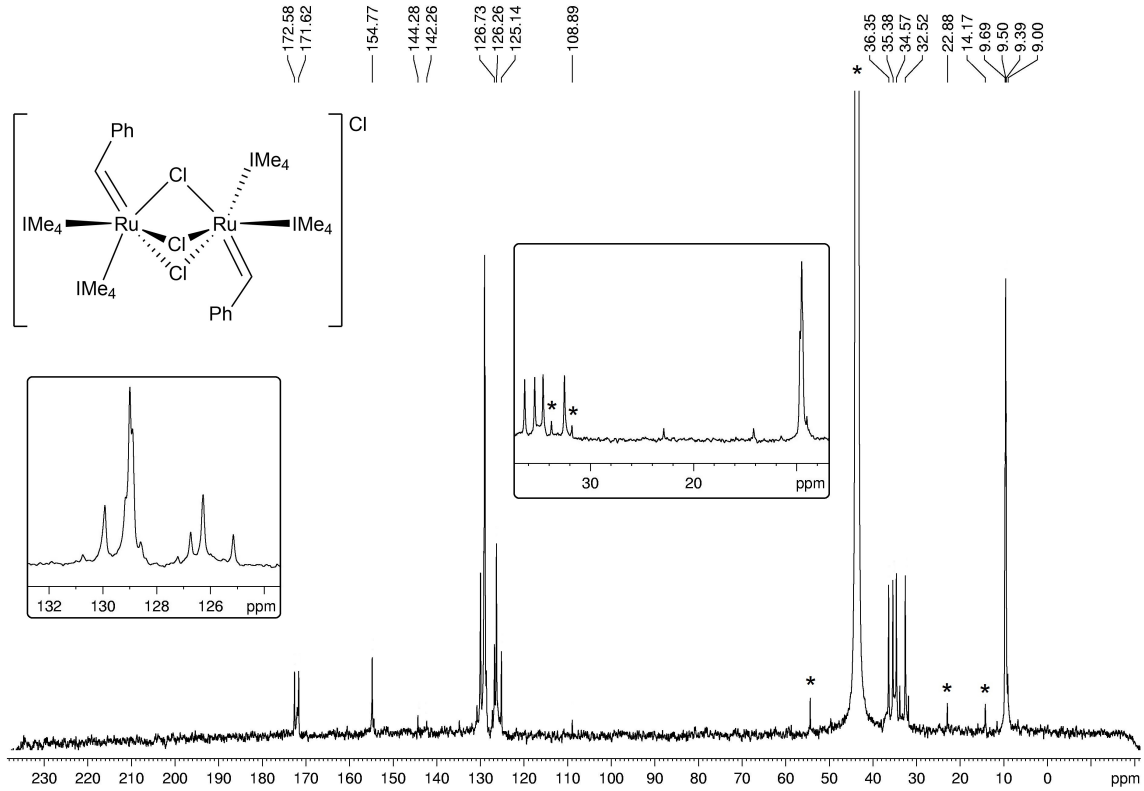

Figure D3. $^{13}C\{^{1}H\}$ NMR spectrum of **Ru-4** (DCE-d4, 125.7 MHz).

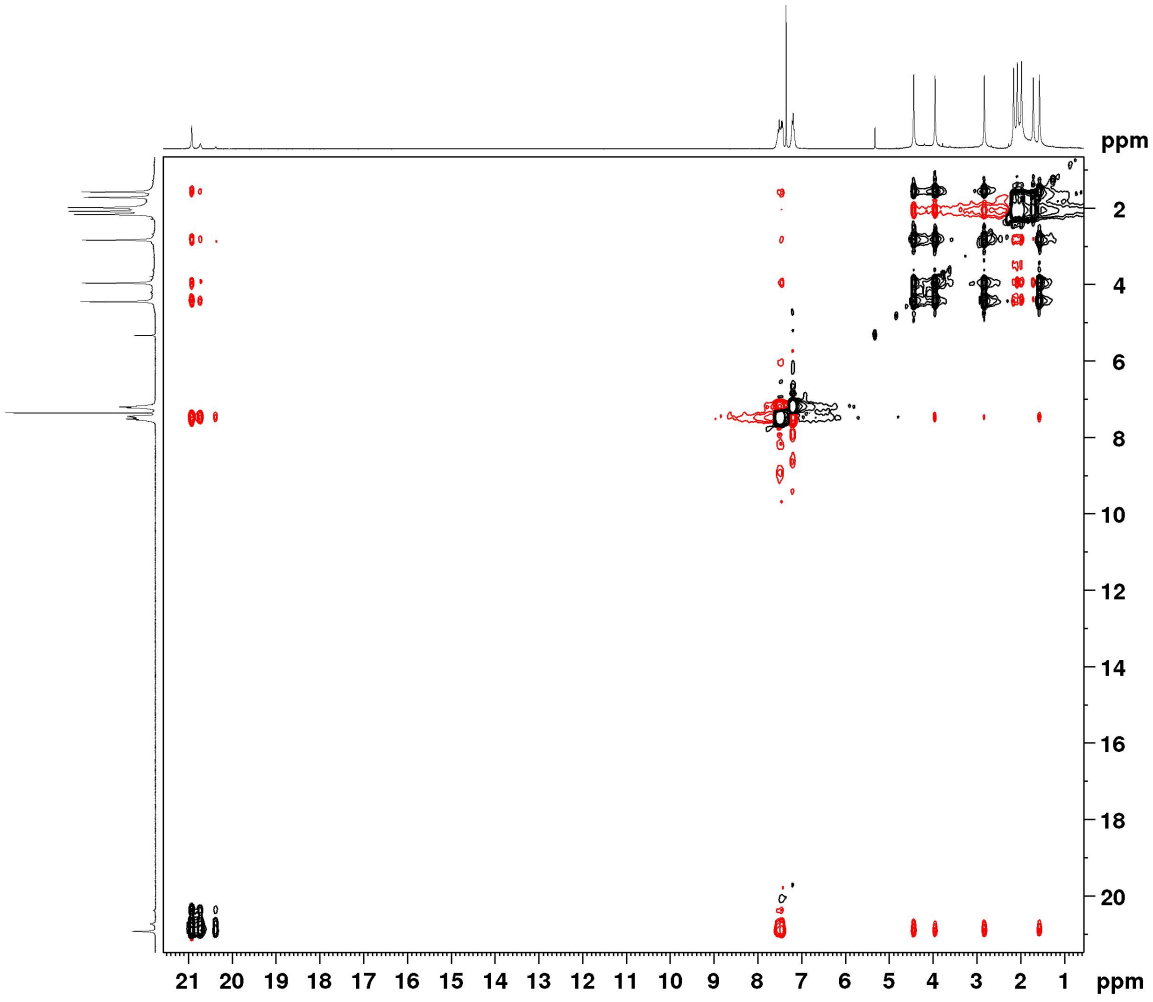

Figure D4. ^{1}H-^{1}H EXSY/NOESY spectrum of **Ru-4** (CD_2Cl_2, 300 MHz). EXSY correlations are shown in black; NOESY in red.

E. Crystallographic Data

Table E1. Crystallographic parameters for **Ru-4**.

A. Crystal Data	
formula	$C_{45}H_{66}Cl_7N_8Ru_2$
formula weight	1169.34
crystal dimensions (mm)	0.27 × 0.21 × 0.06
crystal system	triclinic
space group	$P\bar{1}$ (No. 2)
unit cell parameters[a]	
a (Å)	15.2175 (3)
b (Å)	16.4594 (3)
c (Å)	21.4365 (4)
α (deg)	85.8940 (9)
β (deg)	86.8717 (10)
γ (deg)	78.4456 (9)
V (Å^3)	5242.46 (17)
Z	4
ρ_{calcd} (g cm^{-3})	1.482
μ (mm^{-1})	8.252
B. Data Collection and Refinement Conditions	
diffractometer	Bruker D8/APEX II CCD[b]
radiation (λ [Å])	Cu Kα (1.54178) (microfocus source)
temperature (°C)	–100
scan type	ω and ϕ scans (1.0°) (5 s exposures)
data collection 2θ limit (deg)	148.39
total data collected	298211 (-18 ≤ h ≤ 18, -20 ≤ k ≤ 20, -26 ≤ l ≤ 26)
independent reflections	20288 (R_{int} = 0.0623)
number of observed reflections (*NO*)	18324 [$F_o^2 \geq 2\sigma(F_o^2)$]
structure solution method	intrinsic phasing (*SHELXT-2014*[c])
refinement method	full-matrix least-squares on F^2 (*SHELXL–2014*[d])
absorption correction method	multi-scan (*TWINABS*)
range of transmission factors	0.4095–0.2338
data/restraints/parameters	20288 / 0 / 1150
goodness-of-fit (S)[e] [all data]	1.049
final R indices[f]	
R_1 [$F_o^2 \geq 2\sigma(F_o^2)$]	0.0361
wR_2 [all data]	0.0998
largest difference peak and hole	2.040 and –1.484 e Å^{-3}

[a]Obtained from least-squares refinement of 9546 reflections with 5.94° < 2θ < 147.40°.

[b]Programs for diffractometer operation, data collection, data reduction and absorption correction were those supplied by Bruker. The crystal used for data collection was found to display non-merohedral twinning. Both components of the twin were indexed with the program *CELL_NOW* (Bruker AXS Inc., Madison, WI, 2004). The second twin component can be related to the first component by 180º rotation about the [1 $^{-1}/_{4}$ $^{1}/_{2}$] axis in real space and about the [1 0 1] axis in reciprocal space. Integrated intensities for the reflections from the two components were written into a *SHELXL-2014* HKLF 5 reflection file with the data integration program *SAINT* (version 8.34A), using all reflection data (exactly overlapped, partially overlapped and non-overlapped). The refined value of the twin fraction (*SHELXL-2014* BASF parameter) was 0.3942(7).

[c]Sheldrick, G. M. *Acta Crystallogr.* **2015**, *A71*, 3–8.

[d]Sheldrick, G. M. *Acta Crystallogr.* **2015**, *C71*, 3–8.

[e]$S = [\Sigma w(F_o^2 - F_c^2)^2/(n - p)]^{1/2}$ (n = number of data; p = number of parameters varied; $w = [\sigma^2(F_o^2) + (0.0487P)^2 + 7.7337P]^{-1}$ where $P = [\mathrm{Max}(F_o^2, 0) + 2F_c^2]/3$).

[f]$R_1 = \Sigma||F_o| - |F_c||/\Sigma|F_o|$; $wR_2 = [\Sigma w(F_o^2 - F_c^2)^2/\Sigma w(F_o^4)]^{1/2}$.

F. References

(1) van Lierop, B. J.; Reckling, A. M.; Lummiss, J. A. M.; Fogg, D. E. *ChemCatChem* **2012**, *4*, 2020–2025.

(2) Zhang, Z.; Zha, Z.; Gan, C.; Pan, C.; Zhou, Y.; Wang, Z.; Zhou, M.-M. *J. Org. Chem.* **2006**, *71*, 4339–4342.

(3) Putt, K. S.; Nesterenko, V.; Dothager, R. S.; Hergenrother, P. J. *ChemBioChem* **2006**, *7*, 1916–1922.

(4) Angle, S. R.; Choi, I.; Tham, F. S. *J. Org. Chem.* **2008**, *73*, 6268–6278.

(5) Monhaphol, T.; Albinsson, B.; Wanichwecharungruang, S. P. *J. Pharm. Pharmacol.* **2007**, *59*, 279–288.

(6) Lummiss, J. A. M.; Oliveira, K. C.; Pranckevicius, A.; Santos, A.; dos Santos, E. N.; Fogg, D. E. *J. Am. Chem. Soc.* **2012**, *134*, 18889–18891.

(7) Denmark, S. E.; Butler, C. R. *Org. Lett.* **2006**, *8*, 63–66.

(8) Sharma, A.; Kumar, R.; Sharma, N.; Kumar, V.; Sinha, A. K. *Adv. Synth. Catal.* **2008**, *350*, 2910–2920.

(9) Lebel, H.; Ladjel, C. *Organometallics* **2008**, *27*, 2676–2678.

(10) Khartulyari, A. S.; Kapur, M.; Maier, M. E. *Org. Lett.* **2006**, *8*, 5833–5836.

(11) Li, L.; Seeram, N. P. *J. Agric. Food Chem.* **2011**, *58*, 11673–11679.

(12) Hua, G.; Li, Y.; Slawin, A. M. Z.; Woollins, J. D. *Dalton Trans.* **2007**, 1477–1480.

G. List of Contributions

PUBLICATIONS (C = COMMUNICATION, F= FULL PAPER, R = REVIEW, †*EQUAL CONTRIBUTIONS*)

8C. **C.S. Higman**, A.E. Lanterna, M.L. Marin, J.C. Scaiano, D.E. Fogg. "Ruthenium Nanoparticles as Unsuspected Triggers for Isomerization during Olefin Metathesis." **2016**, *submitted*.

7F. **C.S. Higman**, M. Peres de Araujo, D.E. Fogg. "Tandem Catalysis versus One-Pot Catalysis: Ensuring Process Orthogonality in the Transformation of Essential-Oil Phenylpropenoids into High-Value Products via Olefin Isomerization-Metathesis." *Catal. Sci. Tech.* **2016**, *Advance Article,* DOI: 10.1039/c5cy02038g (selected as Cover Article).

6R. **C.S. Higman**†, J.A.M. Lummiss†, D.E. Fogg. "Olefin Metathesis at the Dawn of Uptake in Pharmaceutical and Specialty Chemicals Manufacturing." *Angew. Chem. Int. Ed*., **2016,** *55*, 3553-3565; invited review.

5F. J.A.M. Lummiss, **C.S. Higman**, D.L. Fyson, R. McDonald, D.E. Fogg. "The Divergent Effects of Strong NHC Donation in Catalysis." *Chem. Sci.* **2015**, *6*, 6739-6746.

4F. J.E.C. Wren, B.J. Greer, V.K. Michaelis, **C.S. Higman**, S. Kroeker. "Multinuclear Magnetic Resonance Investigation of Crystalline Alkali Molybdates." *Inorg. Chem*. **2015**, *54*, 9853-9861.

3C. **C.S. Higman**, L. Plais, D.E. Fogg. "Isomerization During Olefin Metathesis: An Assessment of Potential Catalyst Culprits." *ChemCatChem* **2013**, *5*, 3548-3551.

2F. J.M. Blacquiere, **C.S. Higman**, R. McDonald, D.E. Fogg. "A reactive Ru-binaphtholate building block with self-tuning hapticity." *J. Am. Chem. Soc.* **2011**, *133*, 14054-14062.

1F. J.M. Blacquiere, **C.S. Higman**, S.I. Gorelsky, N.J. Beach, D.E. Fogg. "Unprecedentedly Strong Binding of Dinitrogen by a Ruthenium–N-Heterocyclic Carbene Complex." *Angew. Chem. Int. Ed.* **2011***, 50*, 916-919.

MANUSCRIPTS IN PREPARATION

1F. **C.S. Higman**, S.A. Rufh, R. McDonald, D.E. Fogg. " A Truncated N-Heterocyclic Carbene for Olefin Metathesis: A Quest for Improved Catalyst Lifetime and Productivity."

PRESENTATIONS (O=ORAL, P=POSTER; PRESENTING AUTHOR IN BOLD)

P15. **C.S. Higman**, A.E. Lanterna, M.L. Marin, J.C. Scaiano, and D.E. Fogg "Ruthenium nanoparticles in olefin metathesis: their formation and non-innocence." 21st International Symposium on Olefin Metathesis and Related Chemistry (ISOM XXI), Graz, Austria, July 12-16, 2015 (International)

O14. **C.S. Higman**, A.E. Lanterna, M.L. Marin, J.C. Scaiano, and D.E. Fogg. "Ruthenium nanoparticles in olefin metathesis: their formation and non-innocence." 98th Canadian Society for Chemistry Conference, Ottawa, June 17th, 2015 (National)

O13. J.A.M. Lummiss, C.S. Higman, and **D.E. Fogg**. "Strong NHC donation can inhibit

catalysis: A showcase study in olefin metathesis." 98th Canadian Society for Chemistry Conference, Ottawa, June 17th, 2015 (National)

O12. **G.A. Bailey**, C.S. Higman, and D.E. Fogg. "Deactivation of the Hoveyda catalyst: impact of ethylene." 98th Canadian Society for Chemistry Conference, Ottawa, June 17th, 2015 (National)

O11. **C.S. Higman**, A.E. Lanterna, M.L. Marin, J.C. Scaiano, and D.E. Fogg. "Ruthenium nanoparticles in olefin metathesis: their formation and non-innocence." Centre for Catalysts Research and Innovation Annual Meeting, Ottawa, June 5, 2013 (Institutional)

P10. **G.A. Bailey**, C.S. Higman, and D.E. Fogg. "Deactivation of the Hoveyda catalyst: impact of ethylene." Centre for Catalysts Research and Innovation Annual Meeting, Ottawa, June 5, 2013 (Institutional)

O9. **C.S. Higman**, A.E. Lanterna, M.L. Marin, J.C. Scaiano, and D.E. Fogg "Exploring nanoparticle formation during synthesis and use of metathesis catalysts." 47th Inorganic Discussion Weekend, Montreal, Quebec, November 14-16, 2015 (Regional)

P8. **C.S. Higman**, P. Plouffe, M. Peres de Araujo, A. Macchi, and D.E. Fogg. "High-value targets via phenylpropenoid isomerization." 19th International Symposium on Homogeneous Catalysis, Ottawa, July 6-11, 2014 (International)

P7. **C.S. Higman**, and D.E. Fogg. "Unwanted isomerization during metathesis: interrogating potential culprits and establishing a spectrum of guilt." Centre for Catalysts Research and Innovation Annual Meeting, Ottawa, September 12, 2013 (Institutional)

P6. **C.S. Higman**, L. Plais, and D.E. Fogg. "Ruthenium hydrides as olefin isomerization catalysts: Exploring key parameters relating to catalyst productivity." 96th Canadian Society for Chemistry Conference, Quebec City, May 28th, 2013 (National)

P5. **C.S. Higman**, and D.E. Fogg. "NHCs for Olefin Metathesis: Standard to "Stumpy"." Inorganic Discussion Weekend, Ottawa, November 2-4, 2012 (Regional)

P4. **C.S. Higman**, and D.E. Fogg. "Studying the steric and electronic properties of Ruthenium-NHC complexes." 95th Canadian Society for Chemistry Conference, Calgary, May 27th, 2013 (National)

P3. **C.S. Higman**, J.M. Blacquiere, S.I. Gorelsky, and D.E. Fogg. "Unprecedentedly Strong Binding of Dinitrogen at Ruthenium." 2011 Entretiens Jacques Cartier Colloquium on 21st Century Catalysis Science and Applications, Ottawa, September 29-30, 2011 (National)

P2. **C.S. Higman**, J.M. Blacquiere, S.I. Gorelsky, and D.E. Fogg. "Exploring the Strong Binding of Dinitrogen to Ruthenium Centers." Centre for Catalysts Research and Innovation Annual Meeting, Ottawa, September 15, 2011 (Institutional)

P1. **C.S. Higman**, J.M. Blacquiere, S.I. Gorelsky, and D.E. Fogg. "Exploring the Strong Binding of Dinitrogen to Ruthenium Centers." 94th Canadian Society for Chemistry Conference, Montreal, June 5-9, 2011 (National)